# SIMULATION OF VERTICAL SHIP RESPONSES IN HIGH SEAS

A Thesis

by

SURESH RAJENDRAN

Submitted to the Office of Graduate Studies of
Texas A&M University
in partial fulfillment of the requirements for the degree of

MASTER OF SCIENCE

December 2008

Major Subject: Ocean Engineering

# SIMULATION OF VERTICAL SHIP RESPONSES IN HIGH SEAS

A Thesis

by

SURESH RAJENDRAN

Submitted to the Office of Graduate Studies of
Texas A&M University
in partial fulfillment of the requirements for the degree of

MASTER OF SCIENCE

Approved by:

| | |
|---|---|
| Chair of Committee, | Cheung Hun Kim |
| Committee Members, | Richard Mercier |
| | Bob Stewart |
| Head of Department, | David Rosowsky |

December 2008

Major Subject: Ocean Engineering

# ABSTRACT

Simulation of Vertical Ship Responses in High Seas.

(December 2008)

Suresh Rajendran, B.Tech, Cochin University of Science and Technology, India

Chair of Advisory Committee: Dr. Cheung Hun Kim

This research was done to study the effect of sea severity on the vertical ship responses like heave and pitch. Model testing of a 175m moored container ship with zero heading speed was done for different sea states varying from very rough to very high seas. Transfer functions were extracted using Volterra model which constitutes both linear and quadratic part. The experimental linear transfer functions were calculated using Volterra linear model and were compared with linear transfer function from the hydrodynamic theory. Experimental second order transfer functions were also extracted using Volterra quadratic model and their behavior was studied for different sea states. After the extraction of linear and second order transfer functions total responses were reconstructed and compared with the measured responses. This also helped to investigate the contribution of second order part to the total vertical ship responses.

In the last stage of the research a new semi- empirical method was developed called as 'UNIOM' for the prediction of the responses. Laboratory input waves and theoretical LTFs were used for the simulation of ship response and these were compared with measured responses.

*To my parents and sister*

# ACKNOWLEDGEMENTS

I would like to thank my advisor and committee chair, Dr.Cheung.H.Kim for his guidance, inspiration, assistance and patience in explaining the statistics and hydrodynamics part of this research which was completely unknown to me in the initial stage. I would also like to thank Dr.Richard Mercier and Dr.Bob Stewart for sharing their highly valued knowledge and providing right guidance during the course of study and their willingness to serve on my committee. I am very grateful to the Advanced Ship Engineering Research Center at Pusan National University, Busan, Korea, for the support of this research. Also, I am very thankful to Professor Young Hwan Kim, Department of Naval Architecture and Ocean Engineering, Seoul National University, Seoul Korea, for providing us the theoretical LTFs for heave, pitch and vertical relative motion of S175 hull.

I am indebted to my classmates and professors of Texas A&M University for their constant support and motivation. I personally thank my friends Dr.KamalDev Raghavan, Mr.Basil Theckumpurath, Mr.Muneer and Mr.Rajith Padmanabhan for their support and love which was always a source of inspiration during this study.

Finally, thanks to my mother, father and sister for their love for me.

TABLE OF CONTENTS

CHAPTER Page

CHAPTER Page

# LIST OF FIGURES

Page

Page

Page

Page

Page

# LIST OF TABLES

Page

# CHAPTER I

# INTRODUCTION

## 1.1 Problem statement

Ship motions in high seas have been the area of interest for the last three, four decades. But very few experiments were conducted in real random sea environment which may be due to difficulty in setting up the experiment and measurement of the data. Most of the experiments have relied on regular waves for the prediction of ship response in high seas. Again, lots of experiments were conducted on the lateral motion of ship for the detailed study of mooring problems. But Ship response in the high seas has been little studied especially in the area of vertical responses to the high seas causing green water and slamming. In order to achieve the objective one needs to have sound understanding of the fundamental physical meaning of the motion. This may be best achieved by doing the careful experiment and detailed analysis. The note herein describes the experiment and analysis of a ship model in the seas of various severities, where the model is moored in the head random waves for simpler experiment as the basis for the initial development. The analysis was carried out applying the Volterra linear and quadratic model to find LTF and QTF which are defined in the following pages. Volterra cubic model is desirable but the algorithm has not been prepared by the time of research. Volterra model is shown schematically in Figure 1-1.

---

This thesis follows the style of *Journal of Waterway, Port, Coastal, and Ocean Engineering*.

Our study was done on the vertical ship responses in random non linear waves produced in the wave tank. This gives clearer picture of the ship behavior in highly nonlinear random seas. Now researches are aware that more detailed advanced study on the realistic random sea waves are required.

In Conventional ship building practice, ship response is studied based on linear input output method using linear transfer function (LTF). This is called system characteristic. LTF calculated using hydrodynamic theory is purely independent of the sea characteristics. But the experiments on the highly nonlinear random seas have shown that LTF is affected by the sea severity. Such a phenomenon is only visible in high seas for which linear theory is not applicable. As the sea severity increases the non linearity goes from second order to higher orders. This study has given emphasis on second order waves and its response. Linear and second order response transfer function was developed using Volterra model and the responses were extracted so as to study the effect of nonlinear waves on the vertical ship response.

The above mentioned study necessitates the requirement of a prediction model for high seas. So a new semi-empirical model 'UNIOM-Motion' was developed in the final stage of the research for the prediction of ship response in high seas. This method can be found to be analogous to Volterra model to some extent. Figure1-2 shows the schematic diagram for UNIOM model.

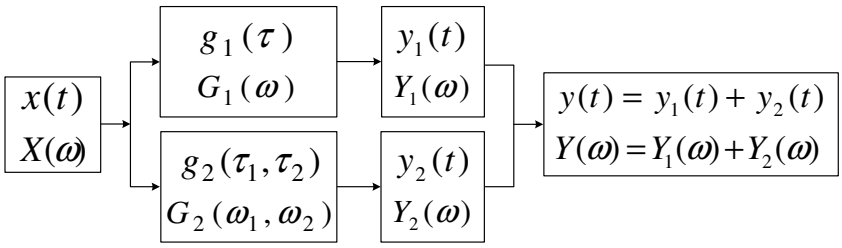


Figure 2-1 Schematic diagram for Volterra Model

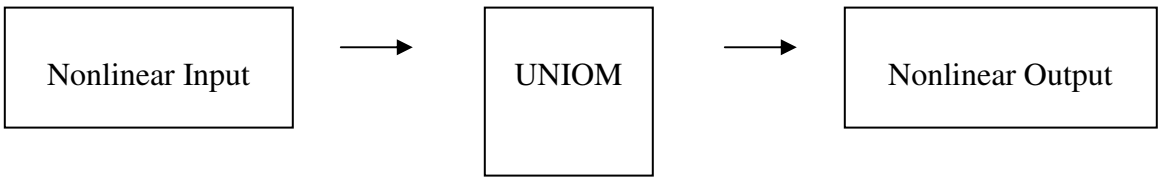


Figure 2-2 Schematic diagram for UNIOM-Motion

## 1.2 Background

Linear theory is based on the assumption that ship is wall sided and travelling on a straight course in very low seas (Cummins 1973). Linear wave assumption was used to calculate the system characteristics of the ship which do not depend upon the sea condition. Dalzell (1962) conducted experiment on the pitch motion of a fast moving destroyer in high seas. It was found that pitch motion was largely affected by sea severity and contrary to the popular belief it decreases as sea severity increases as shown in Figure 1-3.

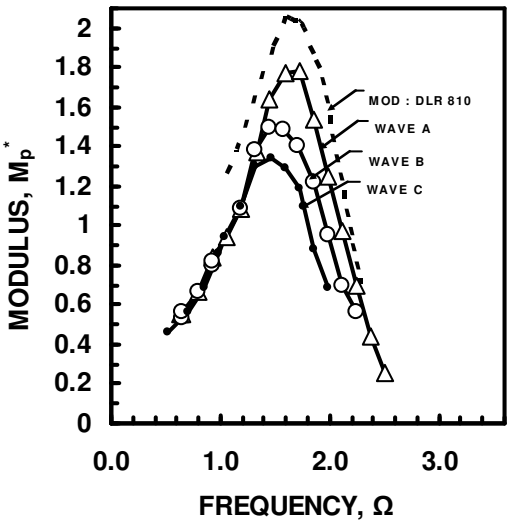


Figure 2-3 Pitch RAO of a destroyer running head seas of A, B, C (Hs = 6, 9, 11m) vs. encounter frequency in non dimensional form. (Dalzell 1962, also available from Cummins, 1973). Dotted line indicates the linear theory prediction

Cummins (1973) conducted experiment on the deck wetting per hour of a destroyer for high seas and found that experimental values are always lower than linear theory as shown in Figure1-4.

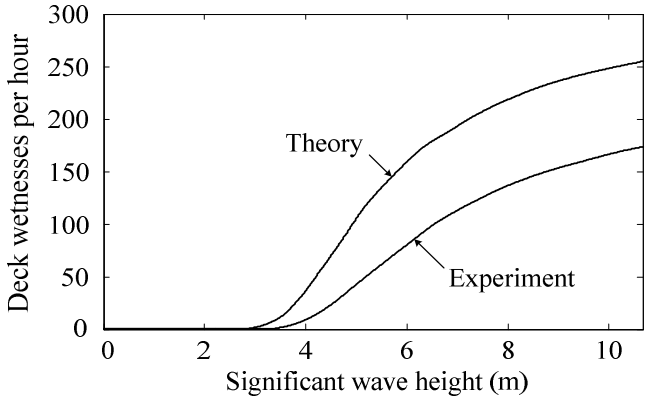


Figure 2-4 Deck wetness per hour of a destroyer (Cummins 1973)

Thus it was clearly observed that vertical ship response in high seas are largely affected by sea severity and the linear theory overestimates the response values compared to experiment.

Since these studies were done experimentally it is necessary to extract second order responses and find the contribution to the total response for better understanding of the problem. Extraction of second order response was done using Volterra quadratic model. Barret (1963) gave general input output model using infinite functional series for the weakly non linear response. Hasselman (1966) paper gives a broad and detailed idea about the second order transfer functions from the nonlinear waves and ship response. He showed that the transfer function characterizing the nonlinear response of ships in irregular seas can be obtained from high order moments of the ship motion by an extension of standard spectral analysis techniques. Even though Hasselman's quadratic model is very much similar to Volterra model he derived it from Taylor's series. Vassilopoulos (1967) showed that Volterra quadratic model can be used for the analysis of ship response. Dalzell (1974; 1976) developed the Volterra quadratic model for practical uses and applied for the calculation of added resistance in head seas in wave tank. Dalzell and Kim (1979) calculated QTFs using hydrodynamic theory for added ship resistance and compared the analytical and experimental results. They found that both cross bi spectrums are fairly in good agreement. It should be noted that Volterra model assumes Gaussian input. So this is applicable to only low sea severities. Kumar et al. (2003) showed that waves are approximately linear below Hs=4m and second order up to a significant wave height of 4m and 9m respectively. Even though our study has

used Gaussian method for analysis of second order response, the response behavior can be easily understood through such an approach. Kim and power (1998) proposed Volterra quadratic model with non-Gaussian input output. A detailed study of Volterra Gaussian and non-Gaussian method for the calculation of QTF can be seen from N.S.Kim and Kim (2004).

In the second stage of the research, 'UNIOM-Motion' was used to predict the responses at high seas. Small variations from this approach were already used for the calculation of ringing of TLP and the force acting on the cylinder due to impact force by Kim.C.H (Kim, 2008). Similar work can be seen from the works of Adil (2004), Richer (2005) and Rajith (2006).

## 1.3 Objective

1) The main objective of the study is to reinvestigate the effect of sea severity on vertical ship responses due to highly nonlinear seas. The system characteristics and responses in high sea condition were checked with that of hydrodynamically calculated linear theory so as to find the discrepancy between the real responses and responses predicted by theory.

2) Extract second order transfer function from the total responses using Volterra model and check the effect of sea severity on these transfer functions. Second order responses were reconstructed from these transfer functions and input waves so as to find the contribution of these responses to the total response. This greatly helped the better understanding of the system and its response.

3) Develop a vertical response prediction model by extending the application of UNIOM-diffraction, a semi-empirical model of Volterra quadratic system which was developed and applied in previous researches.

# CHAPTER II

# APPROACH AND MATHEMATICAL FORMULATION

## 2.1 Classification of sea state

Wind generated waves were generally classified by code 0 to 9 (Tupper 1996) for expressing their sea severity and percentage of occurrence around the globe as listed in table 2.1.

Table 2-1 Classification of sea state

| Code | Description of sea | $H_S$ (m) | Frequency of occurrence | | |
|---|---|---|---|---|---|
| | | | Worldwide | NorthAtlantic | NorthernNorth Atlantic |
| 0 | Calm (glassy) | 0.0 | 11.2486 | 8.3103 | 6.0616 |
| 1 | Calm (rippled) | 0.00 ~ 0.10 | | | |
| 2 | Smooth (wavelets) | 0.10 ~ 0.50 | | | |
| 3 | Slight | 0.50 ~ 1.25 | 31.6851 | 28.1996 | 21.5683 |
| 4 | Moderate | 1.25 ~ 2.50 | 40.1944 | 42.0273 | 40.9915 |
| 5 | Rough | 2.50 ~ 4.00 | 12.8005 | 15.4435 | 21.2383 |
| 6 | Very rough | 4.00 ~ 6.00 | 3.0253 | 4.2938 | 7.0101 |
| 7 | High | 6.00 ~ 9.00 | 0.9263 | 1.4968 | 2.6931 |
| 8 | Very high | 9.00 ~ 14.00 | 0.1190 | 0.2263 | 0.4346 |
| 9 | Phenomenal | over 14.00 | 0.0009 | 0.0016 | 0.0035 |

## 2.2 Gaussian and Non-Gaussian waves

It is well known from Fourier series that any periodic signal can be represented as the sum of large number of sinusoidal waves. Similarly water waves can be created by superimposing large number of sinusoidal waves.

A single sine wave can be represented as

$$\eta(t) = A\cos(kx - \omega t + \varepsilon) \qquad 2\text{-}1$$

Equation 2-1 shows the time history at a particular location x(t). k is the wave number, ω is the circular frequency and ε is any arbitrary phase angle. When we add infinitely many sinusoidal waves with different amplitudes, frequency and random phase angle we get a random wave or a zero mean Gaussian wave.

$$x(t) = \sum_{i=1}^{\infty} A_i \cos\left(k_i x - \omega_i t + \varepsilon_i\right) \qquad 2\text{-}2$$

Where $A_i$ is from the amplitude spectrum which can be obtained by Fourier transforming the input waves.

Crests and troughs of a Gaussian waves are symmetric about the mean level and about the vertical axis passing through peak. Because of this property they have general statistical characteristics which enable them to distinguish from Non-Gaussian waves. Non-Gaussian wave peaks are asymmetrically distributed about mean level and vertical axis passing through the peaks. They are generated by addition of higher order waves to the linear waves. Higher order waves, e.g. stokes second order wave, always have steep peaks and shallow troughs. So when they are added to linear waves it will result in asymmetric distribution of peaks about the mean level. It should be noted here we are considering the waves in deep water and wave breaking is not taken into account. So non-Gaussian waves cannot be created by superimposing the sinusoidal waves since it will always end up in Gaussian waves but they can be created in wave tank.

$$A_i = \sqrt{2U(\omega_i)\Delta\omega} \qquad 2\text{-}3$$

Equation 2-3 describes the method to generate a wave of amplitude $A_i$ with a particular frequency $\omega_i$. $U(\omega)$ is one sided energy spectrum which can be chosen as any standard target spectrum e.g. JONSWAP. In a wave tank, the waves of different frequency generated from equation 2-3 interact with each other resulting in non-Gaussian waves for high sea state.

Statistical properties like skewness and kurtosis are generally used to identify Gaussian and non-Gaussian waves. Skewness is a measure of the vertical symmetry of wave and its sign defines the ratio of crest to trough. A positive skewness in the wave field shows that crest heights are higher than trough heights. Kurtosis is a measure of the degree of peakedness in the distribution and defines the contribution of the big waves. For a normal distribution skewness and kurtosis values are respectively 0 and 3. A Kurtosis value greater than 3 indicates that the contribution from big waves is significant.

Skewness is the average of $(x\text{-}\mu_x)^3$ normalized by $\sigma_x^3$ and expressed in the form:

$$E[\frac{1}{\sigma_x^3}(x-\mu_x)^3] = \frac{1}{T}\int_0^T \frac{(x-\mu_x)^3}{\sigma_x^3}dt = \frac{1}{N-1}\sum_{j=1}^{N}\frac{(x_j-\mu_x)^3}{\sigma_x^3} \qquad 2\text{-}4$$

The kurtosis is the average of $(x-\mu_x)^4$ normalized by $\sigma^4_x$ and expressed in the form:

$$E[\frac{1}{\sigma_x^4}(x-\mu_x)^4] = \frac{1}{T}\int_0^T \frac{(x-\mu_x)^4}{\sigma_x^4} dt = \frac{1}{N-1}\sum_{j=1}^{N} \frac{(x_j-\mu_x)^4}{\sigma_x^4} \quad \text{2-5}$$

Where $\sigma_x$, $\mu_x$ are standard deviation of the process x(t) as a function of time and mean of the process respectively.

## 2.3 Target spectrum

Parameterized spectrums are generally used to generate waves digitally and experimentally depending upon the sea condition. Even though there are large number parameterized spectrums are devolved for the last fifty years here we will mainly talk about two spectrums which were used for the generation of waves in tanks for this study.

### 2.3.1 ITTC spectrum

Given the significant wave height and characteristic period, one can calculate the energy spectrum using the formula

$$U(\omega) = \frac{A}{\omega^5}\exp\left(-\frac{B}{\omega^4}\right), \quad A = 173H_s^2T_1^{-4}, \; B = 691T_1^{-4} \quad \text{2-6}$$

Significant wave height ($H_s$) is the average of highest one third waves and characteristic period $T_1$ is the average period derived from average frequency of the component waves. These are basically used for the generation of sea conditions of average height.

### 2.3.2 JONSWAP spectrum

JONSWAP spectrum is a three parameter spectrum with variables significant wave height ($H_s$), peak period ($T_p$) and peakedness parameter ($\gamma$). They have the advantage that they can represent high sea states using peakedness ($\gamma$) parameter which

ranges from 1 to 7 depending upon the sea state. High laboratory waves generated from this spectrum are non Gaussian in nature and hence can be used to study the effect of high seas on the ships. Waves simulated digitally from the JONSWAP are Gaussian waves since the spectrum doesn't carry any phase information.

JONSWAP spectrum can be derived from the following equation

$$U(\omega) = \frac{5}{16} H_s^2 \omega_m^4 \omega^{-5} \exp\left[ -1.25 \left( \frac{\omega_m}{\omega} \right)^4 \right] (1 - 0.287 \ln \gamma) \gamma^{\exp\left[ -\frac{(\omega - \omega_m)^2}{2\sigma^2 \omega_m^2} \right]} \quad 2\text{-}7$$

Where

$$\sigma = \begin{cases} 0.07 & \text{for } \omega \leq \omega_m \\ 0.09 & \text{for } \omega > \omega_m \end{cases} \quad 2\text{-}8$$

$\omega_m$ is the model frequency derived from the model period of frequency spectrum which in turn is derived from peak period of the period spectrum by the following equation

$$T_p = 0.880\ T_m \quad 2\text{-}9$$

## 2.4 Rayleigh distribution

A random process is said to be stationary if the statistics of the samples does not depend on the absolute time of measurement. A random process is said to be homogeneous if the statistics of the samples does not depend upon the space or the place of measurement. A process which is both homogenous and stationary is called as ergodic process. An ergodic random process is said to be narrow banded if the energy is distributed between a finite limited ranges of frequency. Water waves are considered to be narrow banded since their energy always lies in a finite frequency band. For narrow

banded zero mean Gaussian process it can be shown that probability for a wave crest to exceed a given peak value 'a' is

$$\Pr\{\text{peaks} > a\} = \exp\left[-\frac{a^2}{2m_0}\right] \qquad 2\text{-}10$$

Where $m_0$ is variance of the waves or the area under the energy spectrum which can be found out from the following equation

$$m_0 = \sigma_x^2 = E[(x-\mu_x)^2] = \frac{1}{T}\int_0^T (x-\mu_x)^2\, dt = \frac{1}{N-1}\sum_{j=1}^{N}(x_j-\mu_x)^2 \qquad 2\text{-}11$$

$\mu_x$ and $\sigma_x$ are the mean and standard deviation of the wave time history x(t).

Equation 2-10 is called as Rayleigh probability distribution exceeding 'a'. This equation can be used to identify the nonlinearity of the waves. Peaks from a narrow banded Gaussian will always follow the Rayleigh distribution curve since they are narrow banded. Deviation from the Rayleigh distribution of peak shows that the crests or troughs are asymmetrically distributed about the mean level and hence the process is non Gaussian.

## 2.5 Most probable peak value

Rayleigh Cumulative probability (peaks < a) can be derived from equation 2-10

$$P(a) = \Pr\{\text{peaks} \le a\} = 1 - \exp\left[-\frac{a^2}{2m_0}\right] \qquad 2\text{-}12$$

If we assume N observations, probability of maximum peak value occurrence is

$$1/N = 1 - \exp\left[-\frac{a_N{}^2}{2m_0}\right] \qquad 2\text{-}13$$

Therefore most probable peak value in N observation is

$$\hat{a}_N = \sqrt{2\ln N}\sqrt{m_0} \qquad 2\text{-}14$$

N is number of zero crossings during the time interval 'T' sec.

$$N = \frac{T}{T_z} \qquad 2\text{-}15$$

$T_z$ is the zero crossing period which can be calculated as follows

$$T_z = 2\pi\sqrt{\frac{m_0}{m_2}} \qquad 2\text{-}16$$

Where $m_2$ is the second moment of the one sided spectrum $U_{xx}(\omega)$

$$m_2 = \int_0^\infty \omega^2 U_{xx}(\omega)\, d\omega \qquad 2\text{-}17$$

## 2.6 Volterra Quadratic Model

Volterra Model is a system identification method generally used in signal processing techniques. Methods for analyzing ship responses in irregular seas were developed by Hasselman(1966) and Dalzell(1976) as discussed in Background.

## 2.7 Volterra Model in time domain

Volterra Model assumes that input is zero mean Gaussian process and the system consists of both linear and quadratic part. Depending on whether the system is linear or quadratic, response will also be linear or quadratic respectively. Volterra Model can be expressed in time domain as follows

$$y(t) = \int_{-\infty}^{\infty} g_1(\tau_1)x(t-\tau_1)d\tau + \int_{-\infty}^{\infty}\int_{-\infty}^{\infty} g_2(\tau_1,\tau_2)x(t-\tau_1)x(t-\tau_2)d\tau_1 d\tau_2 \qquad 2\text{-}18$$

$g_1$ ($\tau_1$) is the Linear Impulse Response (LIR) function at time t=$\tau_1$ and $g_2$ is quadratic Impulse response (QIR) function which is function of both $\tau_1$ & $\tau_2$. $g_2$ is time invariant since they are function of time lag $\tau_1$ and $\tau_2$ only.

Convolution of input wave with LIR gives the linear response and the convolution of a monochromatic input wave with another monochromatic input wave and QIR give quadratic response.

## 2.8 Volterra Liner Model in frequency domain

Using Fourier transforms Volterra Model can be expressed in frequency domain which makes it easier to handle.

If x(t) is input and g(t) is the impulse response due to unit impulse then total response can be written as

$$y(t) = x(t) \ * \ g(t) \qquad 2\text{-}19$$

if x(t)= δ(t) i.e. unit impulse input

then y(t)=g(t)

applying Fourier transform on the output

$$Y(\omega) = \int_{-\infty}^{\infty} y(t)e^{-i\omega t}dt = \int_{-\infty}^{\infty} g(t)e^{-i\omega t}dt \qquad 2\text{-}20$$

Similarly applying Fourier transform on the input

$$X(\omega) = \int_{-\infty}^{\infty} x(t)e^{-i\omega t}dt = \int_{-\infty}^{\infty} \delta(t)e^{-i\omega t}dt = 1 \qquad 2\text{-}21$$

Linear transfer function LTF can be defined as the ratio between output and input

$$LTF = G_1(\omega) = Y(\omega)/ X(\omega) \quad 2\text{-}22$$

Inverse Fourier transforming the LTF we will get IRF.

## 2.9 Relationship between linear response and LTF

A bi-frequency wave can written as sum of two sinusoidal waves

$$x(t) = a_1(\omega_1)\cos(\omega_1 t) + a_2(\omega_2)\cos(\omega_2 t) \quad 2\text{-}23$$

$$= \frac{a_1}{2}(\omega_1)(e^{i\omega_1 t} + e^{-i\omega_1 t}) + \frac{a_2}{2}(\omega_2)(e^{i\omega_2 t} + e^{-i\omega_2 t}) \quad 2\text{-}24$$

$$y_1(t) = \int_{-\infty}^{+\infty} g_1(t_1)x(t-t_1)dt$$

$$= \int_{-\infty}^{+\infty} g_1(t_1)\left[\frac{a_1}{2}\left(e^{i(\omega_1(t-t_1)} + e^{-i(\omega_1(t-t_1)}\right) + \frac{a_2}{2}\left(e^{i(\omega_2(t-t_2)} + e^{-i(\omega_2(t-t_2)}\right)\right]dt$$

$$= \int_{-\infty}^{+\infty} g_1(t_1)\left[\frac{a_1}{2}\left(e^{i\omega_1 t}e^{-i\omega_1 t_1} + e^{-i\omega_1 t}e^{i\omega_1 t_1}\right) + \frac{a_2}{2}\left(e^{i\omega_2 t}e^{-i\omega_2 t_2} + e^{-i\omega_2 t}e^{i\omega_2 t_2}\right)\right]dt$$

$$= \int_{-\infty}^{+\infty} g_1(t_1)\left[\frac{a_1}{2}e^{i\omega_1 t}e^{-i\omega_1 t_1}\right]dt + \int_{-\infty}^{+\infty} g_1(t_1)\left[\frac{a_1}{2}e^{-i\omega_1 t}e^{i\omega_1 t_1}\right]dt$$

$$+ \int_{-\infty}^{+\infty} g_1(t_1)\left[\frac{a_2}{2}e^{i\omega_2 t}e^{-i\omega_2 t_2}\right]dt + \int_{-\infty}^{+\infty} g_1(t_1)\left[\frac{a_2}{2}e^{-i\omega_2 t}e^{i\omega_2 t_2}\right]dt \quad 2\text{-}25$$

$$= \frac{a_1}{2}e^{i\omega_1 t}G_1(\omega_1) + \frac{a_1}{2}e^{-i\omega_1 t}G_1(-\omega_1) + \frac{a_2}{2}e^{-i\omega_2 t}G_2(-\omega_2) + \frac{a_2}{2}e^{i\omega_2 t}G_2(\omega_2)$$

$$y_1(t) = \mathrm{Re}\left(a_1 e^{i(\omega_1(t)} G_1(\omega_1) + a_2 e^{i(\omega_2(t)} G_2(\omega_2)\right) \quad \text{2-26}$$

## 2.10 Extraction of LTF from the cross and auto spectra

So far we saw the relationship between LTF and linear response. Now we've to employ a method to extract the LTF for the purpose of our study. We employed the commonly used spectra method for the calculation for which the derivation is given below.

Volterra model assumes that input is Gaussian. Auto correlation between the inputs and Cross correlation between the input and output can be written as

$$\begin{aligned} R_{xx}(\tau) &= E[x(t-\tau)x(t)] \\ R_{xy}(\tau) &= E[x(t-\tau)y(t)] \end{aligned} \quad \text{2-27}$$

From equation 2-18 we have the linear part of response as

$$y(t) = \int_{-\infty}^{\infty} g_1(\tau_1) x(t-\tau_1) d\tau_1 \quad \text{2-28}$$

$$\begin{aligned} R_{xy}(\tau) &= E[x(t-\tau)y(t)] = E[x(t-\tau)\int_{-\infty}^{\infty} g_1(\tau_1)x(t-\tau_1)d\tau_1] \\ &= \int_{-\infty}^{\infty} g_1(\tau_1) E[x(t-\tau_1)x(t-\tau)] d\tau_1 \\ &= \int_{-\infty}^{\infty} g_1(\tau_1) R_{xx}(\tau_1 - \tau)\, d\tau_1 \end{aligned} \quad \text{2-29}$$

Applying Fourier transform on both sides

$$S_{xy} = G_1(\omega) S_{xx} \quad \text{2-30}$$

Where $S_{xx}$ & $S_{xy}$ are the two sided auto and cross spectrum and can be calculated using either generally used Fourier transform method or Blackman-turkey maximum lag

method. This equation can also be written in terms of one sided cross ($U_{xy}$) and auto ($U_{xx}$) spectrum as follows

$$U_{xy} = G_1(\omega)U_{xx} \qquad 2\text{-}31$$

## 2.11 Volterra Quadratic Model in frequency domain

In the previous sections we considered monochromatic waves interacting with the system producing the linear response. But as the sea state increases these monochromatic waves of different frequencies interact with each other and give rise to non linear responses. When two frequencies interact with each other they produce a quadratic effect on the system e.g. slow drift motion of the vessel. For this particular study we need to employ Volterra Quadratic Model which is widely used in electrical engineering for signal processing.

Equation 2-18 gives the Volterra Quadratic model in time domain. Here we used Volterra model in frequency domain developed by Hasselman (1966) and Dalzell (1976) after some manipulation of the equation in time domain. Similar to equation 2-20 and 2-21, Quadratic Transfer Function (QTF) in frequency domain are derived from the Fourier transform of Quadratic Impulse Response Function (QIF) in time domain. On inverse Fourier transform we can get QIF from QTF.

$$G_2(\omega_1,\omega_2) = \int_{-\infty}^{\infty}\int_{-\infty}^{\infty} g_2(\tau_1,\tau_2)e^{-i\omega_1\tau_1 - i\omega_2\tau_2}\,d\tau_1 d\tau_2 \qquad 2\text{-}32$$

$$g_2(\tau_1,\tau_2) = g_2(\tau_2,\tau_1) \qquad 2\text{-}33$$

Where $g_2(\tau_1,\tau_2)$ is the QIF for the time lag $\tau_1$& $\tau_2$ and are assumed to be symmetrical in its arguments which can be shown as

$G_2(\omega_1,\omega_2)$ is the QTF when two waves of two frequencies $\omega_1$ & $\omega_2$ interact with each other.

Similar to QIF, QTF follows the symmetrical relationship in its domain $\omega_1$ & $\omega_2$ which can be shown as

$$\begin{aligned} G_2(\omega_1,\omega_2) &= G_2(\omega_2,\omega_1) \\ G_2^*(\omega_1,\omega_2) &= G_2(-\omega_1,-\omega_2) = G_2(-\omega_2,-\omega_1) \end{aligned} \qquad \text{2-33}$$

It is our objective to extract these frequency components from the given response and study the behavior. For a quadratic system we have

$$y_2(t) = \int_{-\infty}^{+\infty}\int_{-\infty}^{+\infty} g_2(t_1,t_2)x(t-t_1)x(t-t_2)dt_1dt_2 \qquad \text{2-34}$$

$$y_2 = \int_{-\infty}^{+\infty}\int_{-\infty}^{+\infty} g_2(t_1,t_2)\left\{\begin{bmatrix}\frac{a_1}{2}(e^{i(\omega_1(t-t_1)}+e^{-i(\omega_1(t-t_1)})+ \\ \frac{a_2}{2}(e^{i(\omega_2(t-t_1)}+e^{-i(\omega_2(t-t_1)})\end{bmatrix}\right\}dt_1dt_2 \qquad \text{2-35}$$
$$\left\{\begin{bmatrix}\frac{a_1}{2}(e^{i(\omega_1(t-t_2)}+e^{-i(\omega_1(t-t_2)})+ \\ \frac{a_2}{2}(e^{i(\omega_2(t-t_2)}+e^{-i(\omega_2(t-t_2)})\end{bmatrix}\right\}$$

$$y_2 = \int_{-\infty}^{+\infty}\int_{-\infty}^{+\infty} g_2(t_1,t_2)\left\{\begin{array}{l}\left[\begin{array}{l}\frac{a_1^2}{4}(e^{2i\omega_1 t}e^{-i\omega_1(t_1+t_2)})+\frac{a_1^2}{4}e^{-i\omega_1(t_1-t_2)}+\\ \frac{a_1a_2}{4}e^{i(\omega_1+\omega_2)t}e^{-i(\omega_1t_1+\omega_2t_2)}\\ +\frac{a_1a_2}{4}e^{i(\omega_1-\omega_2)t}e^{-i(\omega_1t_1-\omega_2t_2)})\end{array}\right]\\ +\left[\begin{array}{l}\frac{a_1^2}{4}e^{-i\omega_1(-t_1+t_2)}+\frac{a_1^2}{4}e^{-2i\omega_1 t}e^{-i\omega_1(t_1-t_2)}+\\ \frac{a_1a_2}{4}e^{i(-\omega_1+\omega_2)t}e^{-i(-\omega_1t_1+\omega_2t_2)}\\ +\frac{a_1a_2}{4}e^{i(-\omega_1-\omega_2)t}e^{-i(-\omega_1t_1-\omega_2t_2)})\end{array}\right]\\ +\left[\begin{array}{l}\frac{a_1a_2}{4}e^{i(\omega_1+\omega_2)t}e^{-i(\omega_2t_1+\omega_1t_2)}\\ +\frac{a_1a_2}{4}e^{i(-\omega_1+\omega_2)t}e^{-i(-\omega_1t_2+\omega_2t_1)}+\\ \frac{a_2^2}{4}e^{2i\omega_2 t}e^{-i\omega_2(t_1+t_2)}+\frac{a_2^2}{4}e^{-i\omega_2(t_1-t_2)})\end{array}\right]\\ +\left[\begin{array}{l}\frac{a_1a_2}{4}e^{i(\omega_1-\omega_2)t}e^{-i(\omega_1t_2-\omega_2t_1)}\\ +\frac{a_1a_2}{4}e^{i(-\omega_1-\omega_2)t}e^{-i(-\omega_1t_2-\omega_2t_1)}+\\ \frac{a_2^2}{4}e^{-i\omega_2(-t_1+t_2)}+\frac{a_2^2}{4}e^{-2i\omega_2 t}e^{-i\omega_2(-t_1-t_2)})\end{array}\right]\end{array}\right\}dt_1dt_2 \qquad 2\text{-}36$$

$$
y_2 = \left[\begin{array}{l}
\frac{a_1^2}{4} G_2(\omega_1,\omega_1) e^{2i\omega_1 t} + \frac{a_1^2}{4} G_2(\omega_1,-\omega_1) \\
+ \frac{a_1 a_2}{4} G_2(\omega_1,\omega_2) e^{i(\omega_1+\omega_2)t} + \frac{a_1 a_2}{4} e^{i(\omega_1-\omega_2)t} G_2(\omega_1,-\omega_2) \\
+ \frac{a_1^2}{4} G_2(-\omega_1,\omega_1) + \frac{a_1^2}{4} G_2(\omega_1,-\omega_1) e^{-2i\omega_1 t} \\
+ \frac{a_1 a_2}{4} G_2(-\omega_1,\omega_2) e^{i(-\omega_1+\omega_2)t} + \frac{a_1 a_2}{4} G_2(-\omega_1,-\omega_2) e^{i(-\omega_1-\omega_2)t} \\
+ \frac{a_1 a_2}{4} G_2(\omega_1,\omega_2) e^{i(\omega_1+\omega_2)t} + \frac{a_1 a_2}{4} G_2(-\omega_1,\omega_2) e^{i(-\omega_1+\omega_2)t} \\
+ \frac{a_2^2}{4} G_2(\omega_2,\omega_2) e^{2i\omega_2 t} + \frac{a_2^2}{4} G_2(\omega_2,-\omega_2) \\
+ \frac{a_1 a_2}{4} G_2(\omega_1,-\omega_2) e^{i(\omega_1-\omega_2)t} + \frac{a_1 a_2}{4} G_2(-\omega_1,-\omega_2) e^{i(-\omega_1-\omega_2)t} \\
+ \frac{a_2^2}{4} G_2(-\omega_2,\omega_2) + \frac{a_2^2}{4} G_2(-\omega_2,-\omega_2) e^{-2i\omega_2 t}
\end{array}\right] \qquad \text{2-37}
$$

using symmetry relations from equation (2.34) .

$$G_2(\omega_1,\omega_2) = G_2(\omega_2,\omega_1)$$
$$G_2^*(\omega_1,\omega_2) = G_2(-\omega_1,-\omega_2) = G_2(-\omega_2,-\omega_1)$$

$$y_2 = \begin{bmatrix} \mathrm{Re}\left(\frac{a_1^2}{2}G_2(\omega_1,\omega_1)e^{2i\omega_1 t}\right)+\frac{a_1^2}{2}G_2(\omega_1,-\omega_1)+ \\ \mathrm{Re}\left(a_1a_2G_2(\omega_1,\omega_2)e^{i(\omega_1+\omega_2)t}\right)+\mathrm{Re}\left(a_1a_2G_2(\omega_1,-\omega_2)e^{i(\omega_1-\omega_2)t}\right)+ \\ \mathrm{Re}\left(\frac{a_2^2}{2}G_2(\omega_2,\omega_2)e^{2i\omega_2 t}\right)+\frac{a_2^2}{2}G_2(\omega_2,-\omega_2) \end{bmatrix} \quad \text{2-38}$$

$$y_2 = \begin{bmatrix} \overbrace{\mathrm{Re}\left(\frac{a_1^2}{2}G_2(\omega_1,\omega_1)e^{2i\omega_1 t}\right)+\mathrm{Re}\left(\frac{a_2^2}{2}G_2(\omega_2,\omega_2)e^{2i\omega_2 t}\right)}^{\text{double frequency}} \\ +\overbrace{\mathrm{Re}\left(a_1a_2G_2(\omega_1,\omega_2)e^{i(\omega_1+\omega_2)t}\right)}^{\text{sum frequency}}+\overbrace{\mathrm{Re}\left(a_1a_2G_2(\omega_1,-\omega_2)e^{i(\omega_1-\omega_2)t}\right)}^{\text{difference frequency}} \\ +\left(\overbrace{\frac{a_1^2}{2}G_2(\omega_1,-\omega_1)+\frac{a_2^2}{2}G_2(\omega_2,-\omega_2)}^{\text{mean}}\right) \end{bmatrix} \quad \text{2-39}$$

Total response (y) can be written as a sum of linear response ($y_1$) and quadratic response ($y_2$).

$$y = y_1 + y_2 = \left[ \begin{array}{l} \overbrace{\mathrm{Re}\left( a_1 e^{i(\omega_1(t)} G_1(\omega_1) + a_2 e^{i(\omega_2(t)} G_2(\omega_2) \right)}^{\text{Linear frequency}} + \overbrace{\mathrm{Re}\left( \frac{a_1^2}{2} G_2(\omega_1,\omega_1) e^{2i\omega_1 t} \right) + \left( \frac{a_2^2}{2} G_2(\omega_2,\omega_2) e^{2i\omega_2 t} \right)}^{\text{double frequency}} \\ + \overbrace{\mathrm{Re}\left( a_1 a_2 G_2(\omega_1,\omega_2) e^{i(\omega_1+\omega_2)t} \right)}^{\text{sum frequency}} + \overbrace{\mathrm{Re}\left( a_1 a_2 G_2(\omega_1,-\omega_2) e^{i(\omega_1-\omega_2)t} \right)}^{\text{difference frequency}} \\ + \left( \overbrace{\frac{a_1^2}{2} G_2(\omega_1,-\omega_1) + \frac{a_2^2}{2} G_2(\omega_2,-\omega_2)}^{\text{mean}} \right) \end{array} \right] \qquad 2\text{-}40$$

This relation is well expressed through the following diagram. Here frequencies $\omega_1$ & $\omega_2$ plotted on the x and y axes are interacting with each other in their particular domain.

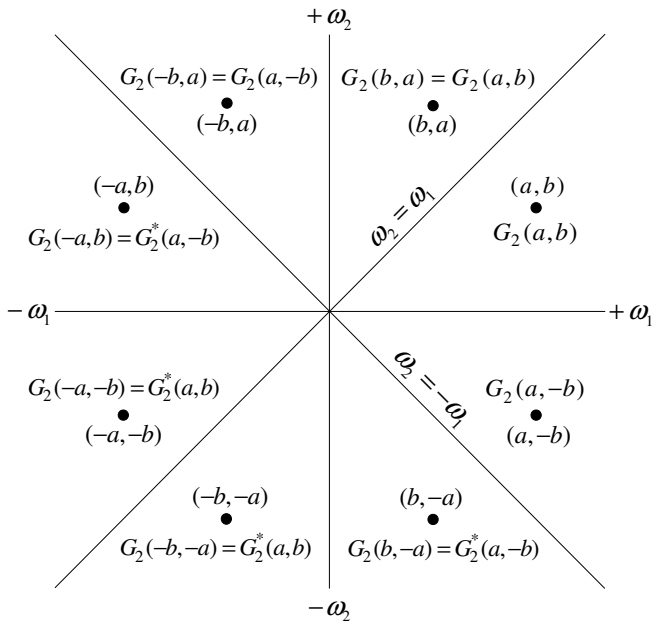


Figure 2-1 Diagram showing the symmetry of quadratic transfer functions

Diagonal lines passing through each quadrant result from the interaction of frequencies of same absolute value. Diagonal in the first quadrant results from the interaction of positive $\omega_1$ & $\omega_2$ which is equivalent to double frequency responses. Diagonal on the fourth quadrant which results from the interaction of $\omega_1$ & $-\omega_2$ gives rise to zero frequency response. The major axis and diagonals divide the diagram into octants where we can apply the symmetry. Applying equation 2-27 we can limit our area of study to the quadrant between the axis $\omega_1 = \omega_2$ & $\omega_1 = |-\omega_2|$ which is better explained from the below diagram

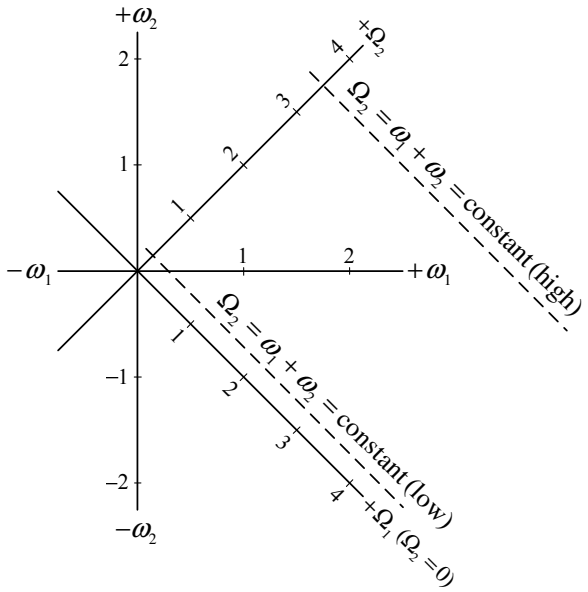


Figure 2-2 Transformation of axis from $\omega_1, \omega_2$ to $\Omega_1, \Omega_2$

Here $\Omega_1$ & $\Omega_2$ are the zero and double frequency axis as discussed earlier. The domain between $\Omega_1$ & $\omega_1$ represent the difference frequency components of the response while

domain between $\Omega_2$ & $\omega_1$ represent the sum frequency component. Therefore bichromatic wave interaction give rise to six different frequency component i.e two individual frequency part or the linear part, mean frequency or zero frequency component, double frequency component, difference frequency and sum frequency parts.

## 2.12 Extraction of QTF from cross bi spectra

In the case of linear response we saw cross correlation of the input wave with response. Here as we are talking about second order effect, wave-wave interaction and their respective responses becomes important. Like cross correlation of wave-response here we will make use of third moment which is correlation between wave-wave-response.

$$M_{xxy}(\tau_1,\tau_2) = E[x(t+\tau_2)x(t+\tau_1)(y(t)-E[y(t)])] \quad \text{2-41}$$

Tick (1961) showed that double Fourier transform of the third moment gives cross bi spectrum

$$CBS(\omega_1,\omega_2) = \frac{1}{(2\pi)^2}\int_{-\infty}^{\infty}\int_{-\infty}^{\infty} e^{-i(\tau_1\omega_1+\tau_2\omega_2)} M_{xxy}(\tau_1,\tau_2)d\tau_1 d\tau_2 \quad \text{2-42}$$

Dalzell (1972) rearranged the equation with a new starting point by defining third moment as

$$M_{xxy}(\tau_1,\tau_2) = E[x(t+\tau_1)x(t-\tau_1)(y(t-\tau_2)-E[y(t-\tau_2)])] \quad \text{2-43}$$

Since output is assumed to be Gaussian $E[y(t-\tau_2)] = 0$

From equation 2-18 we know that

$$y(t)=\int_{-\infty}^{+\infty} g_1(t_1)x(t-t_1)dt_1+\int_{-\infty}^{+\infty}\int_{-\infty}^{+\infty} g_2(t_1,t_2)x(t-t_1)x(t-t_2)dt_1dt_2$$

$$y(t-\tau_2)=\int_{-\infty}^{+\infty} g_1(t_1)x(t-t_1-\tau_2)dt_1+\int_{-\infty}^{+\infty}\int_{-\infty}^{+\infty} g_2(t_1,t_2)x(t-t_1-\tau_2)x(t-t_2-\tau_2)dt_1dt_2$$

$$\begin{aligned}y(t-\tau_2)-E\left[y(t-\tau_2)\right]=&\int_{-\infty}^{+\infty} g_1(t_1)x(t-t_1-\tau_2)dt_1+\int_{-\infty}^{+\infty}\int_{-\infty}^{+\infty} g_2(t_1,t_2)x(t-t_1-\tau_2)x(t-t_2-\tau_2)dt_1dt_2\\&-\int_{-\infty}^{+\infty} g_1(t_1)E\left[x(t-t_1-\tau_2)\right]dt_1+\int_{-\infty}^{+\infty}\int_{-\infty}^{+\infty} g_2(t_1,t_2)E\left[x(t-t_1-\tau_2)x(t-t_2-\tau_2)\right]dt_1dt_2\end{aligned}$$

2-44

For a Gaussian input

$$E\left[x(t-t_1-\tau_2)\right]=0$$

$$\begin{aligned}y(t-\tau_2)-E\left[y(t-\tau_2)\right]=&\int_{-\infty}^{+\infty} g_1(t_1)x(t-t_1-\tau_2)dt_1+\int_{-\infty}^{+\infty}\int_{-\infty}^{+\infty} g_2(t_1,t_2)x(t-t_1-\tau_2)x(t-t_2-\tau_2)dt_1dt_2\\&+\int_{-\infty}^{+\infty}\int_{-\infty}^{+\infty} g_2(t_1,t_2)E\left[x(t-t_1-\tau_2)x(t-t_2-\tau_2)\right]dt_1dt_2\end{aligned}$$

$$\begin{aligned}=&\int_{-\infty}^{+\infty} g_1(t_1)x(t-t_1-\tau_2)dt_1+\int_{-\infty}^{+\infty}\int_{-\infty}^{+\infty} g_2(t_1,t_2)x(t-t_1-\tau_2)x(t-t_2-\tau_2)dt_1dt_2\\&+\int_{-\infty}^{+\infty}\int_{-\infty}^{+\infty} g_2(t_1,t_2)R_{xx}(t_1-t_2)dt_1dt_2\end{aligned}$$

2-45

$$y(t-\tau_2)-E\left[y(t-\tau_2)\right]=\int_{-\infty}^{+\infty} g_1(t_1)x(t-t_1-\tau_2)dt_1+\int_{-\infty}^{+\infty}\int_{-\infty}^{+\infty} g_2(t_1,t_2)\left[x(t-t_1-\tau_2)x(t-t_2-\tau_2)-R_{xx}(t_1-t_2)\right]dt_1dt_2$$

2-46

From equation 2-44

$$M_{xxy}(\tau_1,\tau_2)=E[x(t+\tau_1)x(t-\tau_1)(y(t-\tau_2)-E[y(t-\tau_2)])]$$

$$M_{xxy}(\tau_1,\tau_2)=\int_{-\infty}^{+\infty} g_1(t_1)E\left[x(t+\tau_1)x(t-\tau_1)x(t-t_1-\tau_2)\right]dt_1$$
$$+\int_{-\infty}^{+\infty}\int_{-\infty}^{+\infty} g_2(t_1,t_2)E\left[x(t+\tau_1)x(t-\tau_1)x(t-t_1-\tau_2)x(t-t_2-\tau_2)-x(t+\tau_1)x(t-\tau_1)R_{xx}(t_1-t_2)\right]dt_1dt_2 \quad \text{2-47}$$

Since temporal average of triple product is zero, first term of the equation becomes zero.

Using the property

$$E\left[x(t_1)x(t_2)x(t_3)x(t_4)\right]=R_{xx}(t_2-t_1)R_{xx}(t_4-t_3)+R_{xx}(t_3-t_1)R_{xx}(t_4-t_2)+R_{xx}(t_4-t_1)R_{xx}(t_3-t_2)$$

$$M_{xxy}(\tau_1,\tau_2)=\int_{-\infty}^{+\infty}\int_{-\infty}^{+\infty} g_2(t_1,t_2)\begin{pmatrix}R_{xx}(2\tau_1)R_{xx}(t_1-t_2)+R_{xx}(-\tau_1-\tau_2-t_1)R_{xx}(\tau_1-\tau_2-t_2)\\ +R_{xx}(-\tau_1-\tau_2-t_2)R_{xx}(\tau_1-\tau_2-t_1)-R_{xx}(-2\tau_1)Rxx(t_1-t_2)\end{pmatrix}dt_1dt_2 \quad \text{2-48}$$

Since auto correlation is an even function we can rewrite the equation as

$$M_{xxy}(\tau_1,\tau_2)=\int_{-\infty}^{+\infty}\int_{-\infty}^{+\infty} g_2(t_1,t_2)\begin{pmatrix}R_{xx}(2\tau_1)R_{xx}(t_1-t_2)+R_{xx}(\tau_1+\tau_2+t_1)R_{xx}(\tau_1-\tau_2-t_2)\\ +R_{xx}(\tau_1+\tau_2+t_2)R_{xx}(\tau_1-\tau_2-t_1)-R_{xx}(2\tau_1)Rxx(t_1-t_2)\end{pmatrix}dt_1dt_2 \quad \text{2-49}$$

$$M_{xxy}(\tau_1,\tau_2)=\int_{-\infty}^{+\infty}\int_{-\infty}^{+\infty} g_2(t_1,t_2)\begin{pmatrix}R_{xx}(2\tau_1)R_{xx}(t_1-t_2)+R_{xx}(\tau_1+\tau_2+t_1)R_{xx}(\tau_1-\tau_2-t_2)\\ +R_{xx}(\tau_1+\tau_2+t_2)R_{xx}(\tau_1-\tau_2-t_1)-R_{xx}(2\tau_1)Rxx(t_1-t_2)\end{pmatrix}dt_1dt_2$$

Since $g_2(t_1,t_2)$ is symmetric and the integration limits in between the infinity the terms inside the square bracket are same

$$M_{xxy}(\tau_1,\tau_2)=2\int_{-\infty}^{+\infty}\int_{-\infty}^{+\infty} g_2(t_1,t_2)\left(R_{xx}(\tau_1+\tau_2+t_1)R_{xx}(\tau_1-\tau_2-t_2)\right)dt_1dt_2 \quad \text{2-50}$$

According to Parseval's formula used by Barret (1963)

$$\iiint \ldots \iint f_1(t_1,t_2,\ldots,t_n) f_2(t_1,t_2,\ldots,t_n) dt_1 dt_2 \ldots dt_n$$
$$= \frac{1}{(2\pi)^n} \iiint \ldots \iint F_1^*(\omega_1,\omega_2,\ldots,\omega_n) F_2(\omega_1,\omega_2,\ldots,\omega_n) d\omega_1 d\omega_2 \ldots d\omega_n \quad 2\text{-}51$$

Where * represent the complex conjugate and $f_1$, $F_1$ are the Fourier transform pairs defined as follows

$$F_n(\omega_1,\omega_2,\ldots\omega_n) = \iint f_n(t_1,t_2\ldots t_n) \exp\left(-i\sum_1^n \omega_n t_n\right) dt_1 dt_2 \ldots dt_n$$
$$f_n(t_1,t_2,\ldots t_n) = \iint F_n(\omega_1,\omega_2\ldots\omega_n) \exp\left(i\sum_{n=1}^n \omega_n t_n\right) d\omega_1 d\omega_2 \ldots d\omega_n \quad 2\text{-}52$$

Here $F_1(\omega_1,\omega_2) = G_2(\omega_1,\omega_2)$, $f_1(t_1,t_2) = g_2(t_1,t_2)$, $f_2(t_1,t_2) = R_{xx}(\tau_1+\tau_2+t_1) R_{xx}(\tau_1-\tau_2-t_2)$

$$F_2(\omega_1,\omega_2) = \int_{-\infty}^{+\infty}\int_{-\infty}^{+\infty} \left( R_{xx}(\tau_1+\tau_2+t_1) R_{xx}(\tau_1-\tau_2-t_2) \exp\left(-i\sum_{n=1}^{n=2} \omega_n t_n\right) dt_1 dt_2 \right) \quad 2\text{-}53$$

$$F_2(\omega_1,\omega_2) = \int_{-\infty}^{+\infty}\int_{-\infty}^{+\infty} \begin{pmatrix} R_{xx}(\tau_1+\tau_2+t_1) \mathrm{e}^{-i\omega_1(\tau_1+\tau_2+t_1)} \mathrm{e}^{i\omega_1(\tau_1+\tau_2)} dt_1 \\ \\ R_{xx}(t_2+\tau_2-\tau_1) \mathrm{e}^{-i\omega_2(t_2+\tau_2-\tau_1)} \mathrm{e}^{i\omega_2(\tau_2-\tau_1)} dt_2 \end{pmatrix} \quad 2\text{-}54$$

$$F_2(\omega_1,\omega_2) = S_{xx}(\omega_1) S_{xx}(\omega_2) \mathrm{e}^{i(\tau_1(\omega_1-\omega_2)+\tau_2(\omega_1+\omega_2))}$$

$$M_{xxy}(\tau_1,\tau_2) = \frac{2}{(2\pi)^2} \int_{-\infty}^{+\infty}\int_{-\infty}^{+\infty} \left( G_2^*(\omega_1,\omega_2) S_{xx}(\omega_1) S_{xx}(\omega_2) \mathrm{e}^{i(\tau_1(\omega_1-\omega_2)+\tau_2(\omega_1+\omega_2))} d\omega_1 d\omega_2 \right) \quad 2\text{-}55$$

For an easy understanding of the problem the axis is transformed from $(\omega_1,\omega_2)$ to $(\Omega_1,\Omega_2)$ as discussed above. Applying Jacobian coordinate transform $d\omega_1 d\omega_2 = \frac{1}{2} d\Omega_1 d\Omega_2$ to the differential area, equation 2-56 becomes

$$M_{xxy}(\tau_1,\tau_2) = \frac{1}{(2\pi)^2} \int_{-\infty}^{+\infty}\int_{-\infty}^{+\infty} \left( G_2^*(\frac{\Omega_1+\Omega_2}{2}, \frac{\Omega_2-\Omega_1}{2}) S_{xx}(\frac{\Omega_1+\Omega_2}{2}) S_{xx}(\frac{\Omega_2-\Omega_1}{2}) \mathrm{e}^{i\left(\tau_1\Omega_1+\tau_2\Omega_2\right)} d\Omega_1 d\Omega_2 \right) \quad 2\text{-}56$$

By modifying the equation 2-43 & 2-44 it can be seen that cross bi spectrum is the

double fourier transform of third moment

$$CBS(\omega_1,\omega_2)=\int_{-\infty}^{\infty}\int_{-\infty}^{\infty}e^{-i(\tau_1\omega_1+\tau_2\omega_2)}M_{xxy}(\tau_1,\tau_2)d\tau_1 d\tau_2 \qquad 2\text{-}57$$

On inverse Fourier transforming we'll have

$$M_{xxy}(\tau_1,\tau_2)=\frac{1}{(2\pi)^2}\int_{-\infty}^{\infty}\int_{-\infty}^{\infty}e^{-i(\tau_1\Omega_1+\tau_2\Omega_2)}CBS(\Omega_1,\Omega_2)d\tau_1 d\tau_2 \qquad 2\text{-}58$$

Comparing equation (2.56) & (2.58)

$$G_2^*(\frac{\Omega_1+\Omega_2}{2},\frac{\Omega_2-\Omega_1}{2})=\frac{CBS(\Omega_1,\Omega_2)}{S_{xx}(\frac{\Omega_1+\Omega_2}{2})S_{xx}(\frac{\Omega_2-\Omega_1}{2})} \qquad 2\text{-}59$$

Rewriting the equation

$$G_2^*(\omega_1,\omega_2)=\frac{CBS(\omega_1-\omega_2,\omega_1+\omega_2)}{S_{xx}(\omega_1)S_{xx}(\omega_2)},\qquad -\infty\le\omega_1,\omega_2\le+\infty \qquad 2\text{-}60$$

It was seen that at the tails of auto spectrum $S_{xx}(\omega_1),S_{xx}(\omega_2)$ where the values are really small causes abnormally high values in $G_2^*(\omega_1,\omega_2)$. In order to avoid the uncertainty in the estimation, Kim and Kim (2004) proposed a nominal rule to take the spectral densities at the tails to be 10% of the peak energy spectral density. This is shown in the following diagram Figure 2-3.

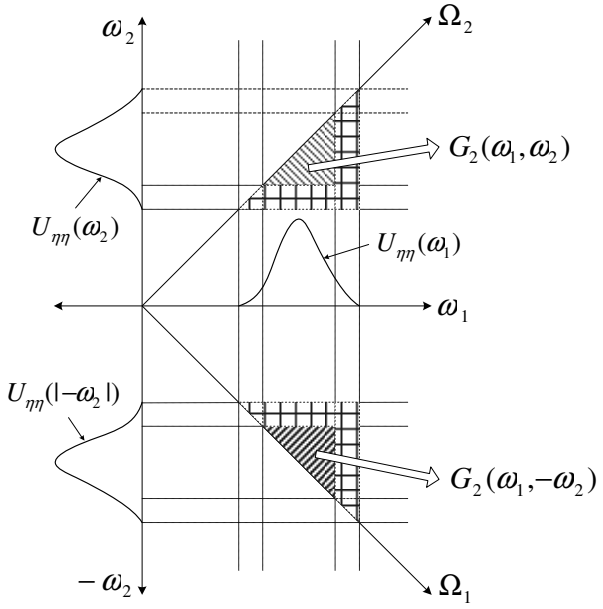


Figure 2-3 Selection of values greater than 10% of peak energy density spectrum

## 2.13 Algorithm for calculation of cross-bi spectrum

Algorithm for cross bi spectrum was developed by applying Blackman-Turkey method in two dimensionsal way. Dalzell(1974) referred to shaman(1963) for the calculation of the algorithm using hamming window with Blackman-Turkey method.

$$\hat{\hat{C}}(\Omega_1,\Omega_2)=\left(\frac{\Delta t}{e_1+e_2}\right)^2\sum_{j=0}^{m}\left\{\begin{array}{l} r(j)(e_1+e_2\cos\pi j/m)\cos(\pi P_1 j/m)\cdot \\ \sum_{k=-n}^{n}\left[\begin{array}{l}(e_1+e_2\cos\pi k/n)\cdot \\ [\cos(\pi P_2 k/n)+i\sin(\pi P_2 k/n)]\cdot \\ \frac{1}{N_S}\sum_{N}x(N+j)x(N-j)y(N+k)\end{array}\right]\end{array}\right\} \qquad 2\text{-}61$$

where $\hat{\hat{C}}$ = estimate of cross-bi spectrum

$\Omega_1=\pi P_1/m\Delta t$ , $\Omega_2=\pi P_2/n\Delta t$ ,

$m$ = maximum lags in the difference frequency ($\Omega_1$)

$n$ = sum frequency direction ($\Omega_2$).

Maximum lag was calculated using the equation given by Kinsman (1965, pp.449)

$$df = 2\left(\frac{N}{m} - \frac{1}{4}\right) \qquad 2\text{-}62$$

Where $df$ is the degree of freedom and a nominal value of 50 to 60 not exceeding 100 is taken as per Kinsman.

N= number of datas

$e_1$ = 0.54 and $e_2$ = 0.46 with a discrete version of the scalar spectrum lag window (Hamming window);

r( j) = 1 for j = 0 and r( j) = 2 for otherwise;

$x(N)$ = the input time series corrected to zero sample mean;

$y(N)$ = the output time series;

$N_s$ = the number of possible products summed;

$\Delta t$ = sampling interval used

## 2.14 Reconstruction test

So far we discussed the methods to extract QTF from the given response and input waves. It was necessary to check the accuracy of these methods used for the calculation of QTFs. This was carried out by conducting the reconstruction test in which the response time series were reconstructed using corresponding QTFs and input waves and were compared with original response time series. Reconstruction test was done using equation 2-41 which can be written in a concise form as shown below

$$y(t) = y_1(t) + y_2(t)$$
$$= \mathrm{Re}\sum_{m=1}^{N} A_m G_1(\omega_m) e^{i(\omega_m t - \varepsilon_m)} + \frac{1}{2}\mathrm{Re}\sum_{j=1}^{N}\sum_{k=1}^{N} A_j A_k G_2^{\pm}(\omega_j, \omega_k) e^{i[(\omega_j \pm \omega_k)t - (\varepsilon_j \pm \varepsilon_k)]} \quad \text{2-63}$$

Nomenclature of the above equation is same as discussed in the previous section i.e. *y(t)* is the total response, $y_1(t)$ is the linear response and $y_2(t)$ is the second order response. $G_1(\omega_m)$ is LTFs calculated as per Volterra linear model with N observed data points . $G_1(\omega_j,\omega_k)$ is QTFs calculated for a combination of frequency $\omega_j$ and $\omega_k$ . $A_j$, $A_k$ and $\varepsilon_j$, $\varepsilon_k$ are amplitudes and phase angles at $\omega_j$ and $\omega_k$ respectively. The reconstructed response series was compared with measured response and the correctness of the method was checked and this is better explained through the below diagram

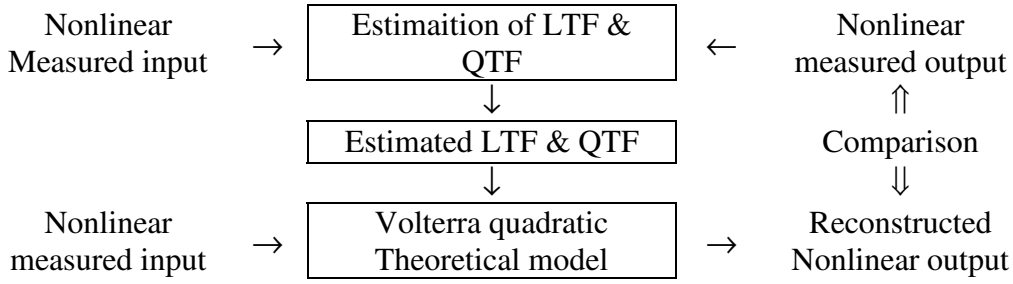


Figure 2-4 Schematic diagram showing the reconstruction of response

## 2.15 Comparison of energy spectrum of the reconstructed and measured response

Energy spectrum of the reconstructed response time series was calculated using conventional Fourier transform method and was compared with energy spectrum of the measured response. This approach was a useful eye check for understanding the contribution of first and second order response to the total response. This also helped to check the presence of any higher order term in the measured response.

## 2.16 Coherency test

Bendat (1990) defined coherency of first and second order response by the following equation

$$\gamma_{xy}^2(\omega) = \frac{U_{y1y1}(\omega)}{U_{yy}(\omega)} \quad \text{2-64}$$

$$q_{xy}^2(\omega) = \frac{U_{y2y2}(\omega)}{U_{yy}(\omega)} \quad \text{2-65}$$

Where the suffixes $y_1$, $y_2$ represent the reconstructed linear and quadratic output, respectively while $y$ is the measured response. $\gamma^2$ and $q^2$ represent the linear and quadratic coherence functions respectively . $U_{y1y1}$, $U_{y2y2}$ indicates one sided spectra of linear and second order response. The sum of the coherency function should lie between 0 and 1. A goodness-of-fit measure for the validity of the quadratic nonlinear model can be found by seeing how close the sum of these linear and quadratic coherence functions is to unity (Bendat, 1990). This helps in to check the presence of any higher order term in the response.

# CHAPTER III

# EXPERIMENTAL SETUP

## 3.1 Experimental study of ITTC model at TAMU

It is our research plan to do a model study to reconfirm the results by Dalzell and Cummins. The experiment will be for measurement of the vertical response of a moored ITTC container ship S175 in head seas of varying severity. The analyses will involve estimates of LTFs based on Linear Volterra model and the results will be compared with linear theory. It is expected that the estimated vertical responses will decrease as the sea severity increases and linear theory will over estimate the experimental result.

Afore mentioned ITTC model was tested in the four varying irregular seas by Prof. Sun Hong Kwon at Pusan National University, whose data were transferred to Texas A & M University for carrying out an in-depth analysis. The model was moored by four soft lines at the head seas. The vertical motions were carefully measured using a specially designed conducts. The model was installed as shown in the below Figure 3-1.

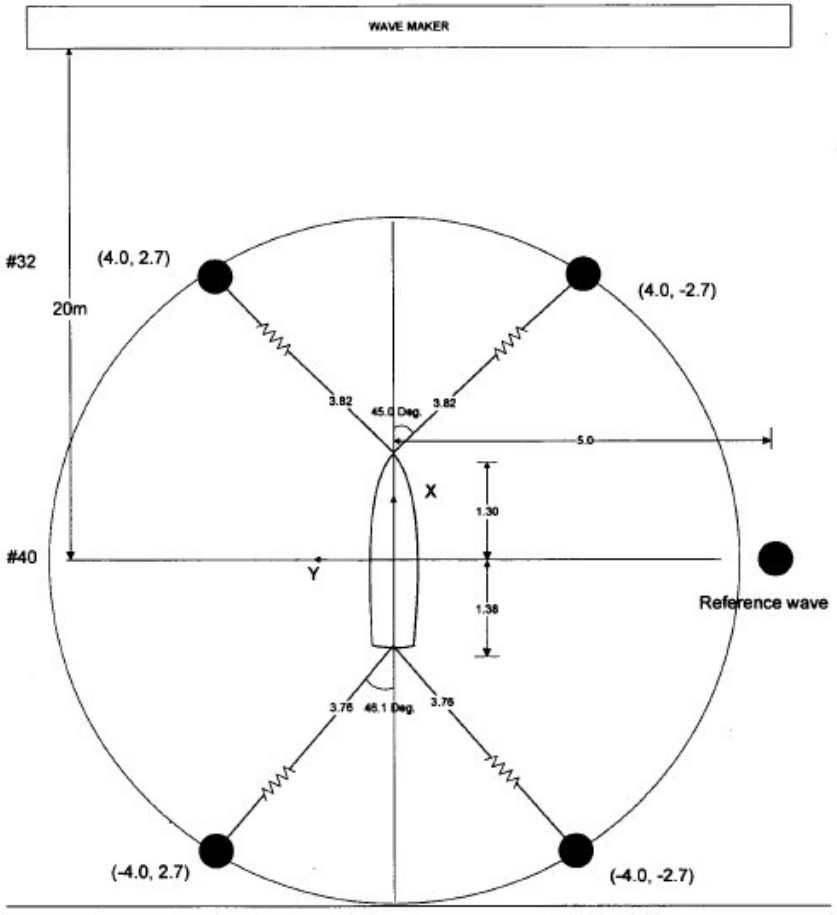


Figure 3-1 View of the model installing area

## 3.2 Data of ship hull

The body plan (transferred data) shows 20 stations with two half stations at either ends. The ship principal particulars are as given in Table 3-1. The stations marked on the hull in the model were used for measuring the vertical motion including relative motions.

Table 3-1 Principal particulars

| Designation | Unit | Ship |
|---|---|---|
| Scale | - | 70.0 |
| Length between perpendicular | M | 175.0 |
| Breath moulded | M | 25.4 |
| Draft mean | M | 9.5 |
| Displacement | $m^3$ | 24119 |
| Wetted surface area | $m^2$ | 5500 |
| Block coefficient | - | 0.5717 |
| Waterplane area coefficient | - | 0.7108 |
| Longitudinal center of gravity (AFT from Midship) | M | 2.48 |
| Vertical Center of Gravity (above Base Line) | M | 9.52 |
| Transverse Metacentric Height | M | 1.0 |
| Radii of Gyration. Pitch and Yaw | M | 202 |
| Radius of Gyration Roll | M | 42 |
| Roll Natural Period | - | 0.382B |
| | Sec | 18.28 |

Table 3.1. Principal particulars continued

| Designation | Unit | Ship |
|---|---|---|
| Propeller | | KP452 |
| Diameter | M | 6.5 |
| Number of blades | | 5 |
| Pitch | M | 6.875 |
| Pitch Ratio | - | 1.055 |
| Expanded Area Ratio | - | 0.73 |
| Hub ratio | - | 0.1846 |
| | - | 0.1846 |
| Appendage | | |
| Rudder | | NACA0018 |
| Bilge Keel | | |
| Length | | 0.25L |
| Maximum breadth | M | 0.45 |

## 3.3 Heave resonance frequency

The heave resonance frequency of the ITTC ship is estimated approximately 0.801 rad/sec (period 7.84 sec) by using an approximate formula given below.

Assuming that damping is negligible and ship's mass is approximately equal to its heaving added mass one may have an approximate natural frequency

$$\omega_3 = \sqrt{(\rho g A_{wp} / 2M_s)}$$

3.4 Particulars of the waves

The current study employed the KRISO data (Korea research institute of ships and ocean engineering). KRISO waves were generated using target spectra ITTC and JONSWAP spectra in the year 2000. The particulars of the waves of varying sea severity are given in Table 3-2, where Hs denotes significant wave height, Tp denotes modal or peak period and gamma represents the peakedness of the spectra. It can be seen from Table 2-1 that first two sea states (Hs=4.5m & 6.5m) belong to very rough and high seas classification respectively while the last two sea states of Hs=10.0m & 12.2m belong to very high seas.

Table 3-2 Particulars of KRISO waves (2000)

| **Data No.** | **Proto** | | **Model** | | **γ** | **Remarks** |
|---|---|---|---|---|---|---|
| | Hs(m) | **Tp** | **Hs(m)** | **Tp** | | |
| #1 | 4.5 | 11.26 | 0.064 | 1.519 | 1.0 | ITTC |
| #2 | 6.5 | 12.09 | 0.092 | 1.630 | 1.5 | JONSWAP |
| #3 | 10.0 | 12.73 | 0.143 | 1.717 | 2.5 | JONSWAP |
| #4 | 12.2 | 13.37 | 0.174 | 1.803 | 2.5 | JONSWAP |

In dealing with the wave, Froude similitude law is applied:

$$Fn = V / \sqrt{gL} \qquad 3\text{-}1$$

Where V and L are the characteristic velocity and length of the ship and g is gravity constant

$$Hs_{\mathrm{mod}\,el} / Hs_{prototype} = \lambda \qquad 3\text{-}2$$

$$Tp_{\mathrm{mod}\,el} / Tp_{prototype} = \lambda^{1/2} \qquad 3\text{-}3$$

Where $\lambda$ is length scale factor.

## 3.5 Measured wave time series

The input waves were generated using the target spectra as defined in the particulars of the KRISO waves in Table 3-2. The wave time series are shown in Figure 3-2 to Figure 3-5. This input data causes the response motions of the structure. Thus it is important to investigate the qualities and severities of the waves. Firstly we examined the qualities of the generated waves with the measured target spectra and then examined the nonlinearities (sea severity) by applying the probability of exceedence of the crest height.

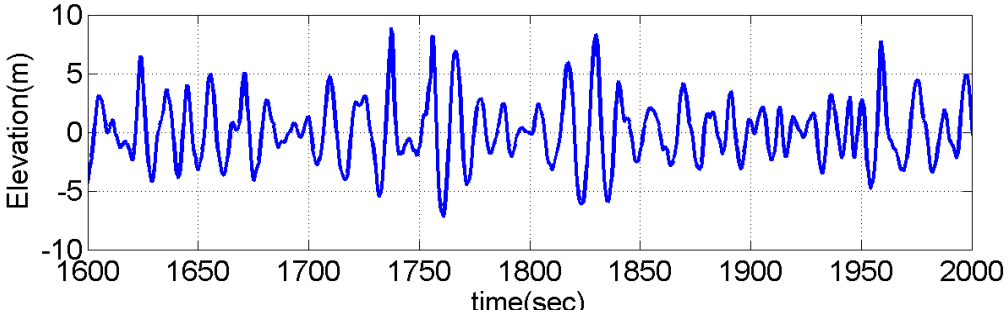


Figure 3-2 Input wave time series Hs=4.5m

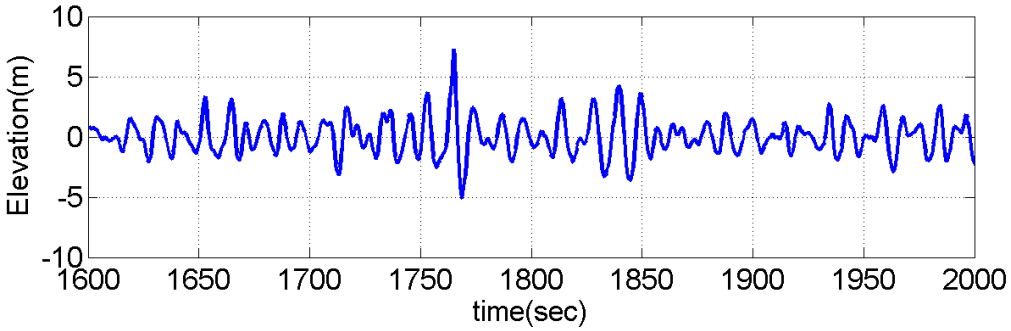


Figure 3-3 Input wave time series Hs=6.5m

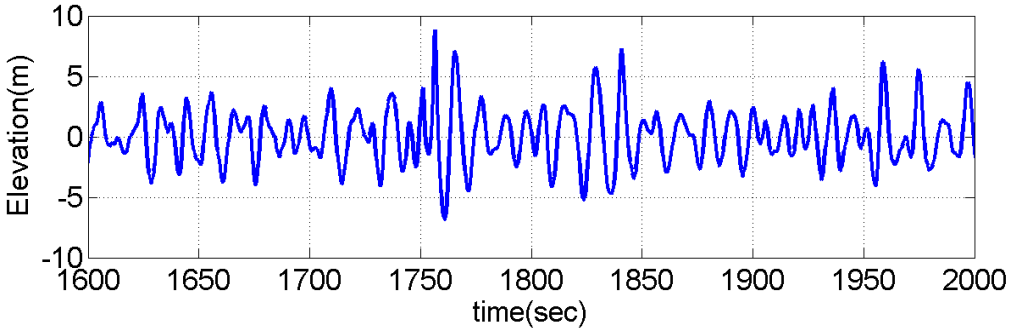


Figure 3-4 Input wave time series Hs=10.0m

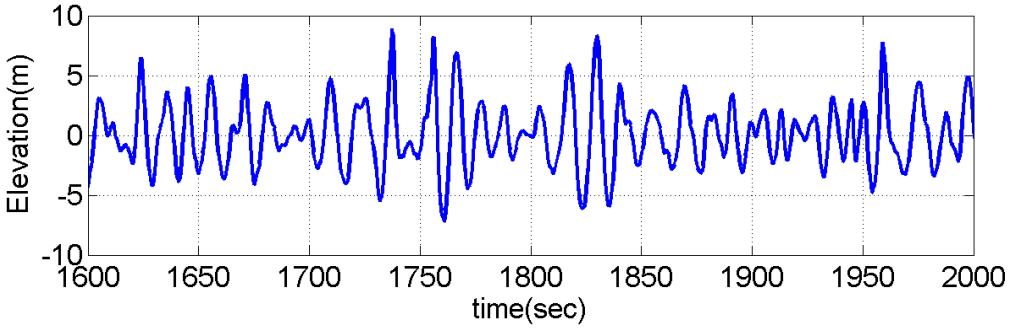


Figure 3-5 Input wave time series Hs=12.2m

## 3.6 Statistics of waves

As a preliminary investigation, statistics of the waves were studied by calculating the mean, variance, skewness and kurtosis values as given table below.

Table 3-3 Statistics of wave motion for different sea state

| | Hs=4.5m | Hs=6.5m | Hs=10.0m | Hs=12.2m |
|---|---|---|---|---|
| Mean | 9.57 x 10^-017 | -6.75 x 10^-017 | 8.04 x 10^-017 | -3.41e-017 |
| Std deviation | 1.5296 | 2.3609 | 3.7953 | 4.6404 |
| Skewness | 0.1001 | 0.2527 | 0.2743 | 0.2955 |
| Kurtosis | 3.2070 | 3.3969 | 3.4180 | 3.2420 |

Mean values were found to be negligible. Skewness value indicates the asymmetry in the distribution of crests and troughs about mean value. Skewness increases as sea state increases indicating increase in nonlinearity for higher seas. It was seen from Table 3-3 that skewness values increases rapidly from Hs=4.5m to Hs=6.5m after which it increase gradually through higher sea states. Kurtosis value is zero for Gaussian distribution. Kurtosis value greater than 3 shows that the wave peakedness is higher than Gaussian distributed waves i.e. there more chance of bigger waves compared to normally distributed linear waves. Non linearity was cross checked by comparing the peaks with Rayleigh distributed peaks in the following section.

## 3.7 Comparison of measured and target spectrum

The time series above represent wave elevations in proto scale, which are subjected to FFT transform and smoothened to get the smooth energy density spectra. Thus we have measured and target spectrums for each sea as shown in Fig. 3.6. It was observed that visually both spectra match very well. However, the foregoing observation

is an eye-view approach. Thus, we need to take account of it in the statistical terms. The variation in the variances between the measured and target spectrum for each sea is computed. Comparison of the variance shows the error to be less than 10% error, which is generally accepted criteria, as shown in Table 3-4. This indicates that the qualities of the measured waves are acceptable.

Input wave frequency range generally lies in between 0.35 to 1.5 for all the waves. It was observed that waves created in wave tank using target spectrum are non linear in high seas. This was verified from the following results where probability of exceedence for the wave crest height was compared with Rayleigh distributed curve.

Table 3-4 Comparison of variance between measured vs target spectrum

| Prototype | Hs | Measured spectrum Variance | Target spectrum Variance | % error |
|---|---|---|---|---|
| Wave no 1 | 4.5m | 0.7077 | 0.7647 | 7.45 |
| Wave no 2 | 6.5m | 1.6861 | 1.8346 | 8.09 |
| Wave no 3 | 10.0m | 4.3572 | 4.1063 | 6.11 |
| Wave no 4 | 12.2m | 6.5139 | 7.075 | 7.93 |

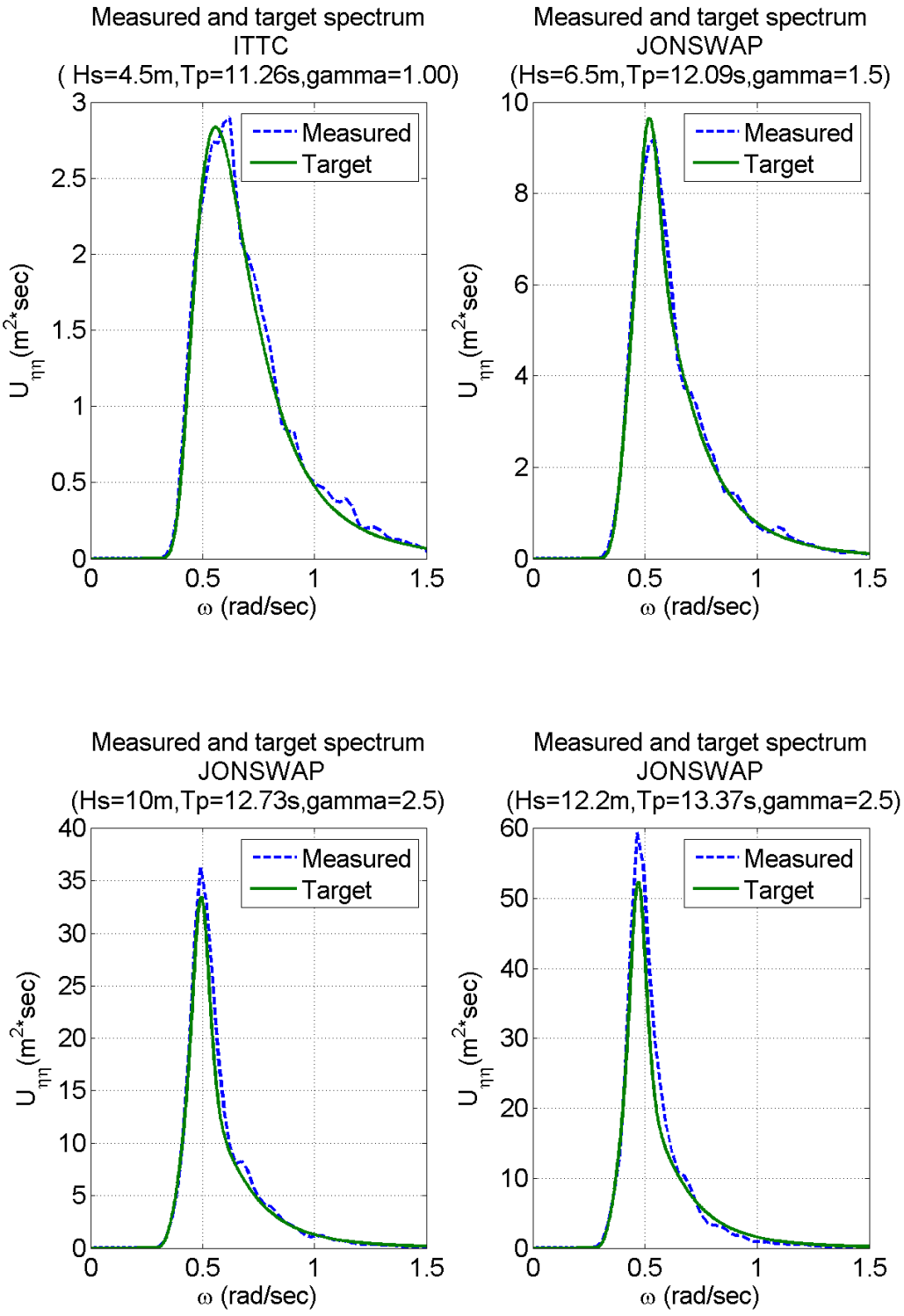


Figure 3-6 Comparison of measured and target wave spectrum

## 3.8 Investigation of nonlinearity of measured wave

Here, we investigated the degree of nonlinearity of waves or sea severity of each sea. As discussed in the previous chapter, the crest heights of narrow banded Gaussian process follow Rayleigh distribution. This proved to be one of the efficient methods for checking the non linearity of the waves. Non linearity was checked using equation 2-10 by comparing the probability of the crest height distributed in the given sea that exceeds a given crest peak.

The probability of exceedence of the linear (Gaussian) sea and those of the real measured waves are compared as shown in Figure 3-6. The comparison of the linear (Gaussian) theory and experiment of the crest height evidently indicates the nonlinearity of the measured wave if the measured points deviate from the linear line. It was found that as the sea severity increases from Hs= 4.5 m to 12.2 m the wave nonlinearity increases gradually.

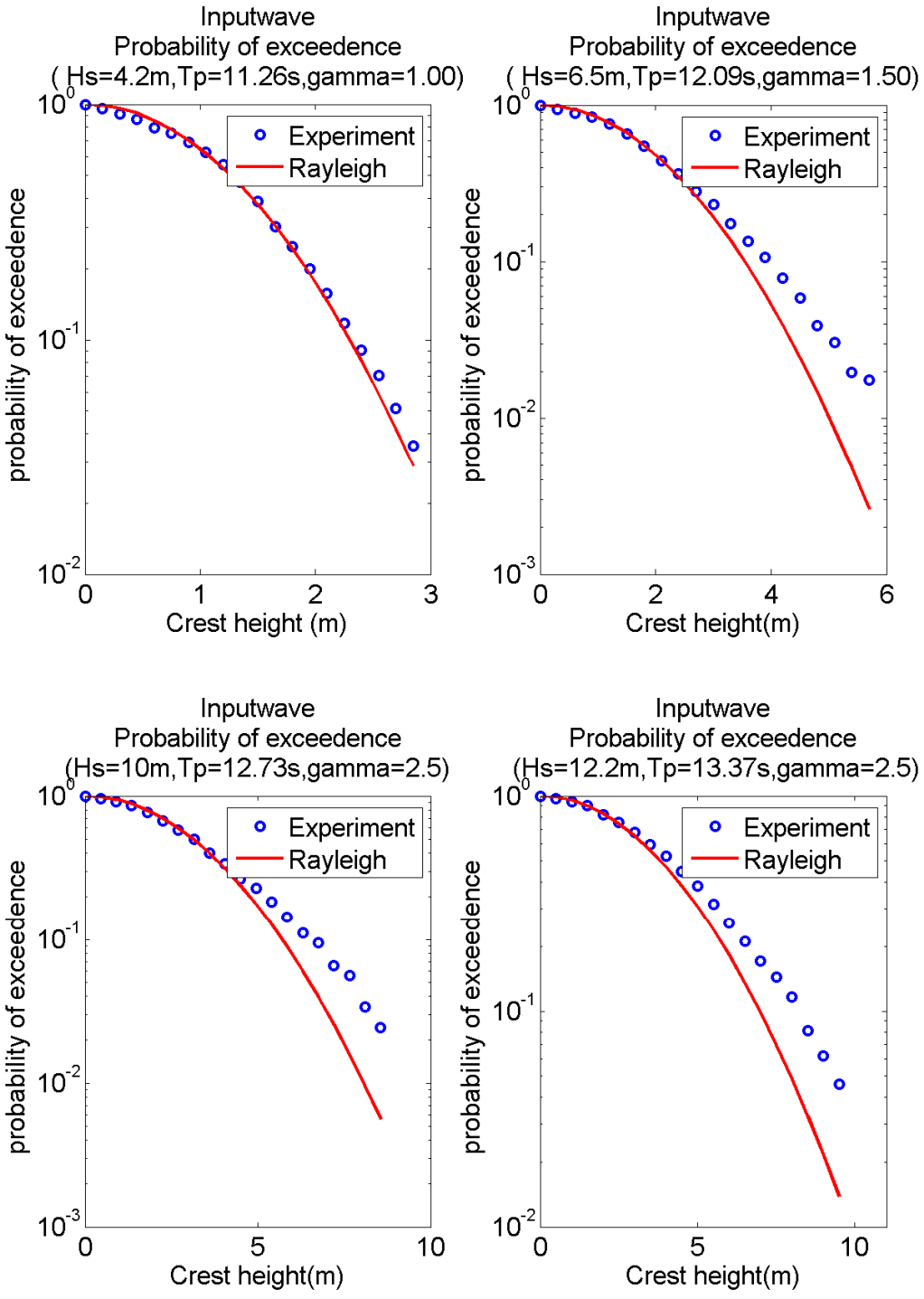


Figure 3-7 Probability of exceedence for input wave crest height

# CHAPTER IV

# RESULTS OF STUDY ON LTF

## 4.1 Measured heave response

Heave response time series from the experiment was plotted as shown from Figure 4-1 to Figure 4-4 for different seas from Hs=4.5 to 12.2m. As a preliminary investigation, statistics of the responses were estimated. Mean, variance, kurtosis and skewness of the heave responses were calculated as in Table 4-1. As discussed in the previous chapter Skewness is a measure of the statistical symmetry of the wave elevation about the mean level. Kurtosis gives idea about peakedness of the data compared with normal distribution.

Table 4-1 Statistics of heave motion for different sea state

| | Hs=4.5m | Hs=6.5m | Hs=10.0m | Hs=12.2m |
|---|---|---|---|---|
| Mean | -2.13 x 10^-17 | -3.43 x 10^-17 | 6.29 x 10^-17 | 2.75 x 10^-016 |
| Variance | 0.1701 | 0.5144 | 1.5230 | 2.8711 |
| Skewness | -0.0015 | 0.0658 | 0.1029 | 0.1596 |
| Kurtosis | 2.9298 | 2.9232 | 2.9050 | 2.9120 |

Mean values of heave responses are practically zero. Zero Skewness represents Gaussian waves with symmetric distribution of crest and trough peaks around mean values. In our analysis Skewness values were found to be small positive values indicating that heave response is asymmetric about the mean value and crest peaks are

slightly larger than trough peaks. Skewness values increases as the sea state increases which is an indication of increase in nonlinearity in higher seas. Kurtosis for Gaussian waves is found to be 3. Kurtosis values deviates from 3 as the sea state increases.

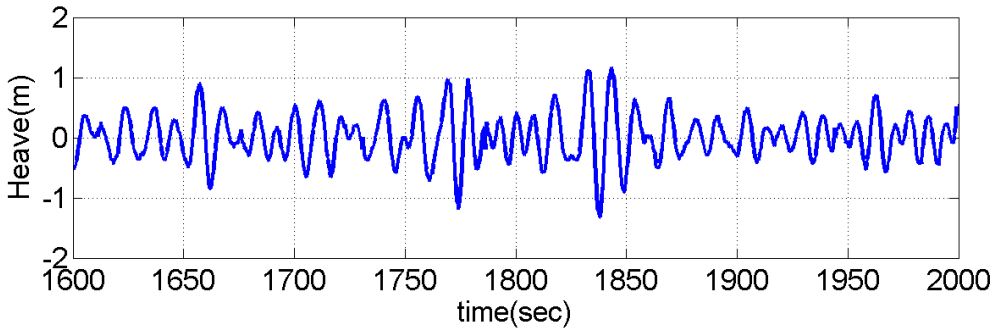


Figure 4-1 Heave motion time series (Hs=4.5m)

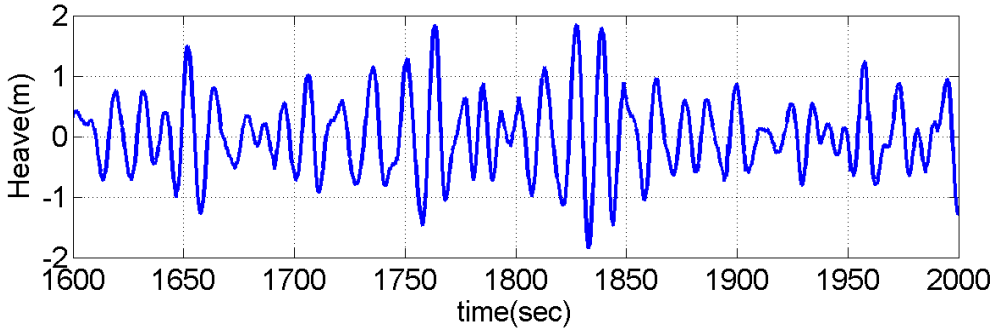


Figure 4-2 Heave motion time series (Hs=6.5m)

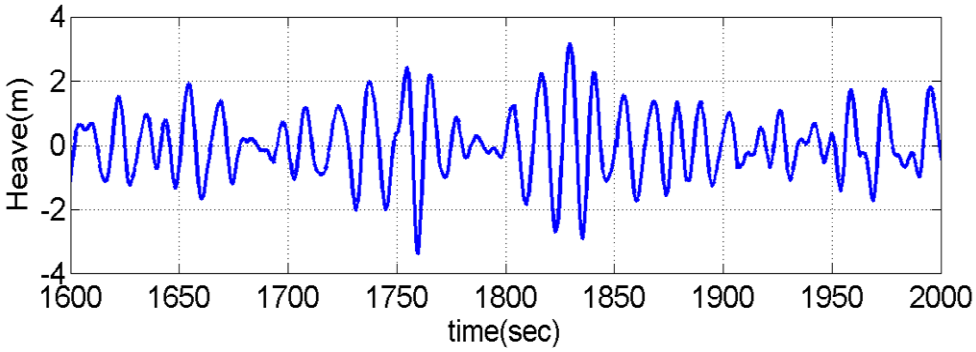


Figure 4-3 Heave motion time series (Hs=10m)

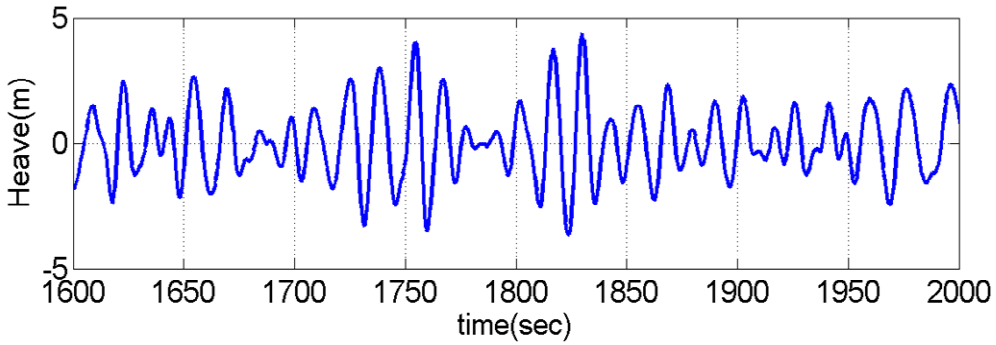


Figure 4-4 Heave motion time series (Hs=12.2m)

## 4.2 Heave auto and cross spectrum

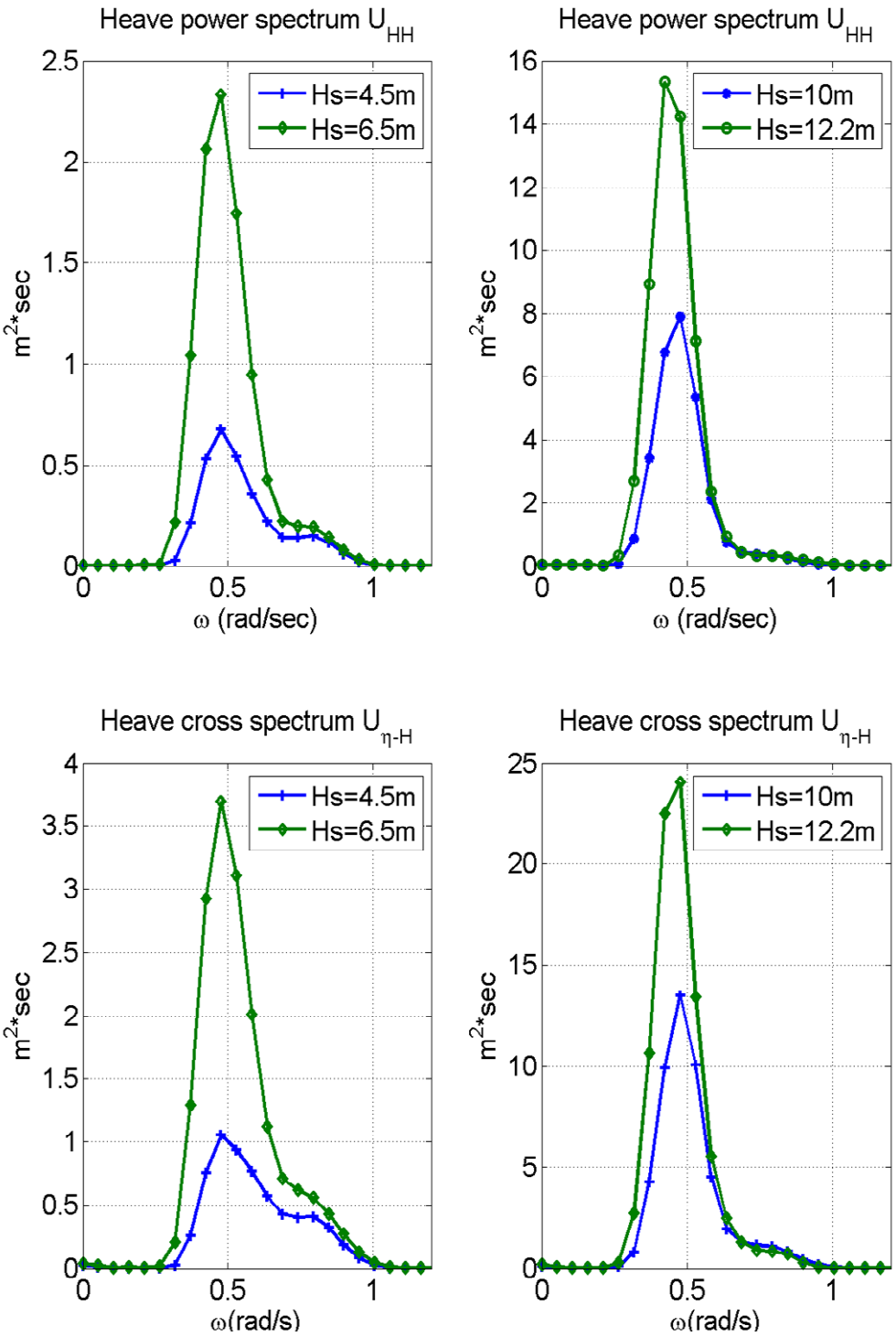


Figure 4-5 Heave motion auto and cross spectrum

## 4.3 Nonlinearity of heave motion

In Figure 4-6 , we compared the probability of exceedence for heave response (positive elevation) to the linear Rayleigh curve. It shows that the probability of the exceedence follows the linear curve for waves #1 and #2 indicating the heave response is linear in these seas. In the waves #3 and #4 the experimental heave data slightly deviates from the linear curve indicating slightly nonlinear heave. However the heaves in all the seas may be regarded practically linear.

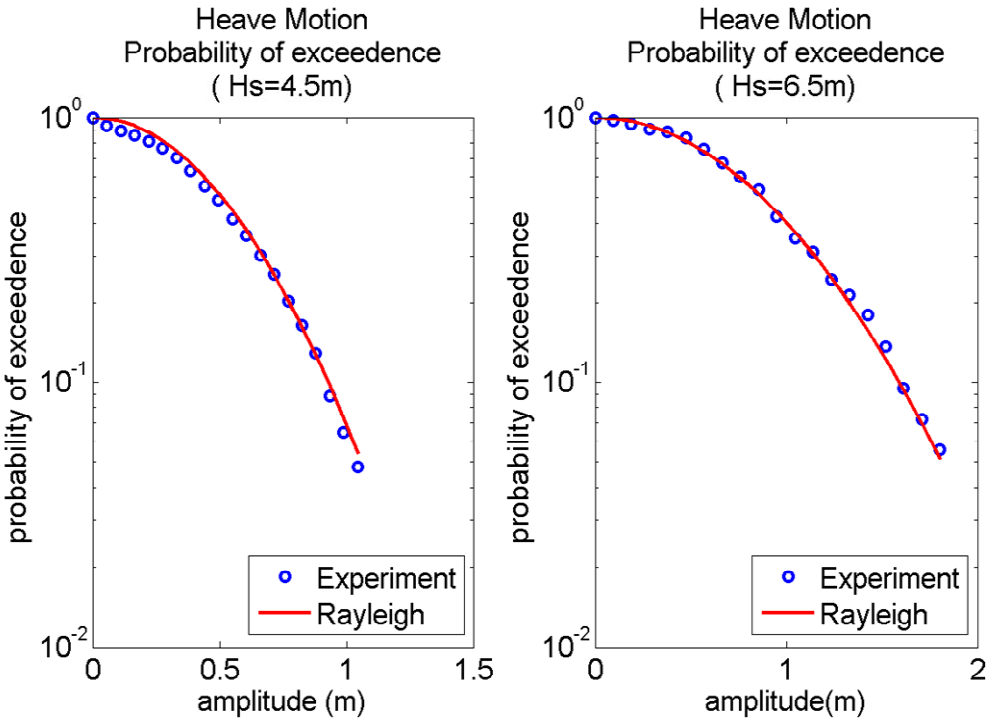


Figure 4-6 Heave motion probabililty of exceedence

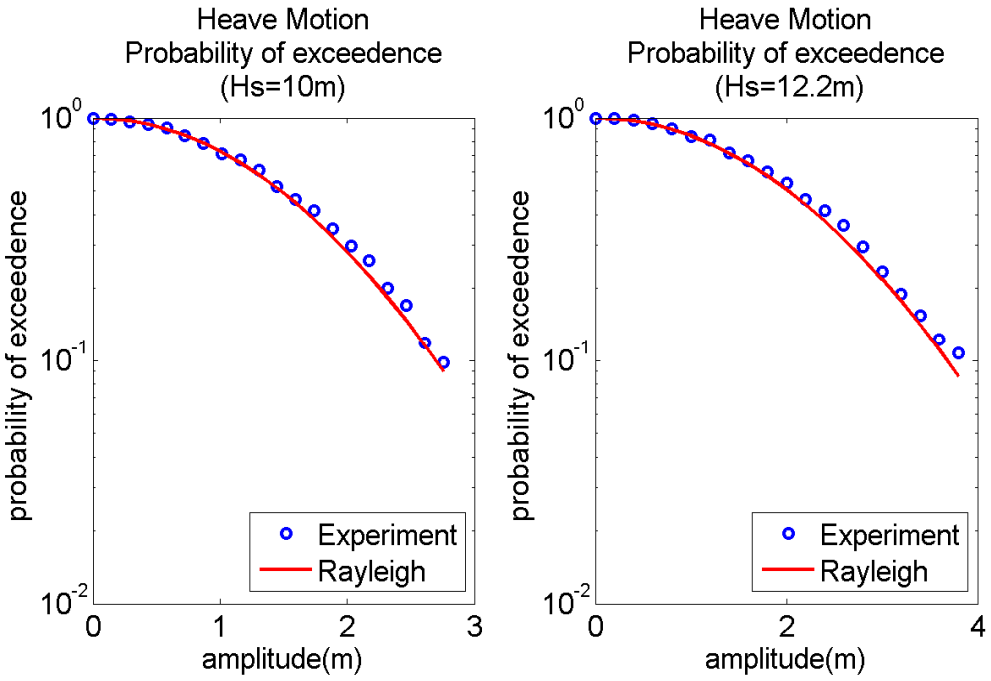


Figure 4-6 (continued)

## 4.4 Heave LTF

We estimated the heave auto and cross spectrum as shown in Figure 4-5. Heave LTFs were determined by applying Volterra linear model using Equation 2-30 . It was observed that heave cross and power spectrum for different seas holds a valid range for a frequency range 0.35 to 0.9 rad/sec which is equivalent to non dimensional frequency range 1.5 to 3.8 and ship to wave length ratio of 0.35 to 2.5. Even though a clear distinction between linear and higher order frequency range was not easy from the experimental values, we assumed that frequency range of heave spectrum as seen from Figure 4-5 is solely due to linear input wave. This frequency range was checked during the calculation of second order part and their reconstruction in the later stage of the

research and found that second order frequency lies out of this assumed linear frequency range. The LTFs are plotted for different seas as shown in Figure 4-7.

Heave resonance frequency was estimated approximately 0.801 rad/sec as per equation.3-1 The humps at frequency 0.83 rad/sec represent heave resonance as observed in Figure 4-7.

Even though LTF for different sea states behaves almost the same way outside natural frequency range, it was evidently seen that LTF decreases as the sea states increase for a frequency range close to natural frequency, i.e. frequency range 0.65 to 0.9 rad/sec. This result is similar to Dalzell.et.al (1973) conclusion regarding pitch motion LTF of destroyer. Phase angle also varies for different sea state and lags behind as the sea state increases around natural frequency.

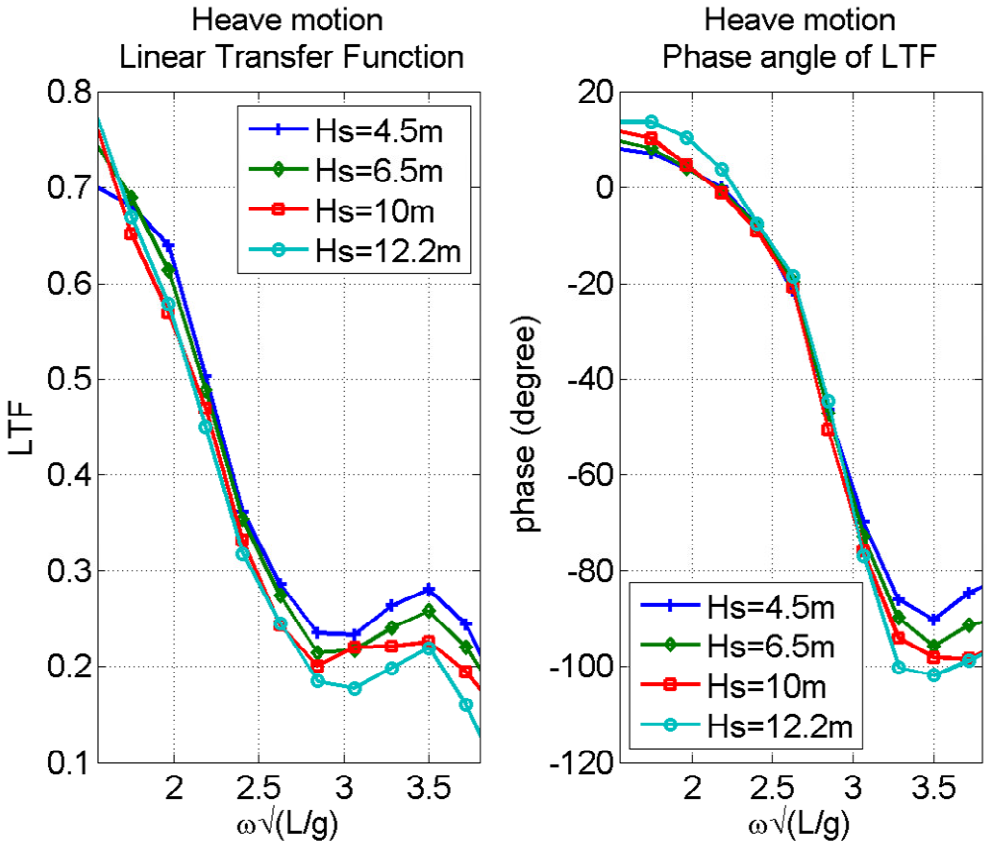


Figure 4-7 Heave motion LTF, phase angle

## 4.5 Comparison of theoretical and experimental LTF

From the foregoing discussions regarding the nonlinearity of input waves and heave response, we saw that input waves were dominantly nonlinear in nature for sea states higher than Hs=4.5m and nonlinearity increases gradually as it goes to higher sea states. Heave responses were almost linear in nature especially for the first two sea states and their peak values followed Rayleigh distribution curve. Since theoretical LTF calculation method assume Gaussian input, difference in the values of experimental and theoretical LTF was expected and noticed for higher sea states especially for the last two

responses due to input waves of Hs=10.0m & 12.2m Figure 4-8 shows the comparison between theoretical and experimental LTFs. It is clear from the figure that theoretical LTF value is higher than experimental LTF for the sea states Hs=10.0m and 12.2 m. Differences between them are large around natural frequency and are close to 25 % more for 10.0m wave and 50% more for 12.2m wave. Experimental LTF for Hs=4.5m and 6.5m almost follows the experimental LTF. It is conventional to apply theoretical LTF in the design of offshore structures. This leads to higher loads resulting in heavy structure.

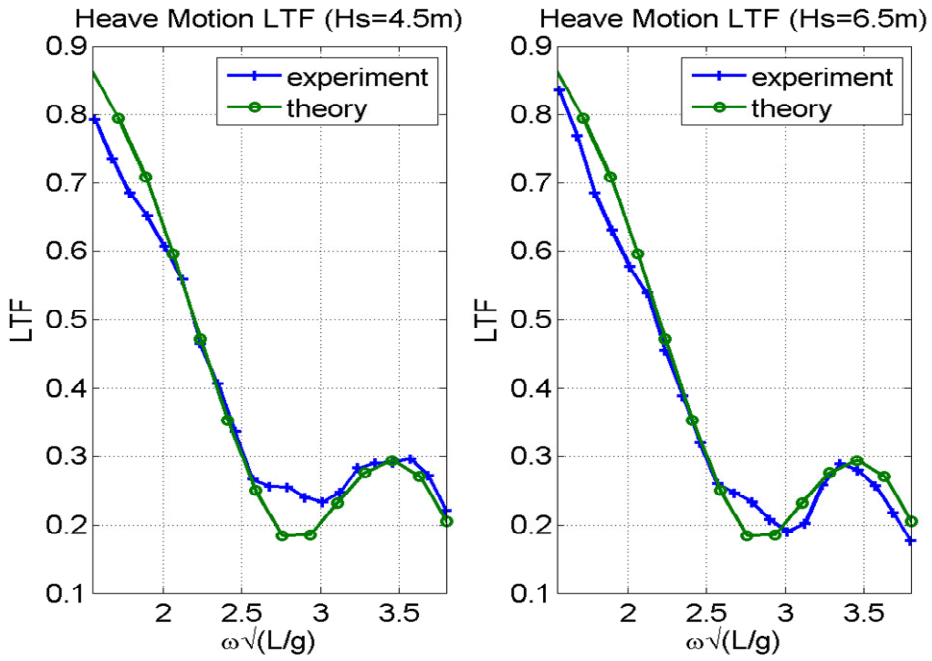


Figure 4-8 Comparison of theoretical and experimental LTF

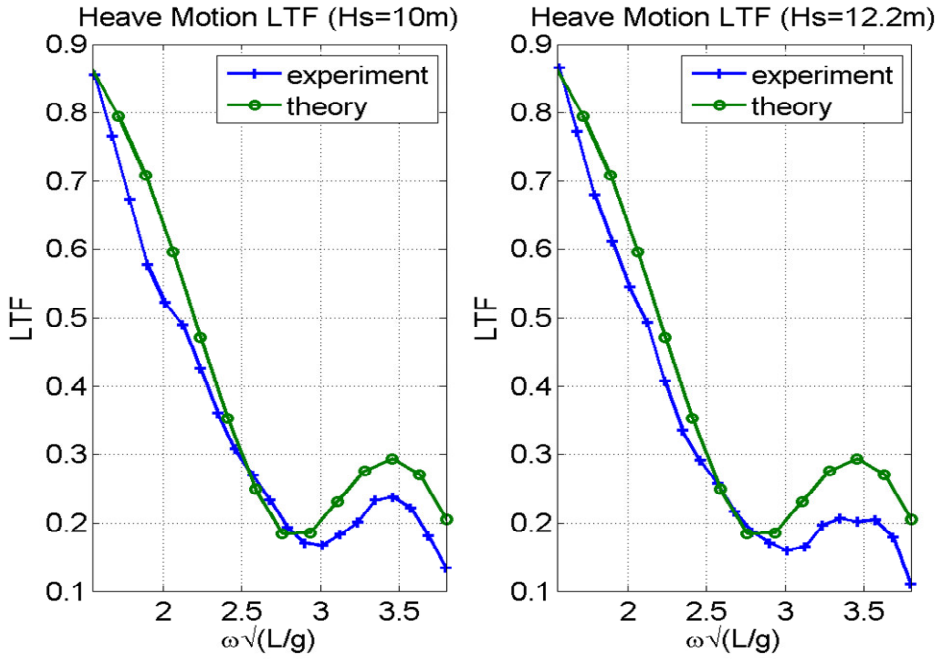


Figure 4-8 (continued)

Similarly phase angles of LTF from linear theory and experiment were compared as shown in Figure 4-9. Theory at low frequency has to be in phase with the measured wave. But measured sea condition shows phase lead about 10 degrees at the low frequency and continue the tendency as the frequency increases. It was observed that phase angles of both experimental and theoretical LTF follows the same trend and phase angle of LTF from experiment lags behind theoretical LTF.

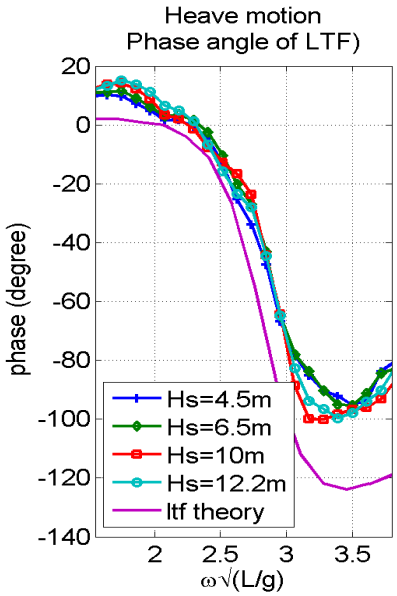


Figure 4-9 Comparison of LTF phase angles from theory and experiment

## 4.6 Heave peaks of experiment and theory

The most probable peak response of Gaussian process is given by equation 2-14 We compared the peak values of heave obtained by the linear theory and experiment at each sea is shown in Figure 4-10. Theory assumes Gaussian seas and theoretical linear response LTFs and employs the most probable peak as given in the above.

Table 4-2 Heave peak value comparison between experiment and theory

| Significant wave height(m) | Peak value (experiment) | Peak value (theory) | % error |
|---|---|---|---|
| 4.5 | 1.2451 | 1.1788 | 5.53 |
| 6.5 | 2.0298 | 2.8964 | 42.69 |
| 10.0 | 3.6516 | 5.0411 | 38.05 |
| 12.2 | 4.9728 | 6.5252 | 31.22 |

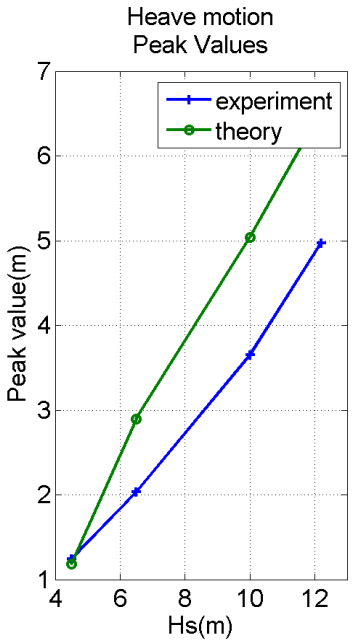


Figure 4-10 Heave motion peak values

It is clear from Figure 4-10 that there is a general trend for linear theory to over estimate the peak values as the sea severity increases. For the responses corresponding to lowest sea (Hs=4.5m) experimental peak value is 5.5% more than theory. For the second response due to input wave of Hs=6.5m we saw that experimental LTF does not vary from theoretical LTF and the system is almost linear. Still the large difference in the peak values can be attributed to the nonlinearity of the input wave which we investigated in Figure 3-3. For the last two responses both the input waves and system were found to be non linear. Peak values from linear theory do not match the experimental peak values.

## 4.7 Pitch motion time series

Pitch motion time series are plotted as shown in Figs. 4.10 to Fig.4.13. Similar to heave response the mean, variance, skewness and kurtosis were calculated and are shown in below table.

Table 4-3 Statistics of pitch motion for different sea state

| | Hs=4.5m | Hs=6.5m | Hs=10.0m | Hs=12.2m |
|---|---|---|---|---|
| Mean | 9.12 x 10^-17 | -2.14 x 10^-17 | 5.37 x 10^-17 | -9.79 x 10^-17 |
| Std deviation | 0.7760 | 1.2972 | 2.0927 | 2.5687 |
| Skewness | 0.0849 | 0.1699 | 0.2577 | 0.2733 |
| Kurtosis | 3.0901 | 3.1839 | 3.1575 | 3.0640 |

Mean values are very small and practically equals to zero. As discussed before skewness of pitch motion shows the non Gaussian behavior. Pitch motion peaks are asymmetrically distributed about the mean value and crest peak heights are larger than trough peak heights. Skewness values increase as the sea state increases and are higher than heave motion. It was inferred from the above observation that nonlinearity involved in pitch motion is higher than heave motion.

Kurtosis values are greater than 3. Therefore it can be assumed that wave peaks are bigger than Gaussian waves.

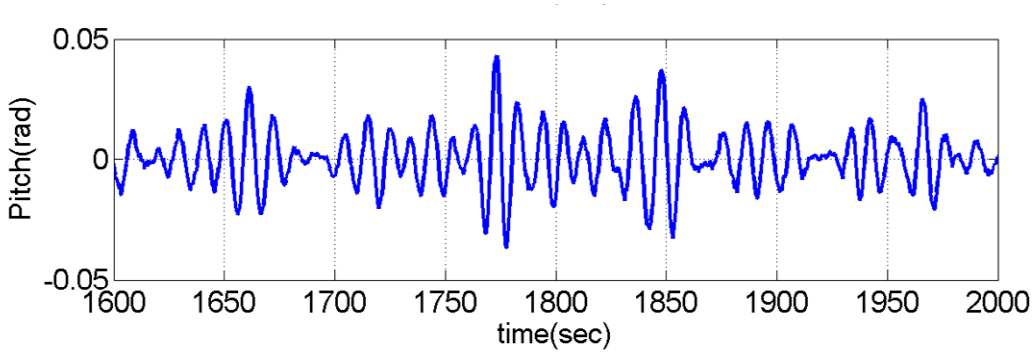


Figure 4-11 Pitch motion time series (Hs=4.5m)

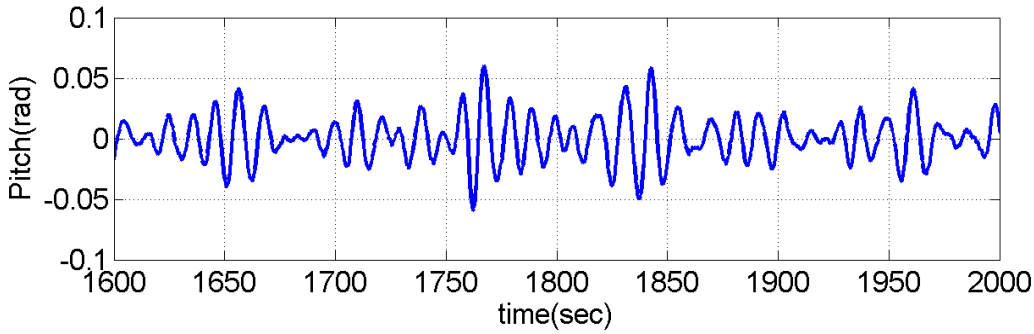


Figure 4-12 Pitch motion time series (Hs=6.5m)

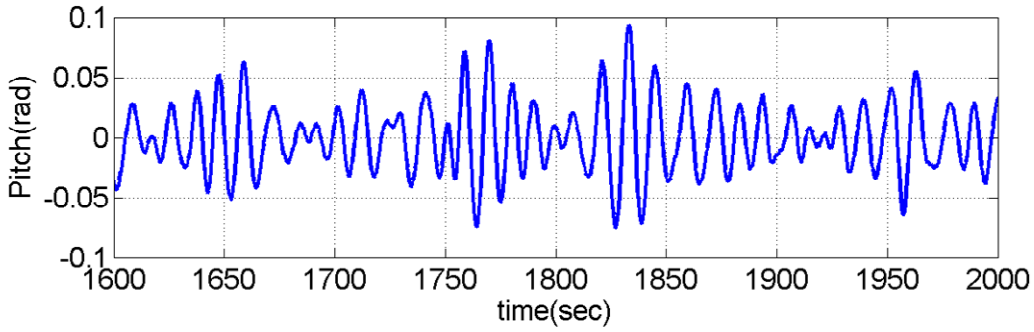


Figure 4-13 Pitch motion time series (Hs=10.0m)

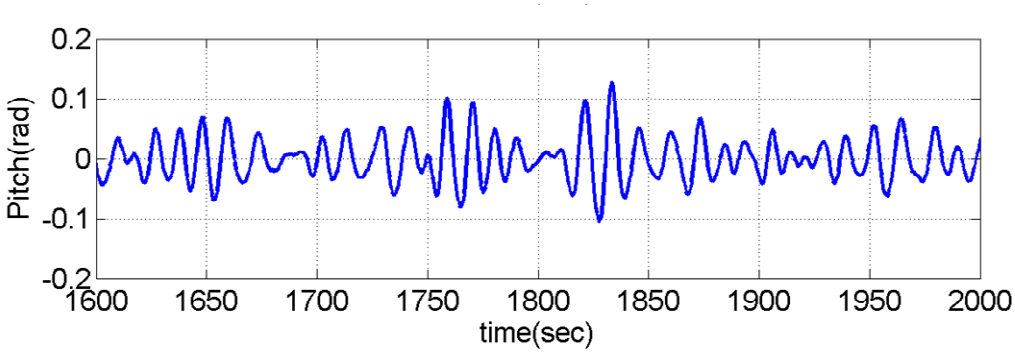


Figure 4-14 Pitch motion time series (Hs=12.2m)

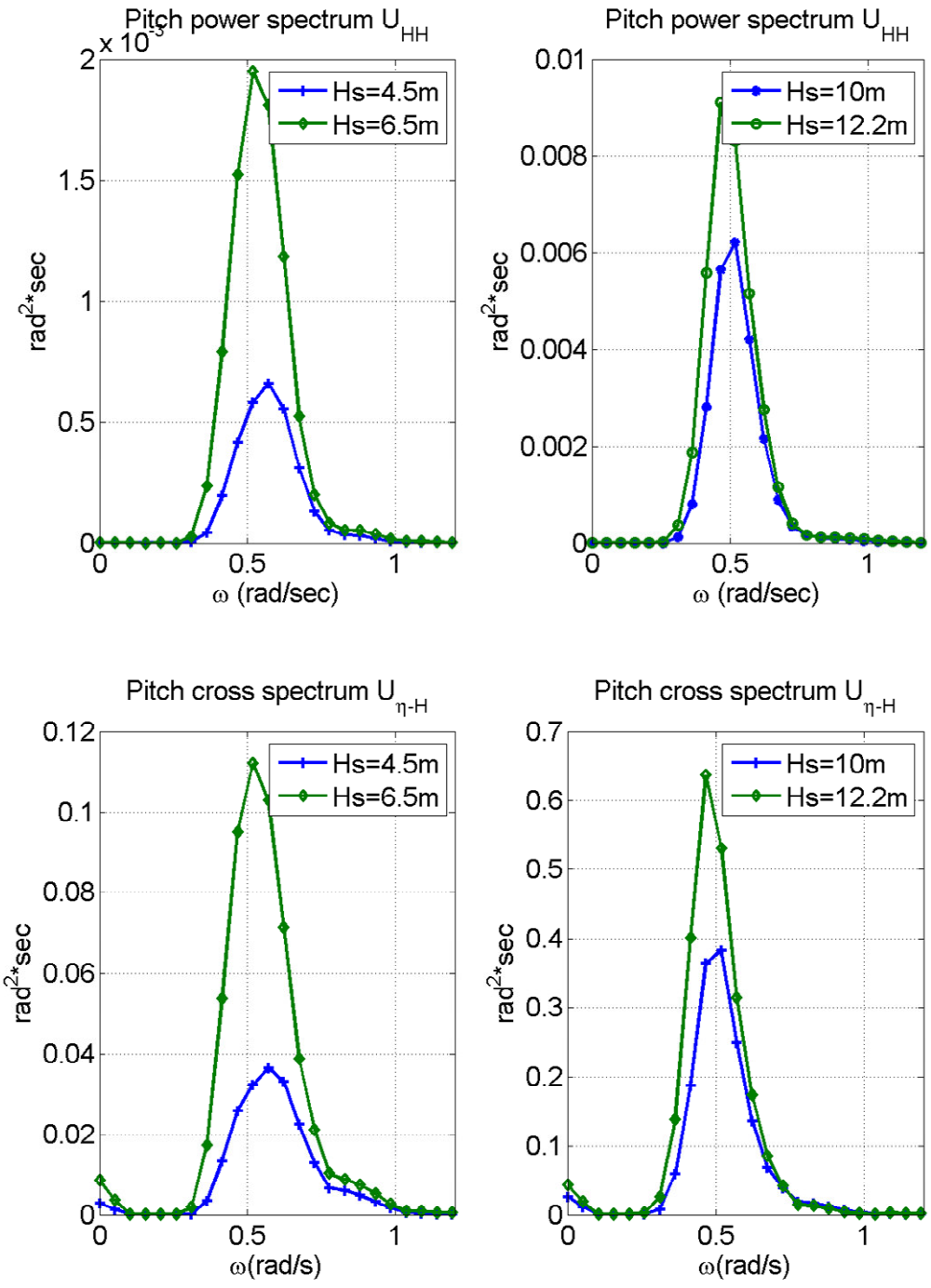


Figure 4-15 Pitch auto and cross spectrum

## 4.8 Pitch LTFs

Above data in Figure 4-15 are used to estimate pitch LTFs as shown in Figure 4-16. Second order effect is hardly present in the pitch auto power spectrum. A small peak at the low frequency range of the cross spectrum is visible. This property was investigated in the later stage of the research but found the effect of second order waves negligible. Similar to heave motion, it was observed that heave cross and power spectrum for different seas holds a valid range for a frequency range 0.36 to 0.9 rad/sec which is equivalent to non dimensional frequency range 1.5 to 3.8.

The experimental LTF values are same for the first two sea states while it decreases for higher sea states for some particular frequency range as shown in Figure 4-16. It was evidently seen that pitch LTF values due to input waves of Hs=10.0m & 12.2m decrease as the sea states increase in the frequency range 0.35 to 0.6 rad/sec (i.e. for non dimensional frequency range of 1.5 to 2.5) . The same phenomenon was observed near the natural frequency range even though in between frequency range there is not much difference in the LTF values.

Pitch resonance frequency was observed at 0.876 rad/sec where the humps were present in LTF plot. Natural frequency of pitch motion is slightly different from heave motion which was observed at 0.83 rad/sec as in Figure 4-7.

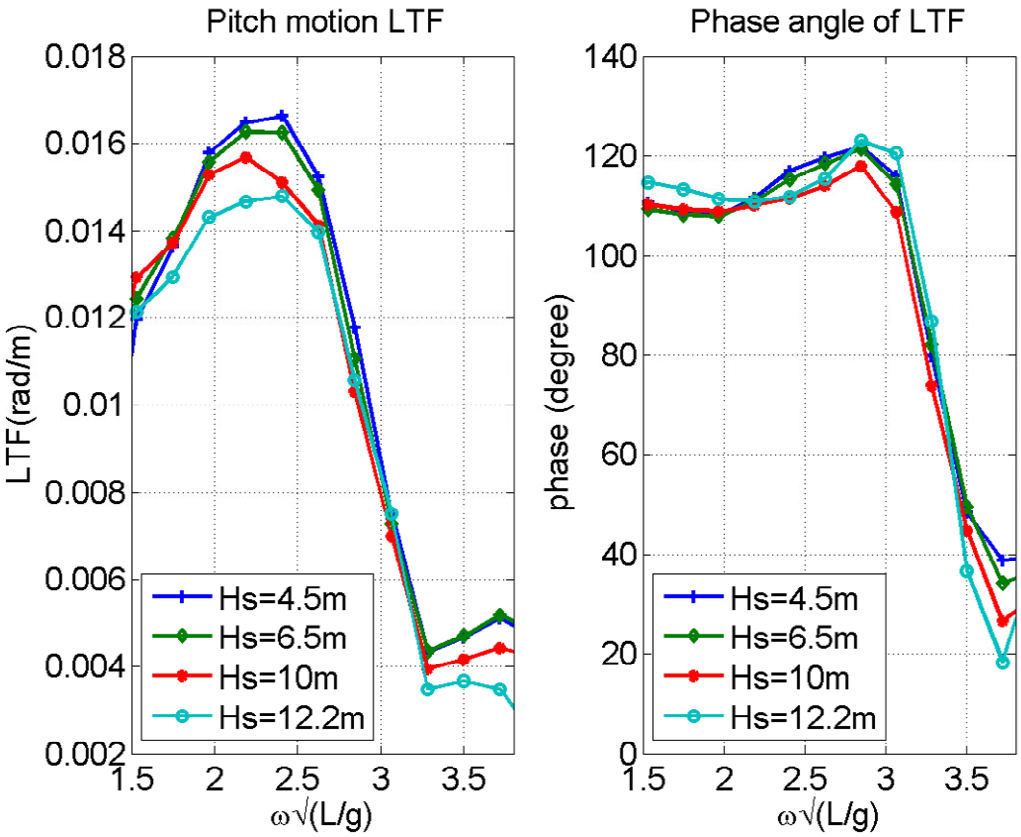


Figure 4-16 Pitch motion experimental LTF and phase angle

## 4.9 Nonlinearity of pitch motion

We investigated the nonlinearity of the pitch response in the time-domain similar to the heave motion. This was carried out by comparing the probability of exceedence of crest height of the linear theoretical pitch motion in the Gaussian Sea with the measured ones in the non-Gaussian seas as shown in Figure 4-17. Similar to heave motion it is observed that measured pitch probability of exceedence follows Rayleigh curve for lower seas and slightly deviates for wave 3& 4. Hence pitch motion is weakly nonlinear for all the seas.

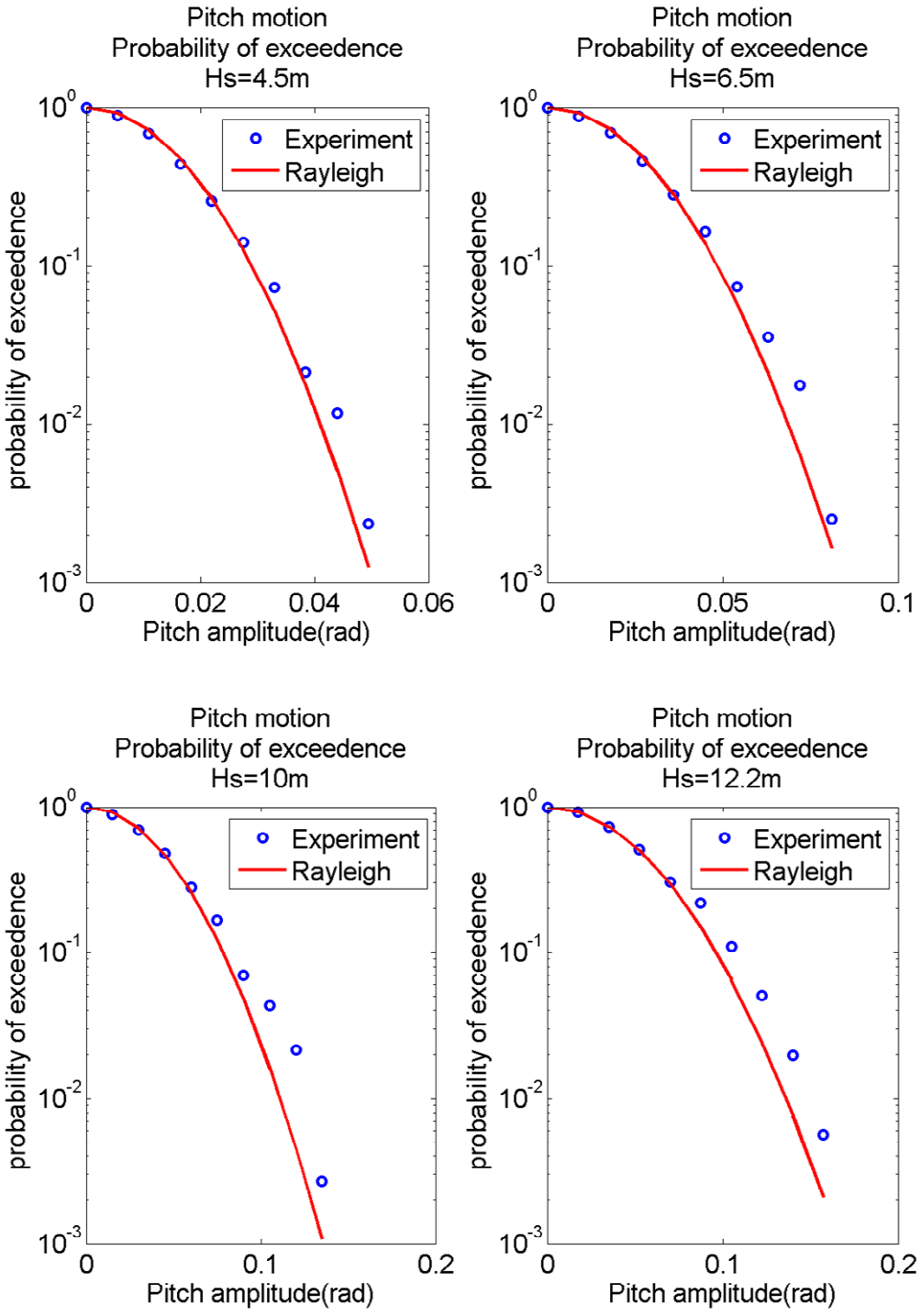


Figure 4-17 Pitch motion probability of exceedence

## 4.10 Pitch LTF theory vs. experiment

LTFs and its phase angles from theory were compared with experiment values as shown in Figure 4-198 and Figure 4-19. Difference between theoretical and experimental LTF values was clearly visible from the plot for a non dimensional frequency range of 1.5-2.5. Theoretical LTF values were always higher than the experimental LTF values for all the sea states during this frequency range and near natural frequency. Theoretical LTF values were found to be 25% to 33% more than experiment for the different sea states. It was seen that phase angles of experimental LTF and theoretical LTF were following same trend as in the case of heave motion.

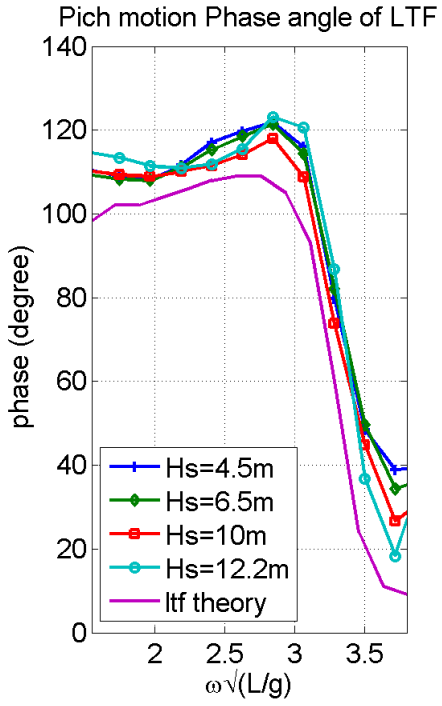


Figure 4-18 Comparison of phase angles of theoretical and experimental LTF

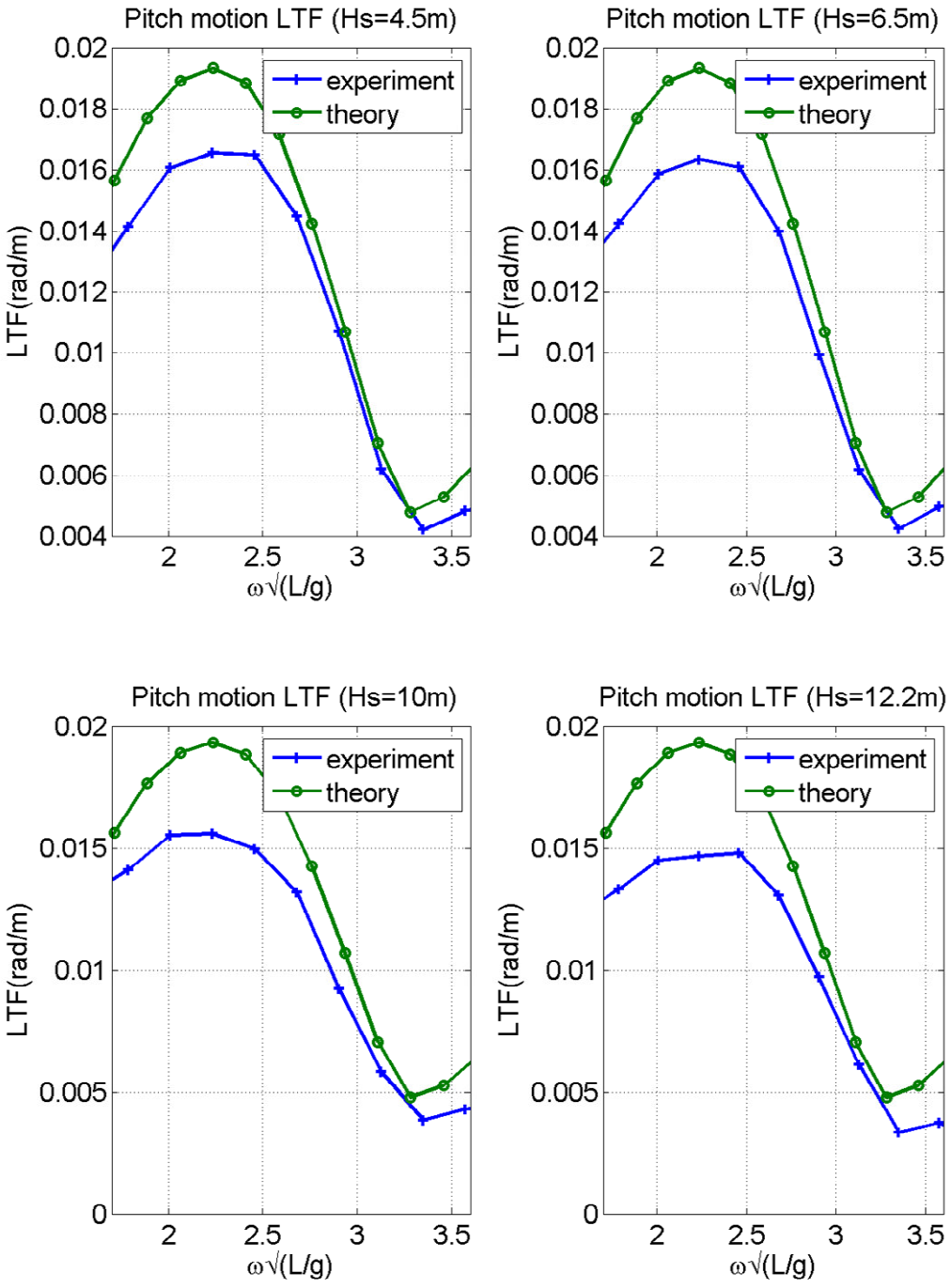


Figure 4-19 Comparison of theoretical and experimental pitch motion LTF

## 4.11 Pitch peaks for theory and experiment

Peak pitch values estimated using Equation 2-14 and were found to be higher than the experiment values at the respective seas. Here the percentage errors between the theory and experimental peak value are found to be up to 30% (Table 4-4).

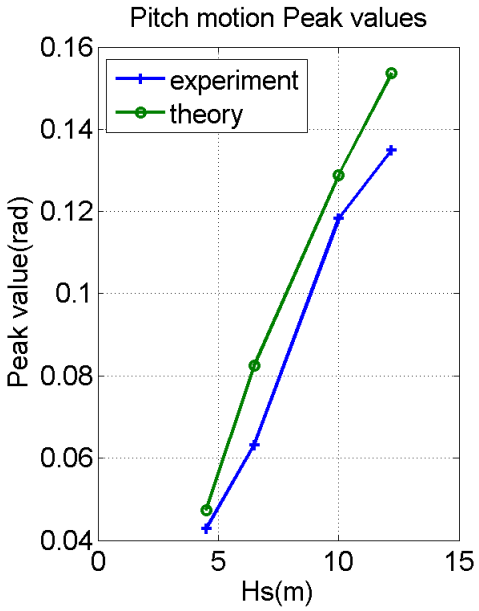


Figure 4-20 Comparison of theoretical and experimental pitch motions peak values

Table 4-4 Pitch motion peak values comparison

| Significant wave height(m) | Peak value (rad) (experiment) | Peak value (rad) (theory) | % error |
|---|---|---|---|
| 4.5 | 0.04298 | 0.0474 | 10.2 |
| 6.5 | 0.0632 | 0.0825 | 30.5 |
| 10.0 | 0.1183 | 0.1289 | 8.9 |
| 12.2 | 0.1346 | 0.1536 | 14.11 |

# CHAPTER V

# RESULTS OF VOLTERRA QUADRATIC MODEL

## 5.1 Heave motion cross-bi spectrum & QTF

Here we employed Volterra quadratic model with assumption of Gaussian input for the calculation of cross bi spectrum shown in Figure 5-1. Using equation 2-62 , cross-bi spectrum for heave motion was calculated for different sea conditions. Heave cross-bi spectra are having two peaks on the low and high output frequency range. The spectrum at low output frequency appears larger in general compared to the higher frequency.

Similarly QTF was calculated using equation 2.62 and plotted as shown in Figure 5-2 . The heave QTFs at low output frequency range are much larger than those at high output frequency range. The QTFs in the low output frequency range are the difference frequency components, while the QTFs in the high output frequency range are the sum frequency components. Second order sum and difference frequency effect at the resonance frequency is visible for output frequency around 0.8 rad/sec. But their effect found to be very small compared with input wave frequency range which was studied during comparison of reconstructed linear and second order response.

Mean second order responses were noticed for all the four sea states in Figure 5-2. They are present along $\Omega_1$ axis at $\Omega_2$ =0. It was seen that Mean responses are relatively negligible for lowest sea state i.e. for Hs=4m. But its presence was clearly visible for the next three sea states. Second order QTFs for heave response decrease as the sea severity increases, which is similar to LTFs. This trend clearly exists for wave

no. 1, 2 & 3. For wave Hs =12.2 m, QTFs are larger compared to those at Hs = 10 m. The reason cannot be identified. However it is clear that QTF and mean second order terms not only depend on the system but also on the sea severity.

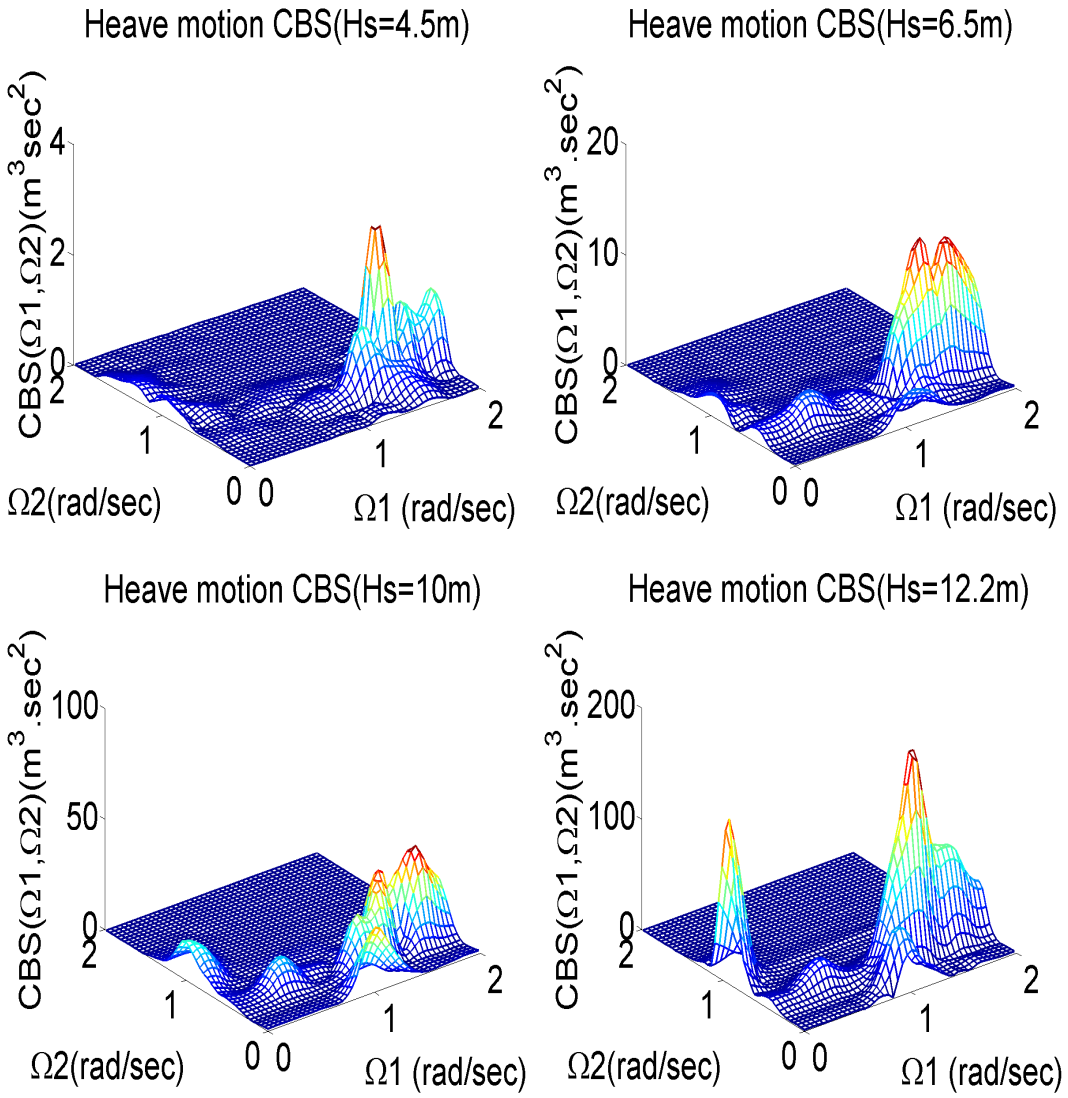


Figure 5-1 Cross bi spectrum of heave motion for different sea states. Cross bi spectrum was plotted against sum and difference frequency axis.

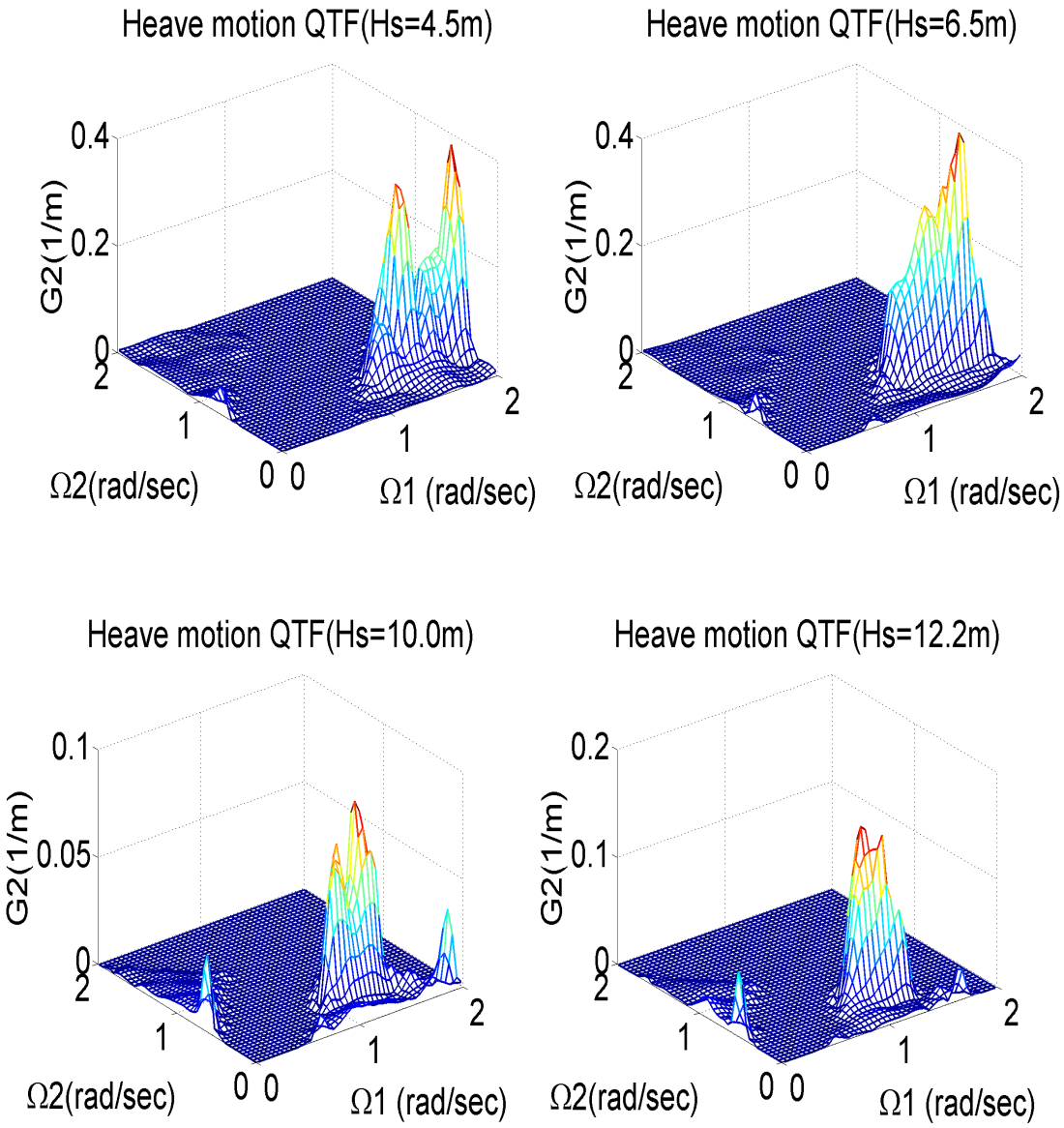


Figure 5-2 QTF of heave motion for sea states from Hs = 4.5m to 12.2m plotted against sum and difference frequency axis

## 5.2 Pitch motion cross-bi spectrum and QTF

Two peaks are visible at high and low output frequency range. The pitch QTFs at low output frequency range is large compared to high frequency range. The QTFs at the high output frequency range are the sum frequency components, whereas those in the low output frequency are the difference frequency components. It was inferred that difference frequency components are dominant in the second order pitch motion compared to sum frequency components. Here also variation in pitch response QTFs with the sea severity was clearly visible for all the four waves. For $2^{nd}$ and $3^{rd}$ responses, QTF decreases with increase in sea severity and $4^{th}$ response does not follow the trend. This phenomenon should be read in conjunction with the reconstruction of responses discussed in the following chapter. Second order sum and difference frequency effect on the pitch resonance frequency was noticed around 0.8 rad/sec. But similar to heave second order responses, these are also very small when compared with resonance effect input frequency range which includes both linear and higher order terms. Mean second order pitch response is found to be negligibly small.

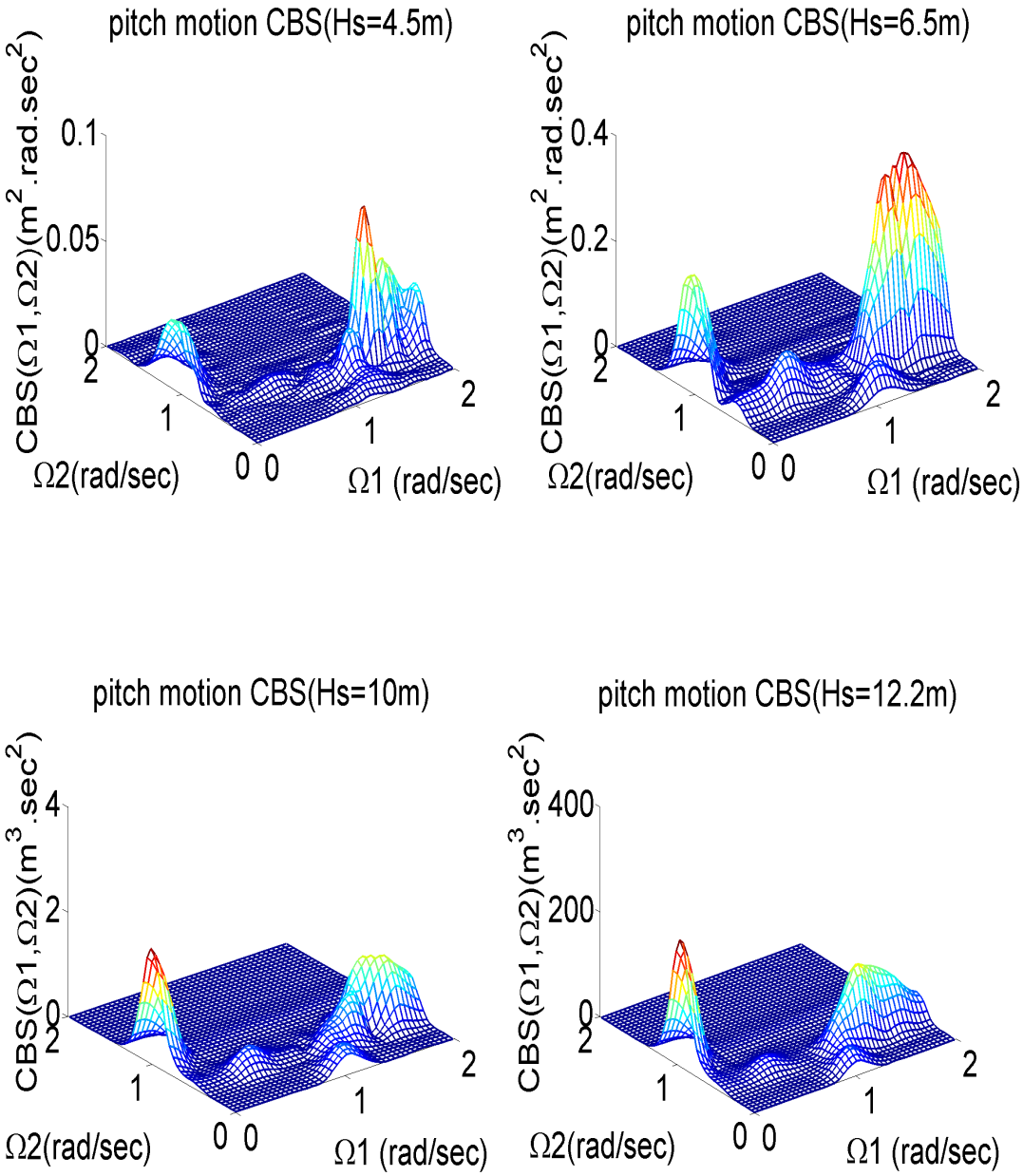


Figure 5-3 Pitch motion cross-bi spectrum for different sea states

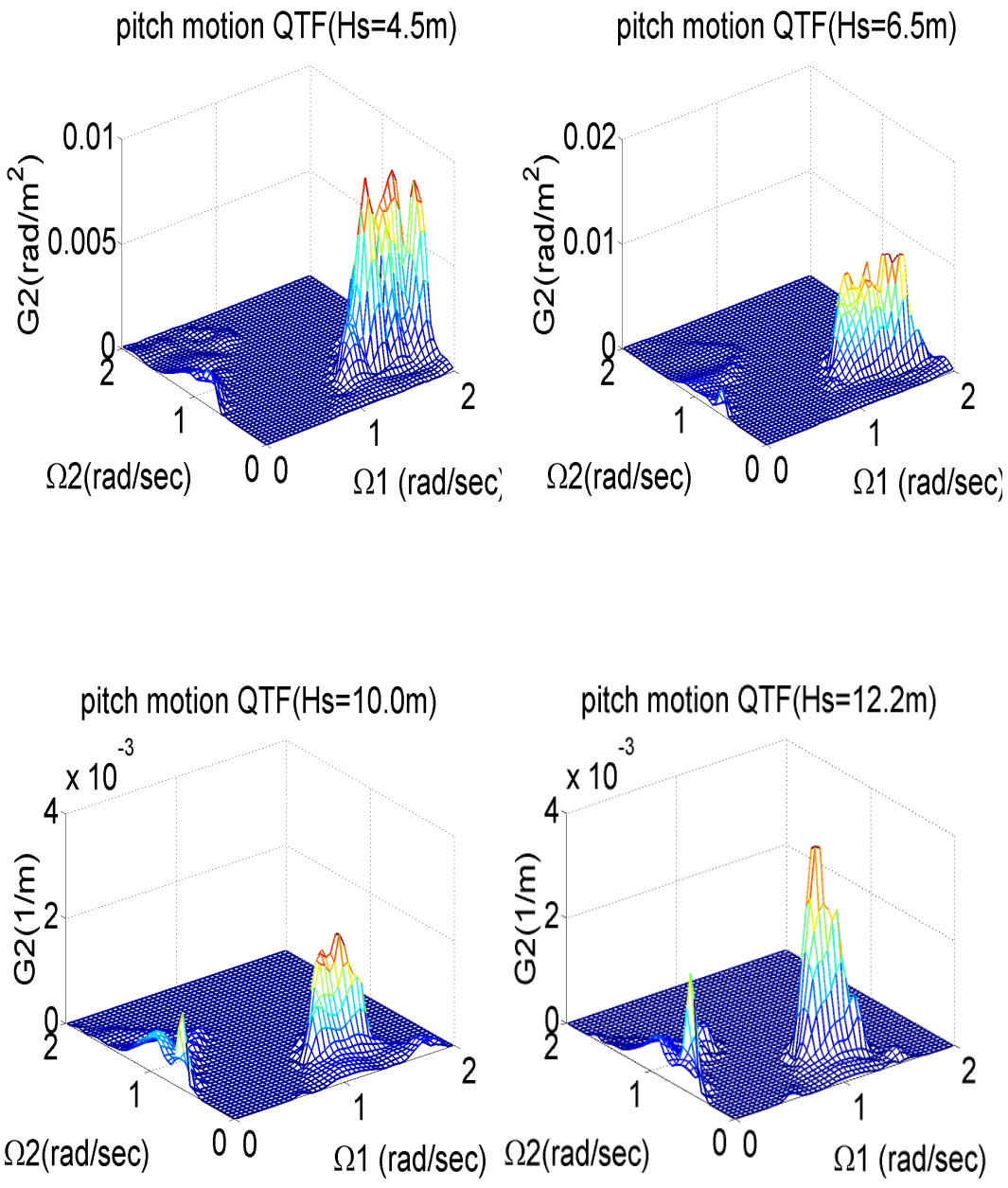


Figure 5-4 Pitch motion QTF for different sea states

# CHAPTER VI

# RECONSTRUCTION AND COHERENCY TEST

## 6.1 Reconstruction of the heave response time series from LTF

Response time series was reconstructed using equation 2-41 which can be written ina concise form as shown below (eqn 2-63).

$$
\begin{aligned}
&y(t) = y_1(t) + y_2(t) \\
&= \mathrm{Re}\sum_{m=1}^{N} A_m G_1(\omega_m) e^{i(\omega_m t - \varepsilon_m)} + \frac{1}{2}\mathrm{Re}\sum_{j=1}^{N}\sum_{k=1}^{N} A_j A_k G_2^{\pm}(\omega_j, \omega_k) e^{i[(\omega_j \pm \omega_k)t - (\varepsilon_j \pm \varepsilon_k)]}
\end{aligned}
$$


$$
\begin{aligned}
&y(t) = y_1(t) + y_2(t) \\
&= \mathrm{Re}\sum_{m=1}^{N} A_m G_1(\omega_m) e^{i(\omega_m t - \varepsilon_m)} + \frac{1}{2}\mathrm{Re}\sum_{j=1}^{N}\sum_{k=1}^{N} A_j A_k G_2^{\pm}(\omega_j, \omega_k) e^{i[(\omega_j \pm \omega_k)t - (\varepsilon_j \pm \varepsilon_k)]}
\end{aligned}
$$


2-63

Reconstruction was done in two steps i.e. Reconstruction of the linear part and reconstruction of the second order part. Linear heave response was reconstructed using experimental LTF as shown in Figure 6-1 to Figure 6-4 using first term of equation 2-64. As discussed earlier experimental LTF range was between 0.36 and 0.9 rad/sec. Reconstruction done between these ranges almost exactly matches with the measured response for the first three waves. It was inferred that measured response is mainly due to input waves in the frequency range 0.36 to 0.9 rad/sec. So contribution of second order response to the total heave response is negligible as discussed in section 3.5. Only for the last response (for input wave Hs=12.2m) noticeable differences in heave between measured and reconstructed response was observed. This is maybe an indication that

second order responses contribution to the total response is very negligible except for very high seas of order great than 10m.

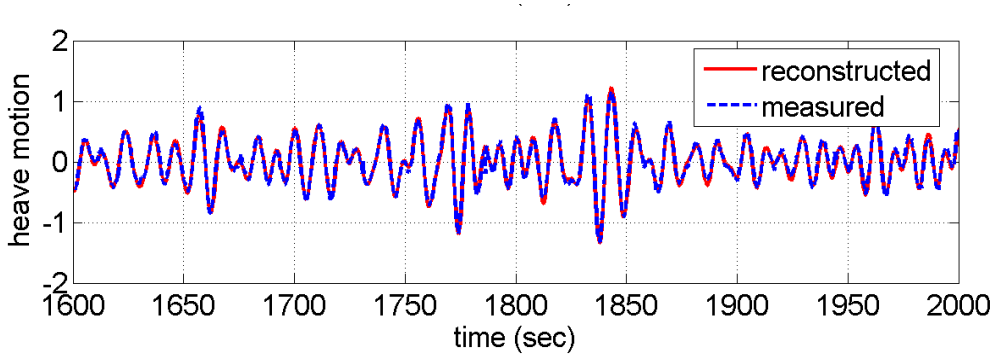


Figure 6-1 Reconstructed heave response from LTF - Hs=4.5m

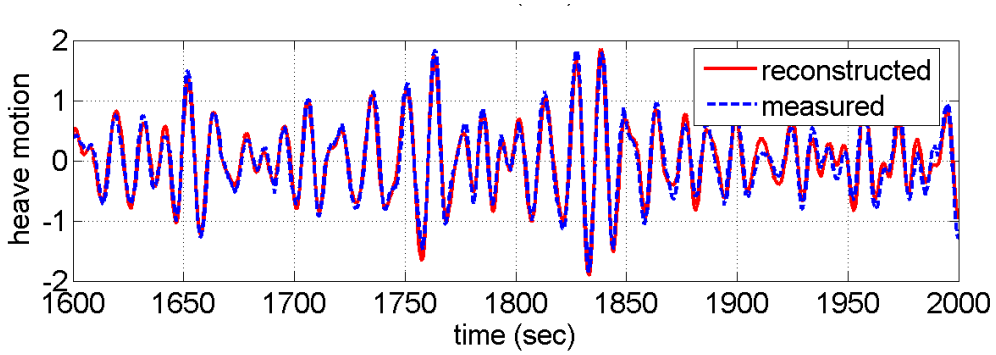


Figure 6-2 Reconstructed heave response from LTF - Hs=6.5m

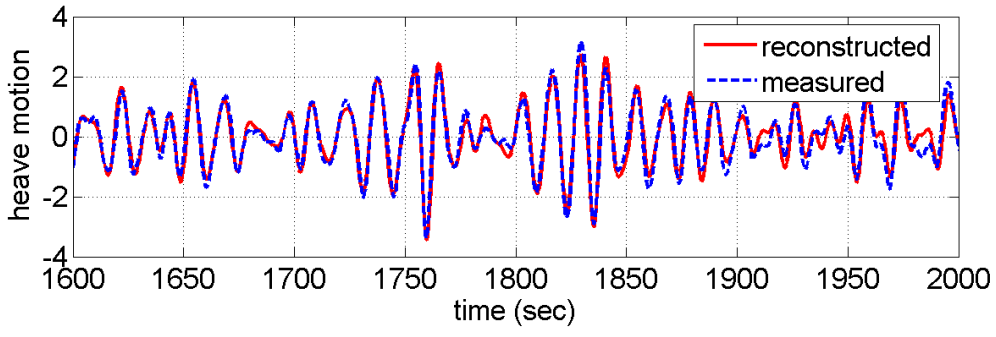


Figure 6-3 Reconstructed heave response from LTF - Hs=10.0m

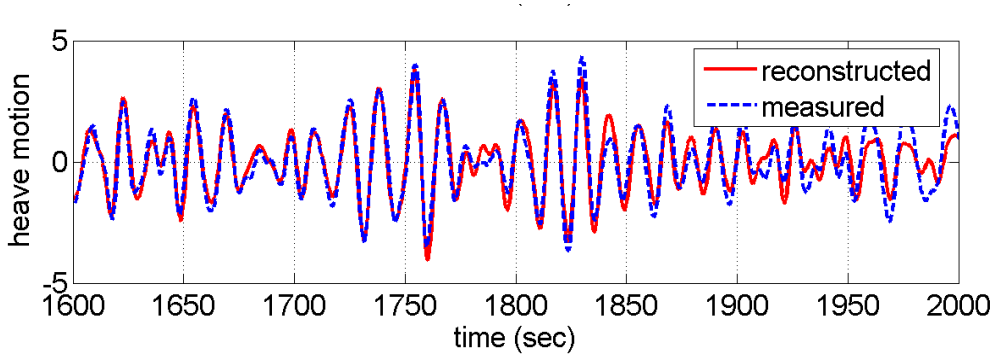


Figure 6-4 Reconstructed heave response from LTF - Hs=12.2m

## 6.2 Reconstruction of second order heave response from QTF

Reconstruction of second order response from QTF was done using second term of equation 2-64. Reconstructed responses were plotted as shown in Figure 6-5 to Figure 6-8. Reconstructed sum and difference frequency components of the second order heave response was calculated up to 2000 seconds and was added to get the total second order response. Transient (high frequency) effects are visible on second order responses especially on sum frequency part as they travel in groups. Contribution of second order response increases gradually from lower to higher seas as expected with an exception to the response from input wave of Hs=6.5m. Second order response from Hs=6.5m is found to be greater than Hs=10.0m. This property was further studied in the following sections of coherency value calculation (section 6.8) where it was noticed that second order responses of 2$^{nd}$ case in the lower frequency range was overestimated. It was expected that peak of second order response should occur at the peak of input wave group. It was observed that second order responses occur at input wave peaks as

expected. Mean and variance of second order heave response was calculated and is as shown in table 5.1.

Table 6-1 Mean values of second order heave response

| | Hs=4.5m | Hs=6.5m | Hs=10.0m | Hs=12.2m |
|---|---|---|---|---|
| Mean | -4.599x10^-4 | -0.0024 | 0.0048 | 0.0026 |
| Variance | 0.0032 | 0.0220 | 0.0080 | 0.0423 |

From the table the variance increases as sea state increases with an exception for Hs=6.5 as discussed before. Mean values clearly exist for second order response while it was negligible for the measured response. Periods of zero up-crossing for second order heave response was calculated and is as shown in Table 5.2.

Table 6-2 Zero upcrossing of second order heave response

| | Hs=4.5m | Hs=6.5m | Hs=10.0m | Hs=12.2m |
|---|---|---|---|---|
| Zero upcrossing | 11.82sec | 13.67sec | 14.03sec | 16.77sec |

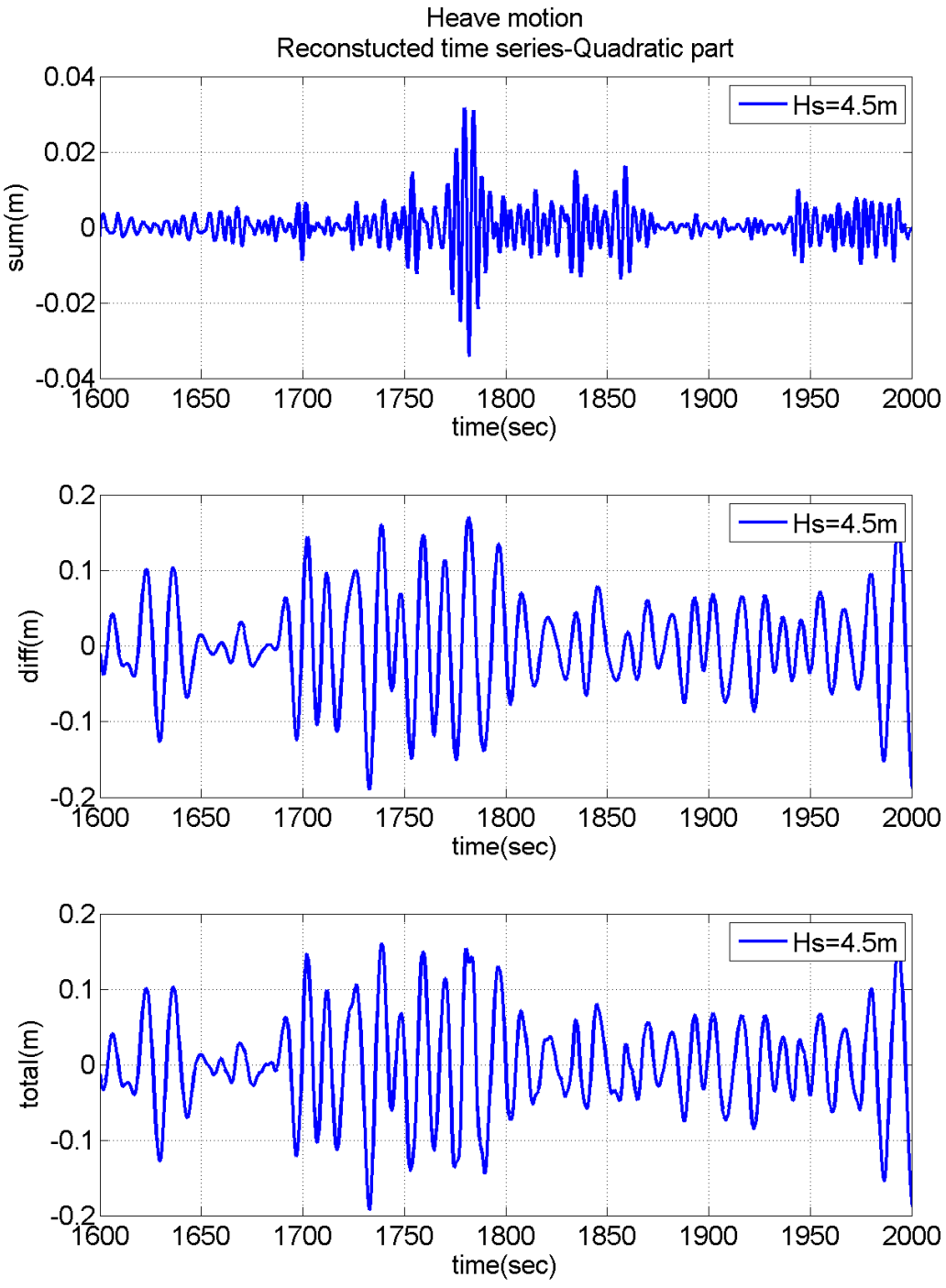


Figure 6-5 Reconstructed second order heave response from QTF - Hs=4.5m

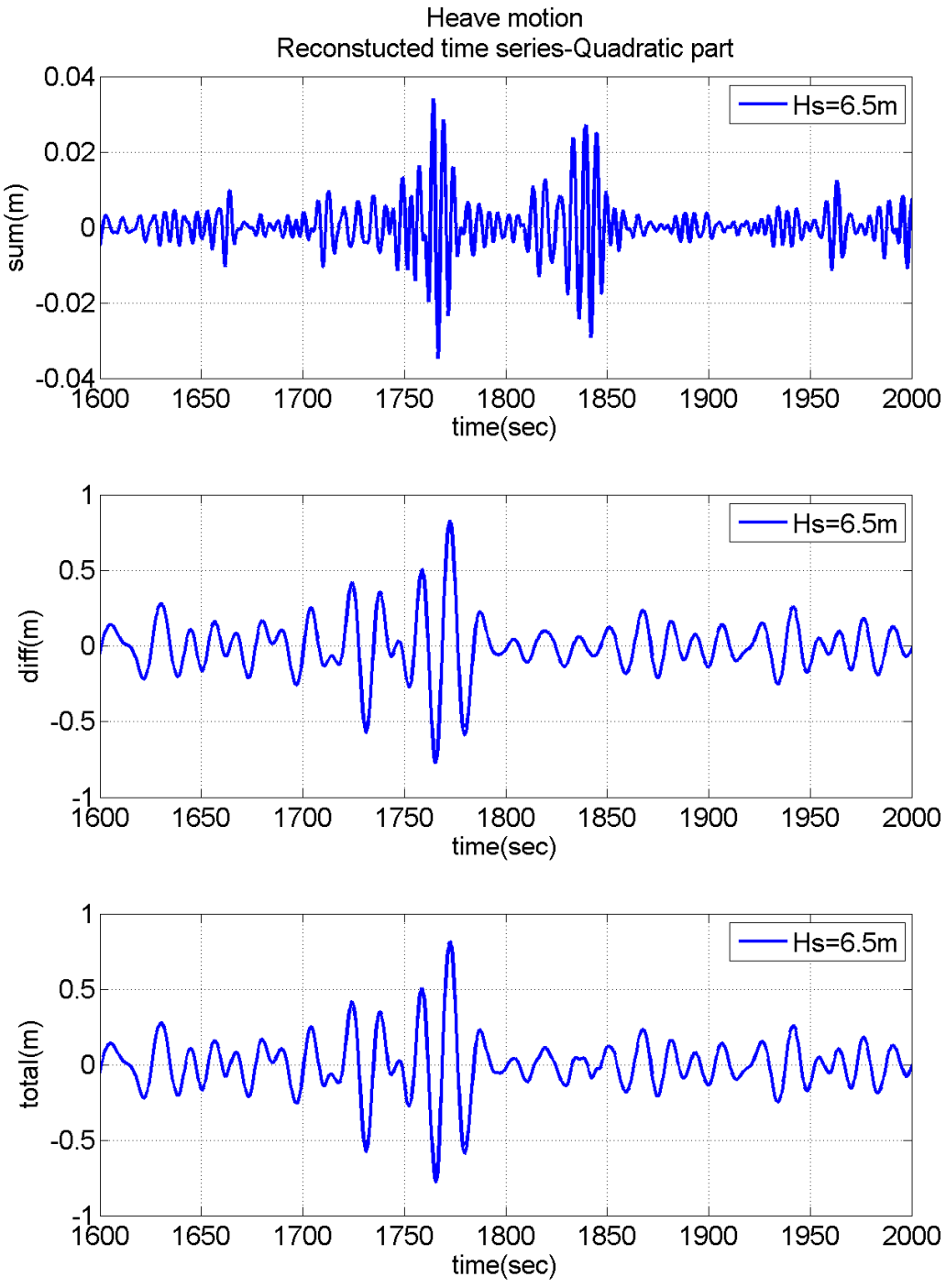


Figure 6-6 Reconstructed second order heave response from QTF - Hs=6.5m

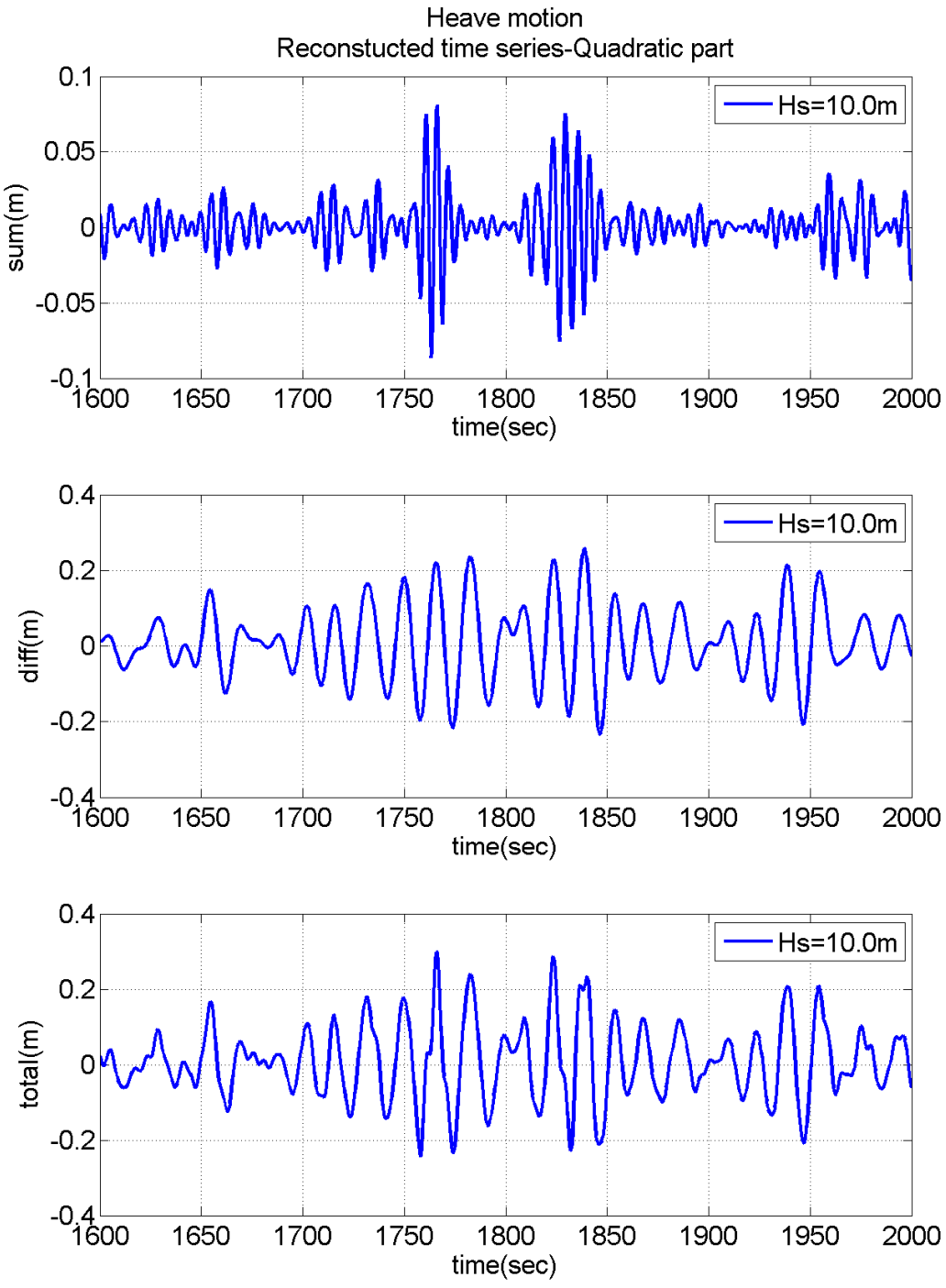


Figure 6-7 Reconstructed second order heave response from QTF - Hs=10.0m

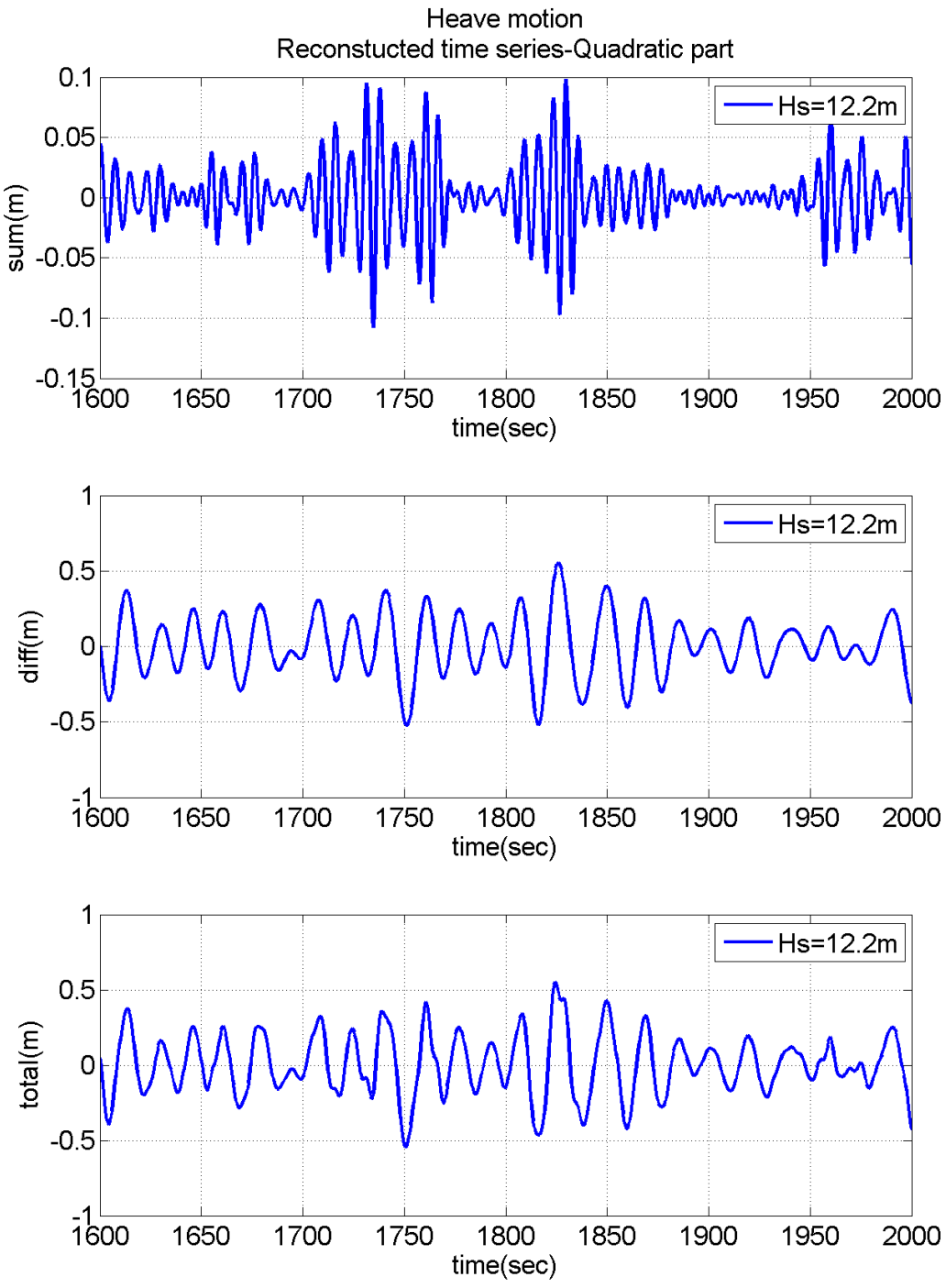


Figure 6-8 Reconstructed second order heave response from QTF - Hs=12.2m

## 6.3 Reconstruction of total heave response – LTF +QTF

Both linear and second order reconstructed response time series were added together to get the total response and were compared with the measured response as shown below from Figure 6-9 to Figure 6-12. Both reconstructed and measured matches very well.

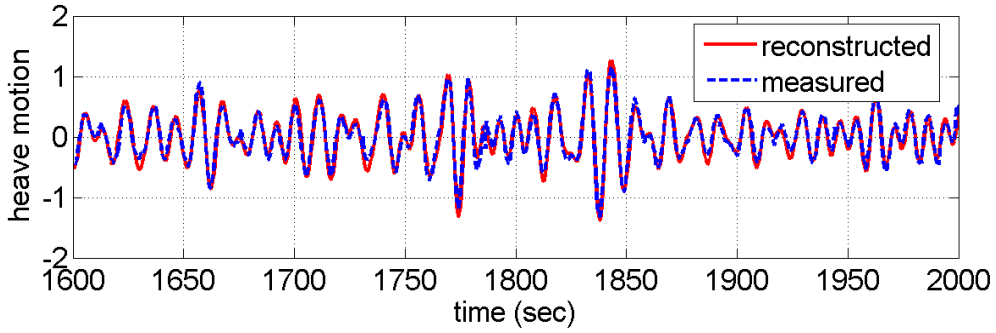


Figure 6-9 Reconstructed heave response from QTF+LTF for (Hs=4.5m)

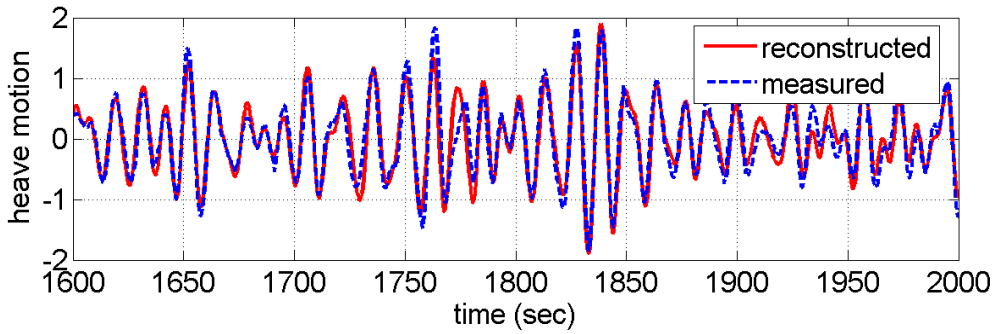


Figure 6-10 Reconstructed heave response from QTF+LTF for (Hs=6.5m)

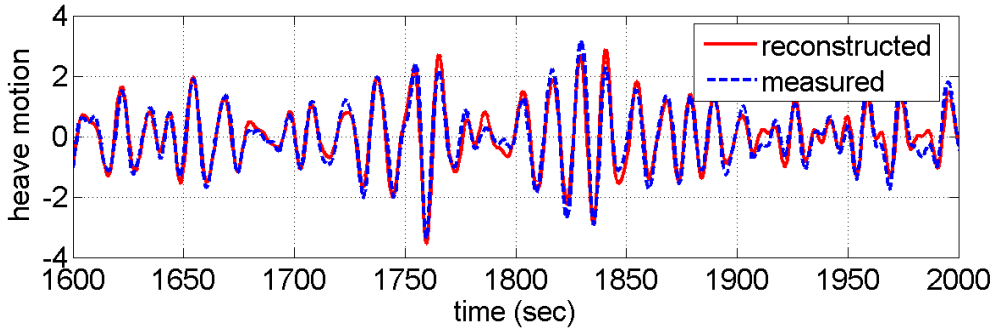


Figure 6-11 Reconstructed heave response from QTF+LTF for (Hs=10.0m)

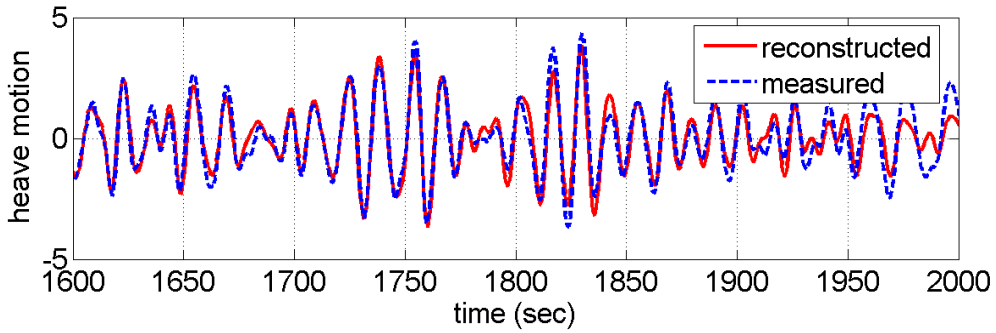


Figure 6-12 Reconstructed heave response from QTF+LTF for (Hs=12.2m)

## 6.4 Reconstruction of the pitch response (linear) from LTF

Similar to heave time series reconstruction, we applied the same method for the reconstruction of the Pitch time series. Pitch linear response was reconstructed from LTF and plotted as shown below from Figure 6-13 to Figure 6-16. Similar to heave response, an experimental LTF frequency range of 0.36 to 0.9 rad/sec was chosen for the reconstruction . Reconstruction from LTF itself exactly matches with measured one for the first two responses which is again an indication that second order contribution to the total response is negligible for them. Small difference in the reconstructed and measured responses was observed in the last two cases.

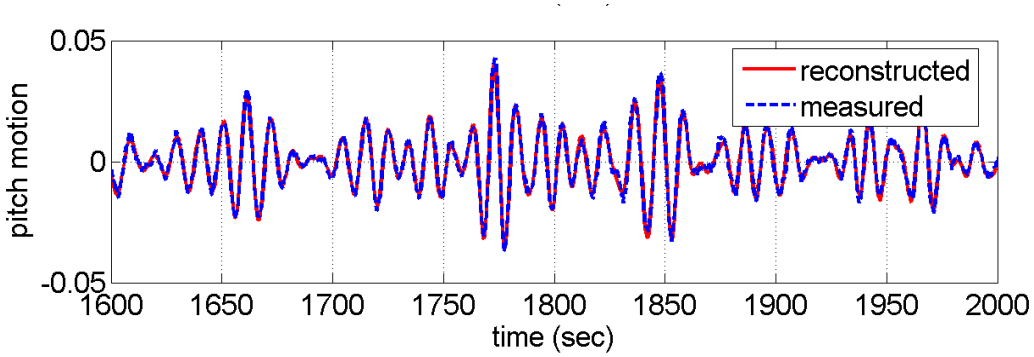


Figure 6-13 Reconstructed pitch linear response from LTF - Hs=4.5m

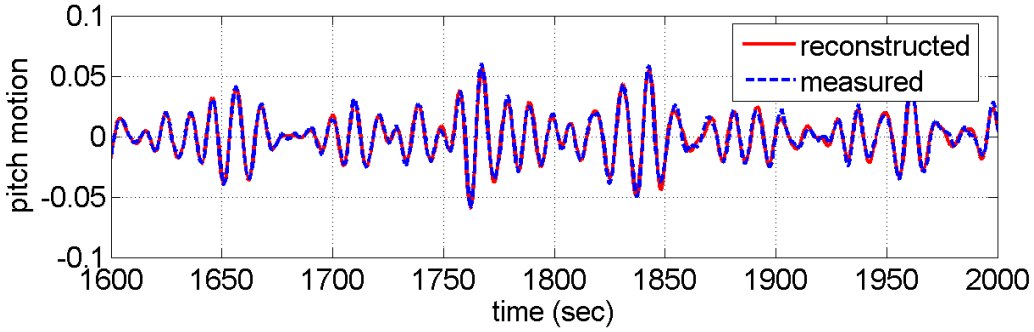


Figure 6-14 Reconstructed pitch linear response from LTF - Hs=6.5m

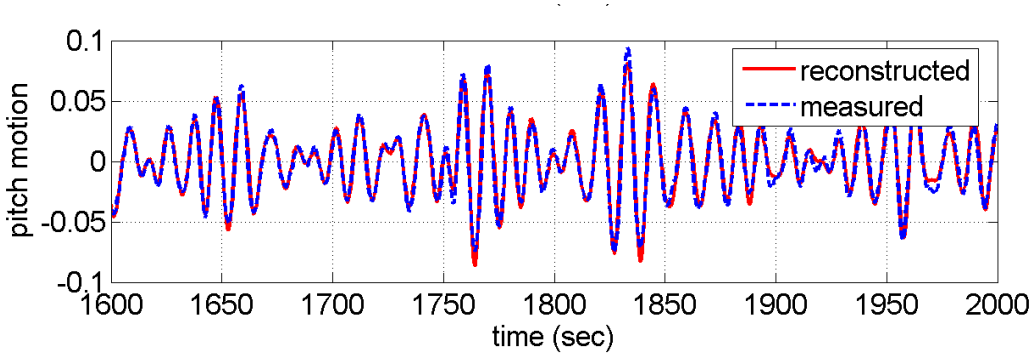


Figure 6-15 Reconstructed pitch linear response from LTF - Hs=10.0m

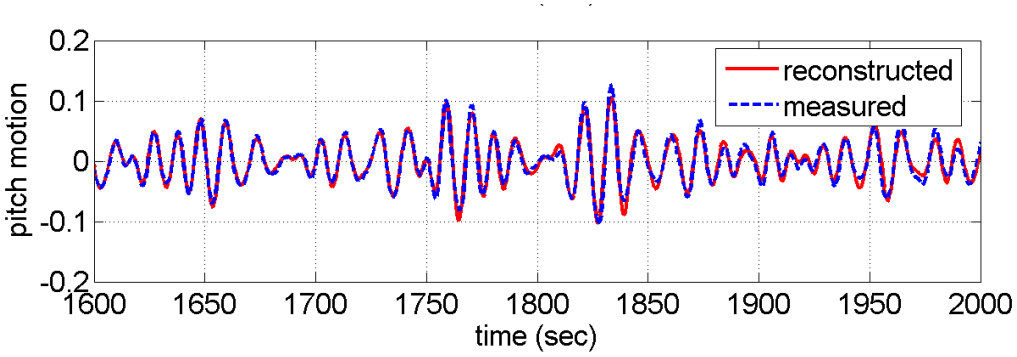


Figure 6-16 Reconstructed pitch linear response from LTF - Hs=12.2m

## 6.5 Reconstruction of second order pitch response from QTF

Second order pitch response was reconstructed from QTF as shown in Figure 6-17 to Figure 6-20 for all the four waves. Sum and difference frequency components move in groups showing the transient nature. Sum frequency component increases as the sea state increases. So unlike heave response both sum and difference frequency components are important in the higher seas. Mean and variance of second order pitch motion was calculated as is shown in Table 6-3.

Table 6-3 Mean and variance of second order pitch response

| | Hs=4.5m | Hs=6.5m | Hs=10.0m | Hs=12.2m |
|---|---|---|---|---|
| Mean | -4.95x10^-6 | -3.65 x 10^-5 | 4.467 x 10^-5 | 4.6135 x 10^-5 |
| Variance | 2.49 x10^-6 | 3.0179 x 10^-5 | 8.457 x 10^-6 | 2.2 x 10^-5 |

Mean pitch response is found to be negligibly small and increases as the sea state increases. Similar to heave response, the variance increases as the sea state increases except for response from input wave of Hs=6.5m which is difficult to explain. Zero upcrossing periods for the pitch response for all the seas were calculated and are shown in Table 6-4.

Table 6-4 Zero upcrossing periods of second order pitch response

| | Hs=4.5m | Hs=6.5m | Hs=10.0m | Hs=12.2m |
|---|---|---|---|---|
| Zero upcrossing period | 11.55 sec | 14.05 sec | 8.1566 sec | 8.7944 sec |

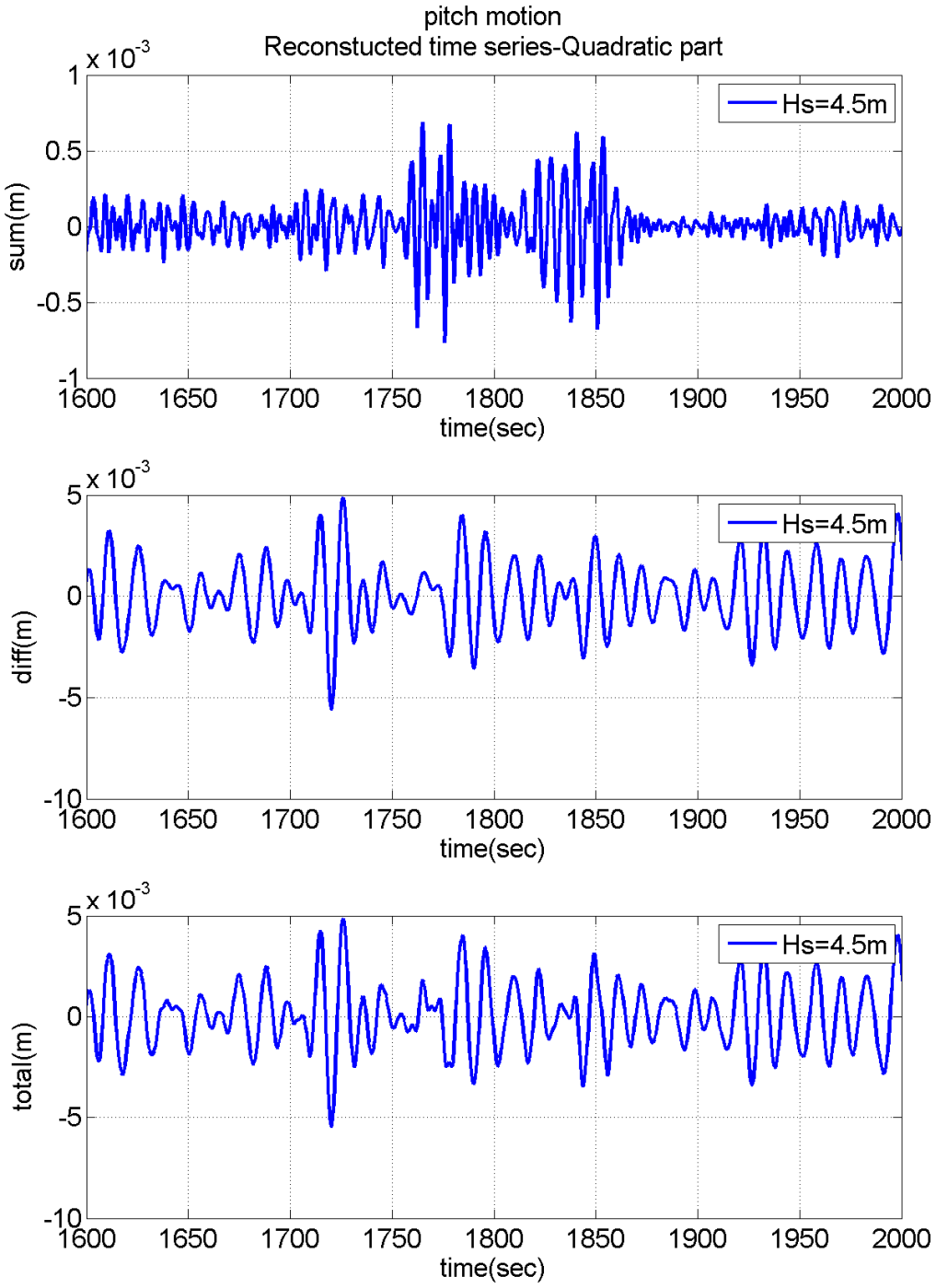


Figure 6-17 Reconstructed pitch response from QTF (Hs=4.5m)

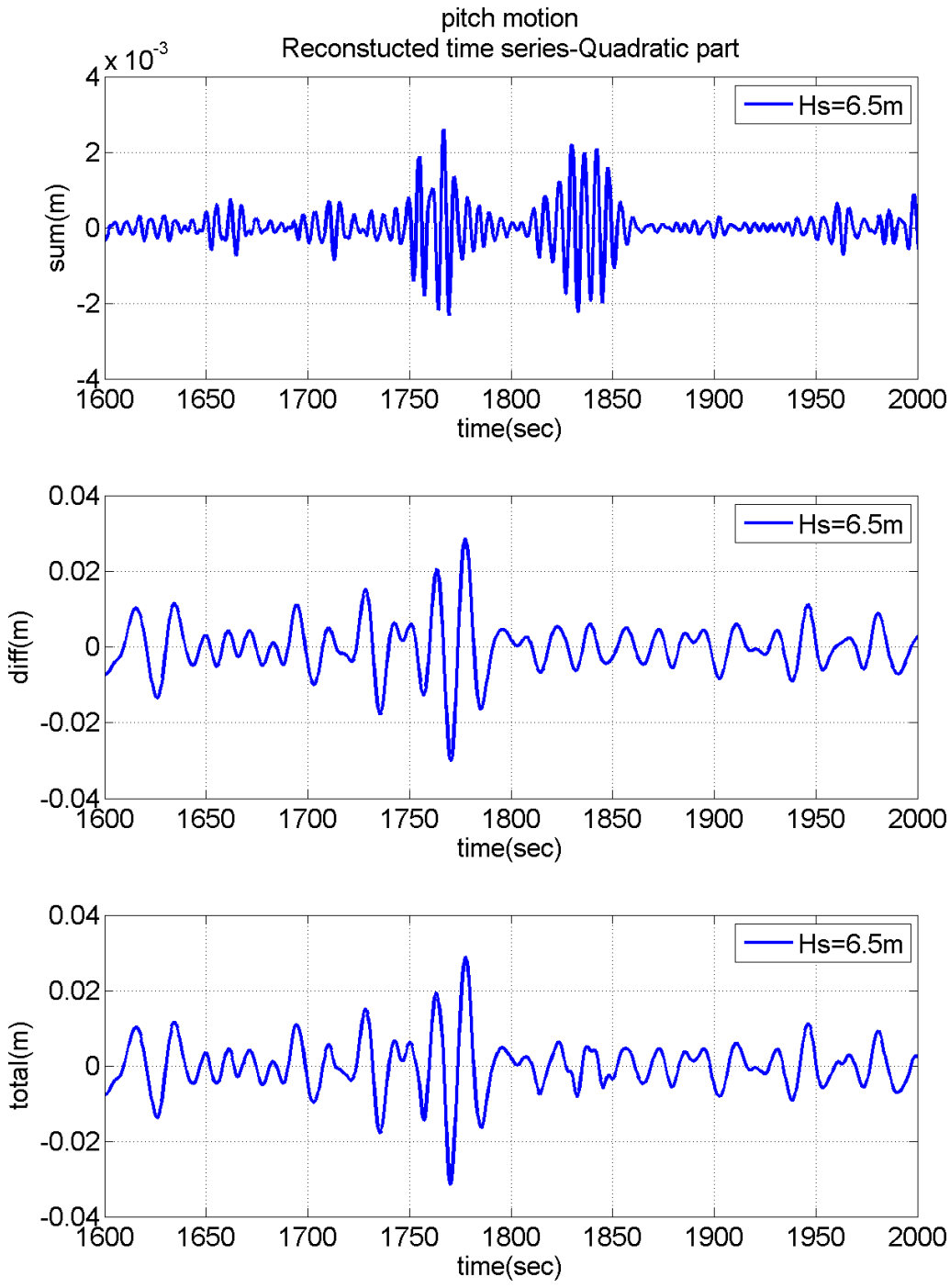


Figure 6-18 Reconstructed pitch response from QTF (Hs=6.5m)

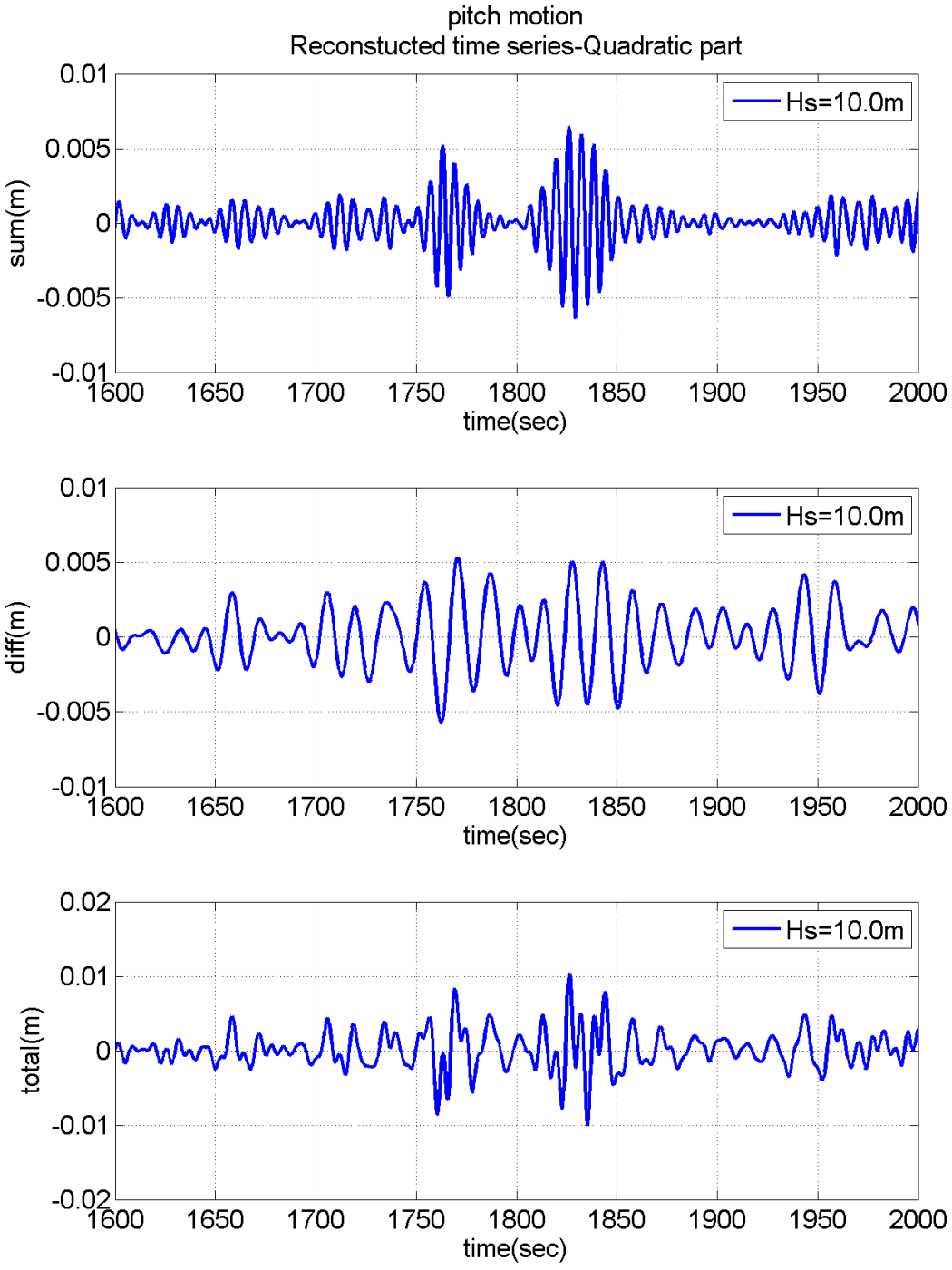


Figure 6-19 Reconstructed pitch response from QTF (Hs=10.0m)

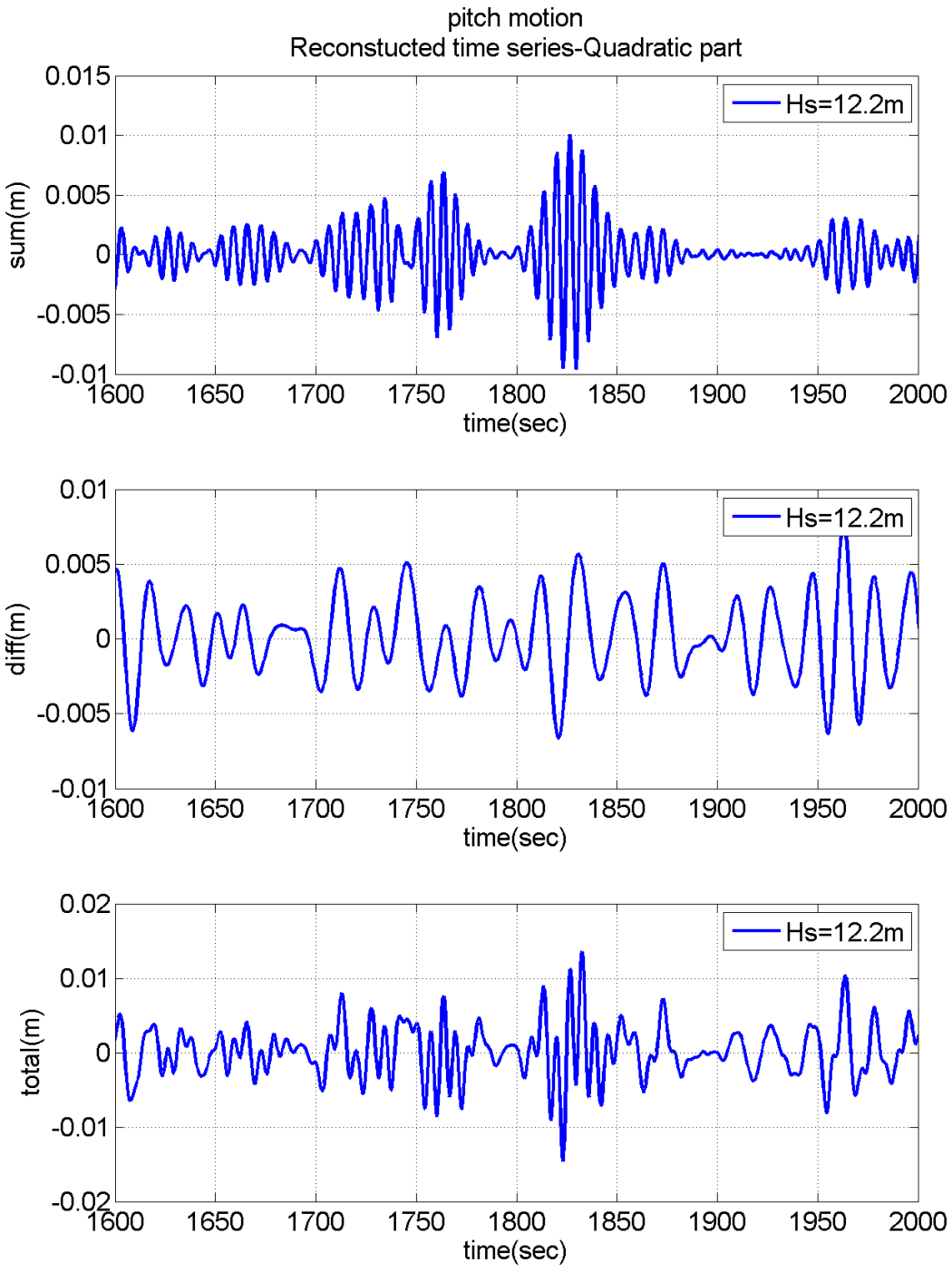


Figure 6-20 Reconstructed pitch response from QTF (Hs=12.2m)

## 6.6 Reconstruction of total pitch response- LTF+QTF

Total pitch responses were calculated from L+Q and plotted as shown in Figure 6-21 to Figure 6-24. The reconstructions are in good agreement with respective measured responses.

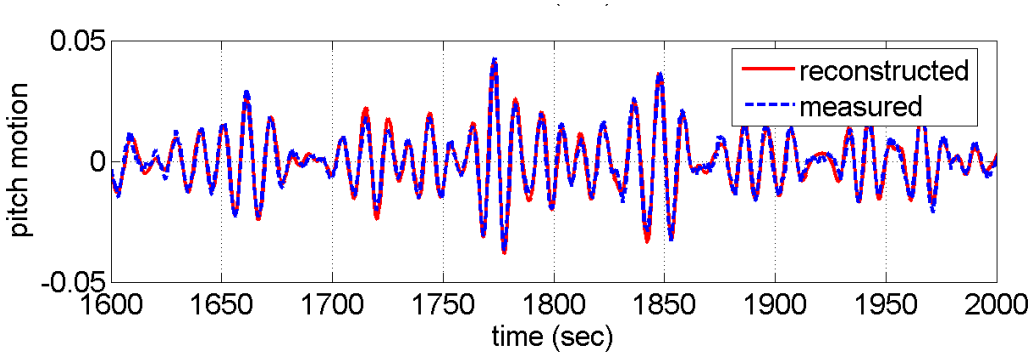


Figure 6-21 Reconstructed total pitch response (LTF+QTF) - Hs=4.5m

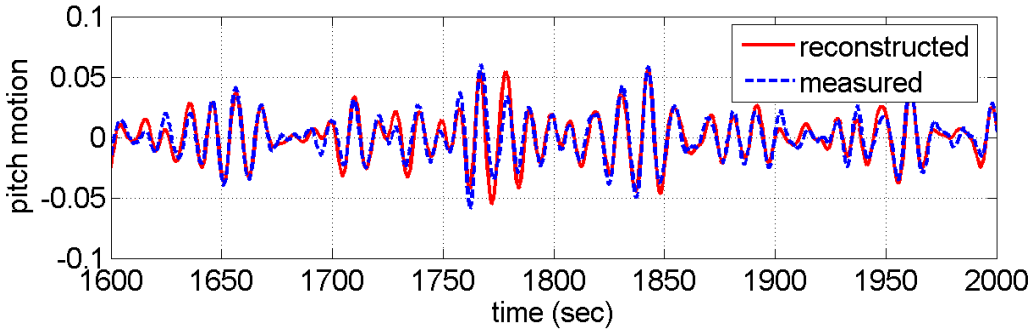


Figure 6-22 Reconstructed total pitch response (LTF+QTF) - Hs=6.5m

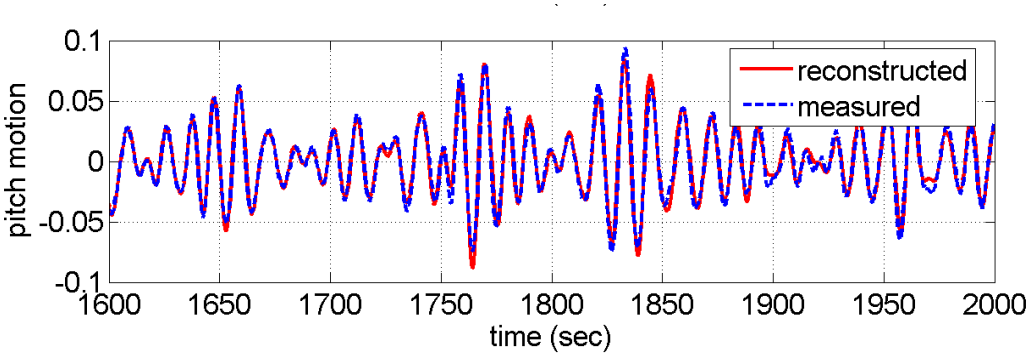


Figure 6-23 Reconstructed total pitch response (LTF+QTF) - Hs=10.0m

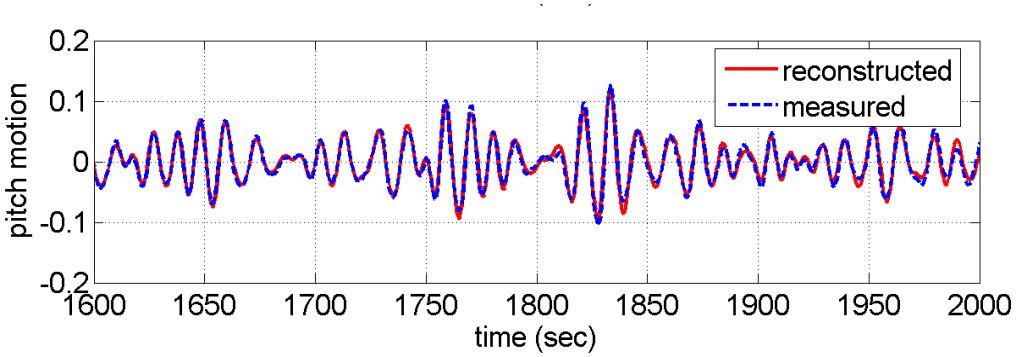


Figure 6-24 Reconstructed total pitch response (LTF+QTF) - Hs=12.2m

## 6.7 Heave response energy spectrum; reconstructed vs. experiment

Energy spectra of total reconstructed heave responses were calculated using Fourier transform and compared with measured response spectra. These were plotted as shown in Figure 6-25 to Figure 6-28 on a semi logarithmic scale so that minute details were available for inspection. It was observed that both spectra match exactly in the experimental LTF frequency range of 0.36 to 0.9 rad/sec. For the responses due to input waves of Hs=6.5 m and 12.2 m, lower frequency response (reconstructed) is higher than measured response in the range between 0.15 to 0.25 rad/sec. The method overestimated

the second order difference frequency component in these range of frequency. This may be due to very low values at the tail of autospectrum resulting in higher values of QTF as discussed in Figure 2-4. Energy spectrum of the reconstructed response does not match with the measured wave spectrum for a frequency ranges outside LTF frequency range. It was inferred that higher order responses greater than second order was present in the total response. It was assumed that proper calculation of higher order response and summing up to the first and second order responses will result in the measured energy spectrum.

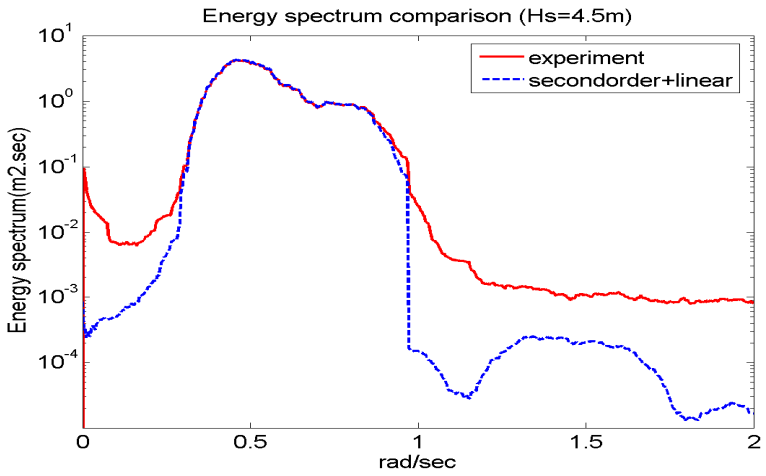


Figure 6-25 Reconstructed vs. measured response energy spectrum (Hs=4.5m)

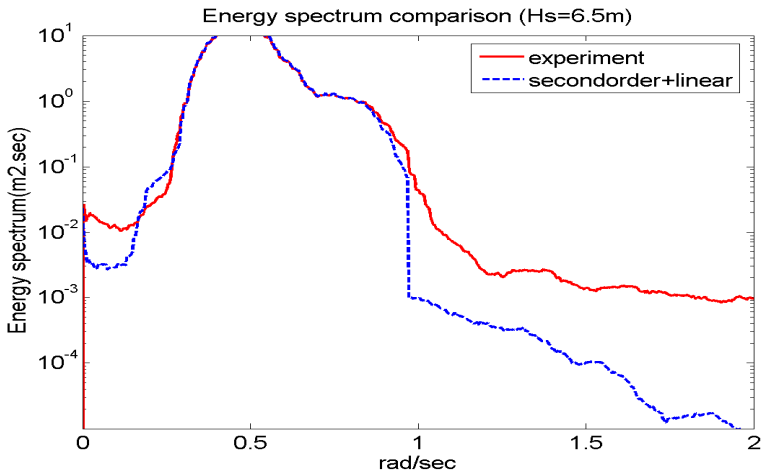


Figure 6-26 Reconstructed vs. measured response energy spectrum (Hs=6.5m)

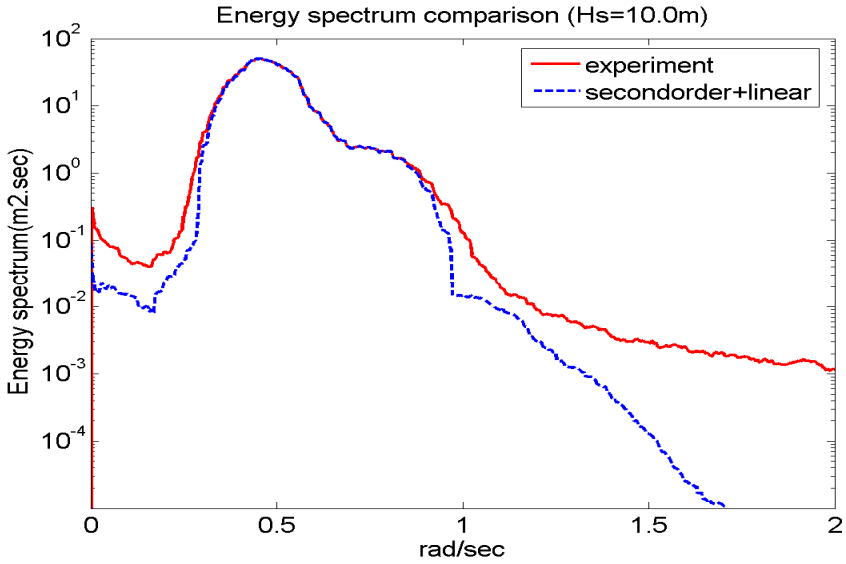


Figure 6-27 Reconstructed vs. measured response energy spectrum (Hs=10.0m)

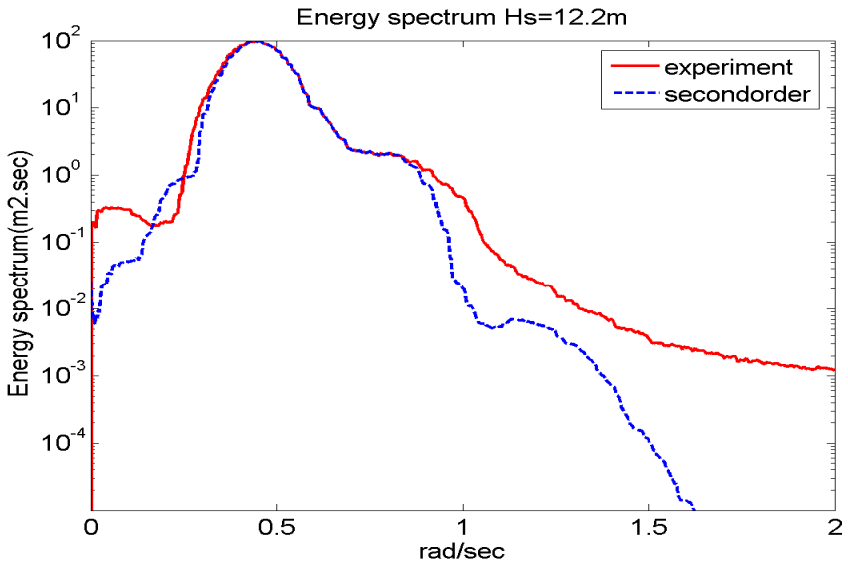


Figure 6-28 Reconstructed vs. measured response energy spectrum (Hs=12.2m)

## 6.8 Coherency of reconstructed heave response

The coherencies of the reconstructed response from experimental LTF and QTF are plotted as shown in Figure 6-29 to Figure 6-32. The reconstruction from experimental LTF shows a coherency of 1. Coherency of second order response almost lies outside the experimental LTF frequency range. This validated our assumption that frequency range between 0.36 to 0.9 rad /sec falls in the linear frequency range, if the higher order term responses greater than second order are absent in these region. Second order responses do not have any effect on the resonance frequency 0.83 rad/sec which lies completely in the linear frequency range. Coherency of response due to input waves of Hs=6.5m and 12.2m are greater than 1 (approx. equal to 2.5) for a frequency range of 0.15 to 0.25 rad /sec which is due to overestimation in calculation as discussed in section

6.7. This may be due to high values in the QTF calculation due to presence of very small values in the tail of the energy spectrum which comes in the denominator in the equation 2-60.Coherency value at 0 rad/sec frequency indicates the second order mean heave motion which was observed for all the responses except for the first wave. This observation is an indication of the presence of second order slowly varying heave drift motion.

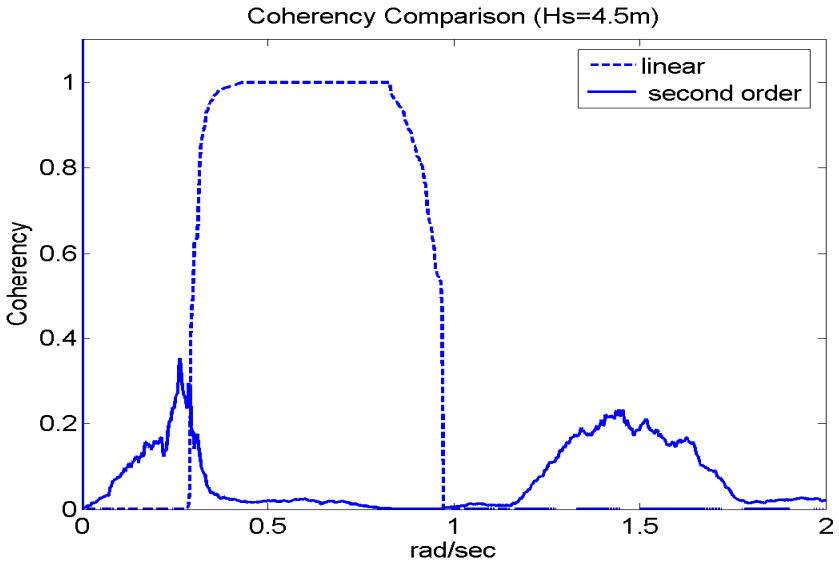


Figure 6-29 Coherency test for the reconstructed heave response - Hs=4.5m

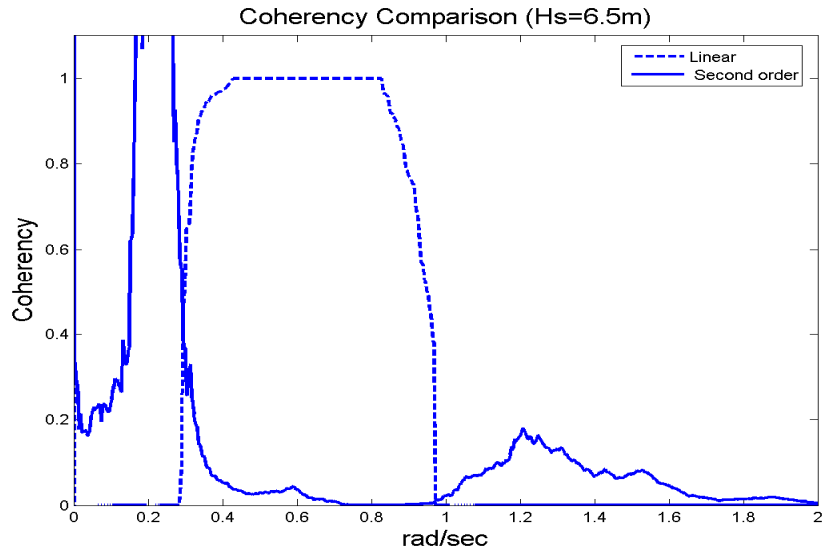


Figure 6-30 Coherency test for the reconstructed heave response - Hs=6.5m

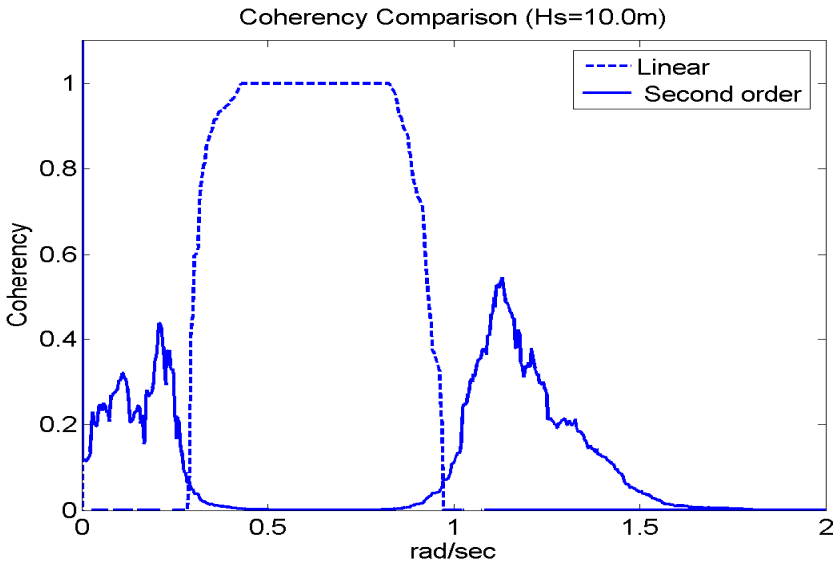


Figure 6-31 Coherency test for the reconstructed heave response - Hs=10.0m

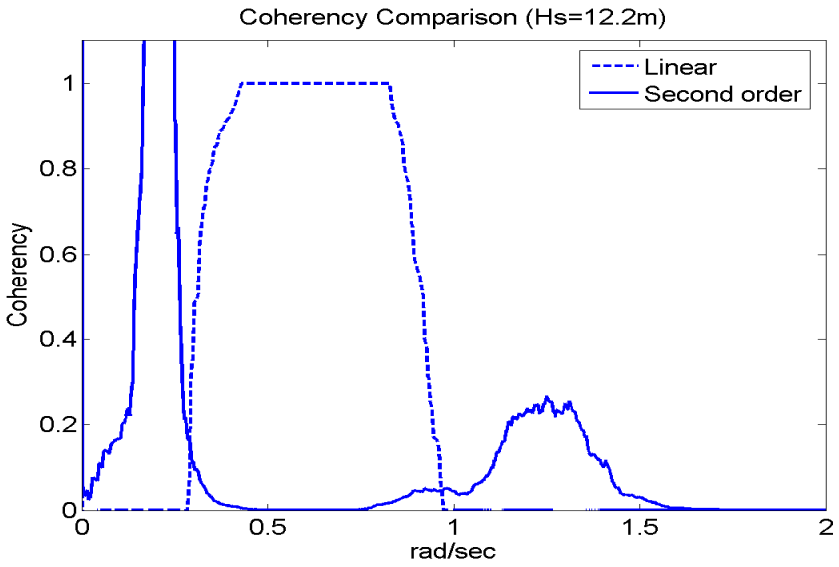


Figure 6-32 Coherency test for the reconstructed heave response - Hs=12.2m

## 6.9 Pitch response energy spectrum; reconstructed vs. experiment

Second order pitch energy spectra were calculated using Fourier transform and were compared with measured spectrum as shown in Figure 6-33 to Figure 6-36. Similar to heave response, pitch energy spectra in the experimental LTF frequency range exactly follows the measured spectra. Addition of higher order terms is required to make total response equivalent to measured response. Overestimation of energy spectra in low frequency range is observed for Hs=6.5m and 12.2m.

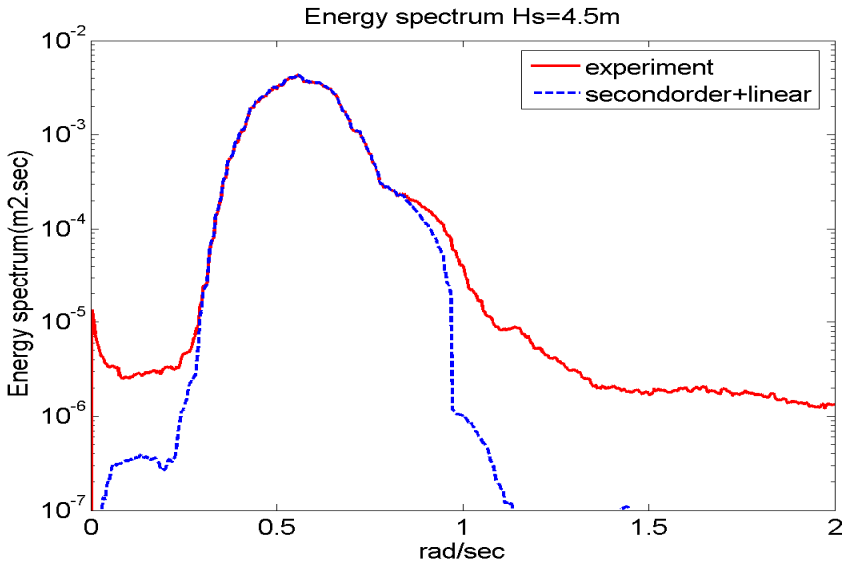


Figure 6-33 Reconstructed vs. measured pitch energy spectrum - Hs=4.5m

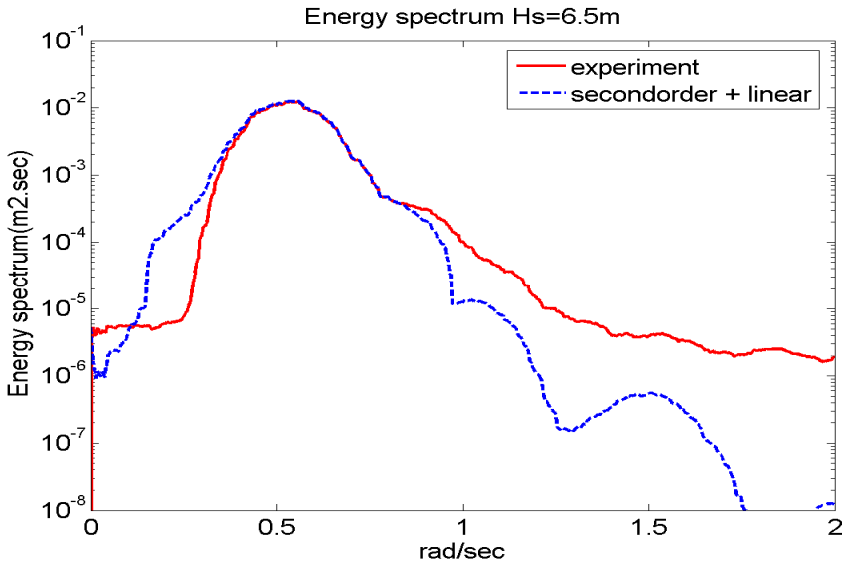


Figure 6-34 Reconstructed vs. measured pitch energy spectrum - Hs=6.5m

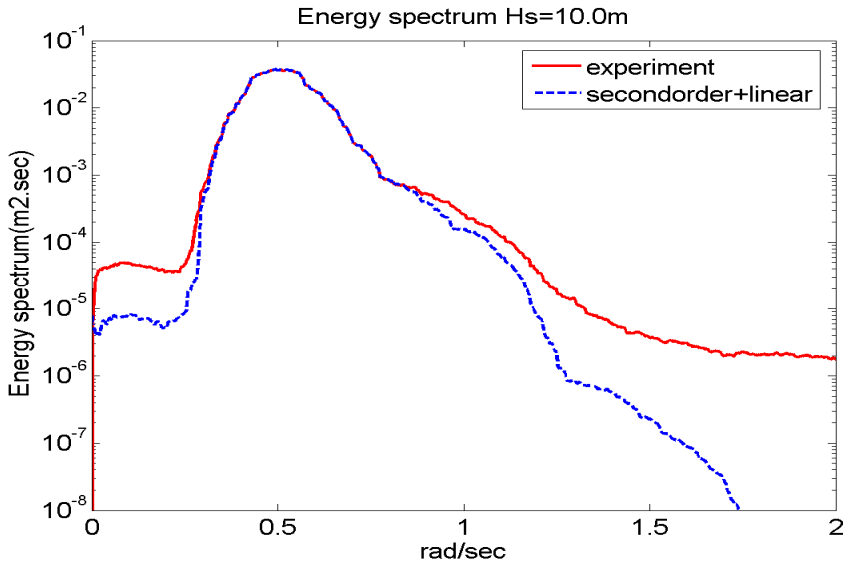


Figure 6-35 Reconstructed vs. measured pitch energy spectrum - Hs=10.0m

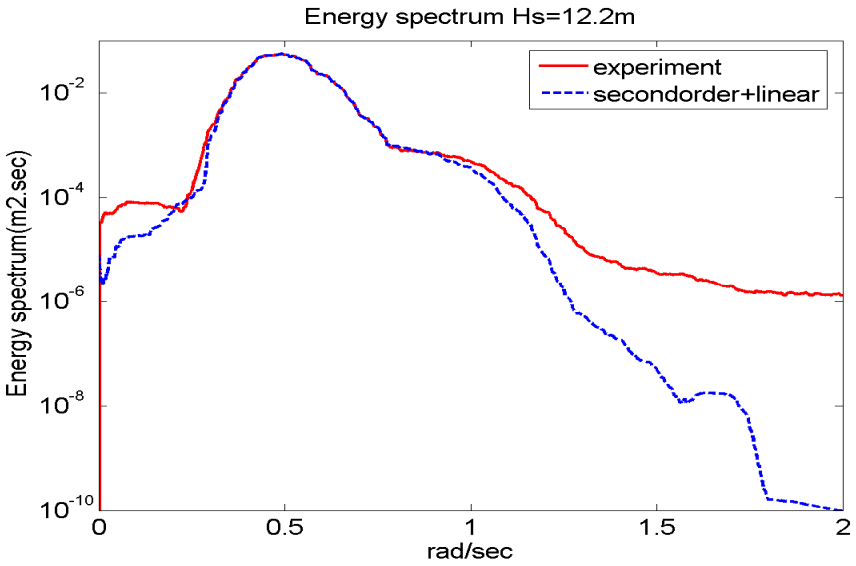


Figure 6-36 Reconstructed vs. measured pitch energy spectrum - Hs=12.2m

## 6.10 Coherency of reconstructed pitch response

Coherency of reconstructed responses from experimental LTF (linear) and QTF are shown in Figure 6-37 to Figure 6-40 . Similar to heave response, total responses mainly constitutes of linear part between 0.35 to 0.9 rad/sec. Contribution from second order response is very small and is almost zero in some regions. High pitch coherency value in high frequency range was noticed. So in high frequency range second order response contribution to the measured response is much higher than low frequency range. Referring to pitch motion cross-bi spectrum and QTF, it was observed that in addition to sum frequency component, output frequency of a small part of difference frequency also lies in the high frequency range. So both sum and a part of difference frequency contribute to the high frequency range. Energy spectra of pitch response due to input waves of Hs=6.5 m and 12.2 m were overestimated similar to heave response.

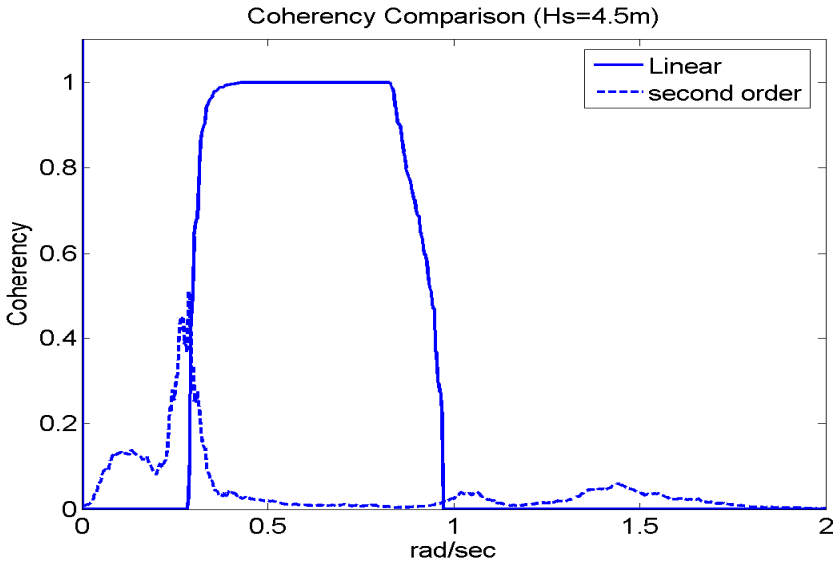


Figure 6-37 Coherency test for the reconstructed pitch response - Hs=4.5m

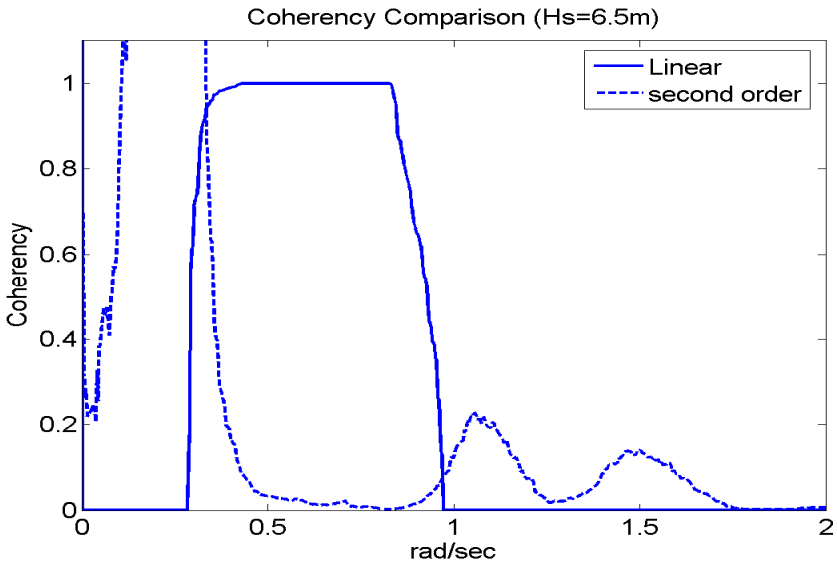


Figure 6-38 Coherency test for the reconstructed pitch response - Hs=6.5m

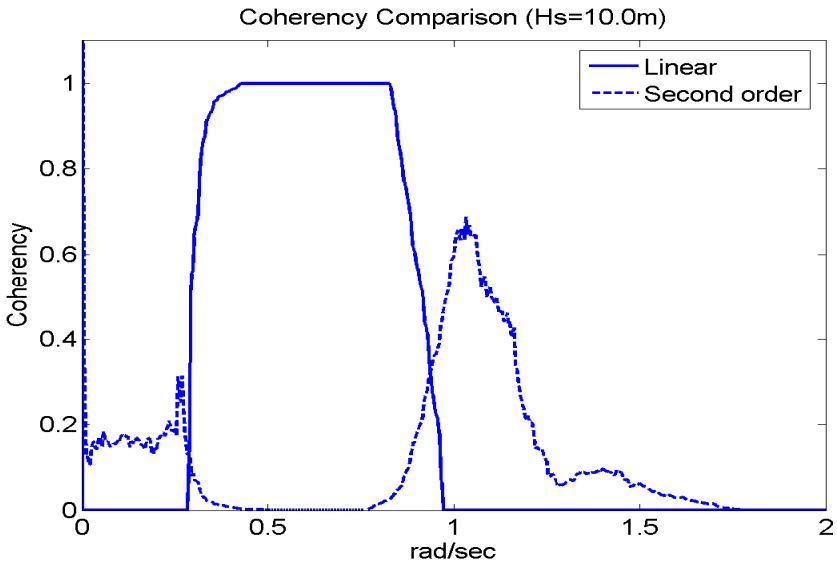


Figure 6-39 Coherency test for the reconstructed pitch response - Hs=10.0m

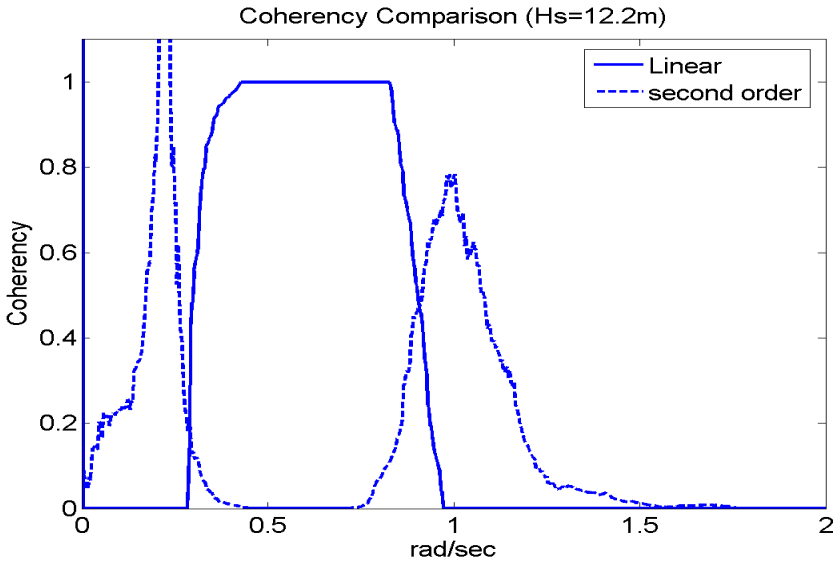


Figure 6-40 Coherency test for the reconstructed pitch response - Hs=12.2m

# CHAPTER VII

# UNIOM-MOTION MODEL

## 7.1 UNIOM-heave and pitch motion

UNIOM (Universal Nonlinear Input-Output Model) is based on the assumption that a non linear real wave input acting on a system will produce non linear output which is best described by the following schematic diagram.

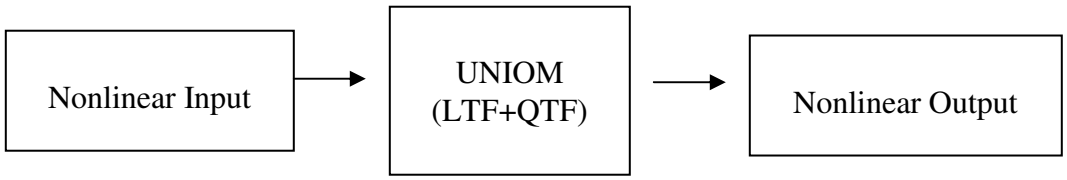


Figure 7-1 Schematic diagram for UNIOM Model

This approach has been previously used by Adil ( Adil 2004) , Richer (Richer 2005), Rajith ( Rajith 2006) for the calculation of forces and motions. A detailed description of this method is given by Kim (2008). Even though proper theoretical background has been developed for the calculation of UNIOM-diffraction and UNIOM-Kinematics, such an approach was not in this case due to insufficient time. But from the previous experience and intuition we applied this method for the prediction of ship vertical response as well and found to be helpful in prediction of the response.

UNIOM is a semi-empirical model which uses the real wave data from the wave tank and hydrodynamically calculated system behavior (e.g. LTF & QTF). For the hydrodynamic LTF (RAO), theoretical LTF values provided by Dr.Yongwan Kim from

Seoul University were used. These values were calculated by a 3D Panel program called as 'WISH' based on a Rankine panel method and time domain approach. This software have already compared and validated the output with other recognized ship motion softwares used in industry like 'SWAN' and 'LAMP'. Calculation and application of theoretical QTF in UNIOM application was beyond the scope of the project and was hence avoided.

UNIOM-Motion equation can be written as given below.

$$y(t) = \mathrm{Re}\left[\sum_{j=1}^{n} A_j (LTF)_j e^{-i\omega_j t}\right] + \mathrm{Re}\frac{1}{2}\left[\sum_{j=1}^{n}\sum_{k=1}^{n} A_j A_k (QTF)_{jk}^{\pm} e^{-i(\omega_j \pm \omega_k)t}\right] \quad 7\text{-}1$$

where $A_j$ denotes the complex amplitude of the measured wave, indicating amplitude and phase angle. Note that this is not the familiar random phase angle as has been used in the Volterra quadratic model that assumes Gaussian input. UNIOM transmits at each time step precisely the effect of the nonlinearity of the wave onto the response. This study used only the first part of equation which includes LTF as discussed before.

## 7.2 Comparison of heave response from UNIOM with measured response

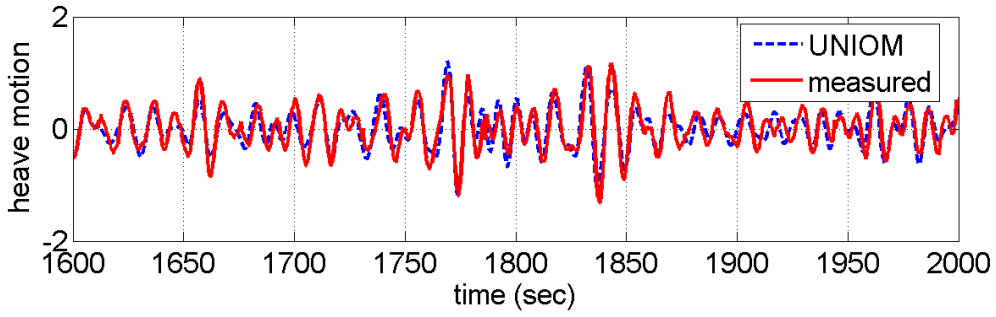


Figure 7-2 Heave response from UNIOM compared with measured response (Hs=4.5m)

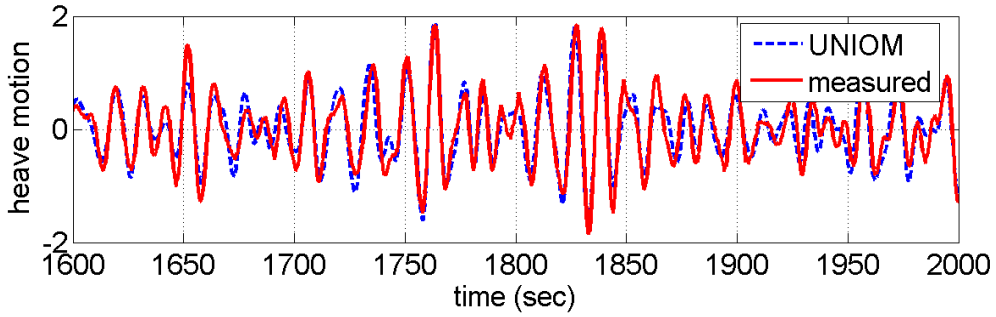


Figure 7-3 Heave response from UNIOM compared with measured response (Hs=6.5m)

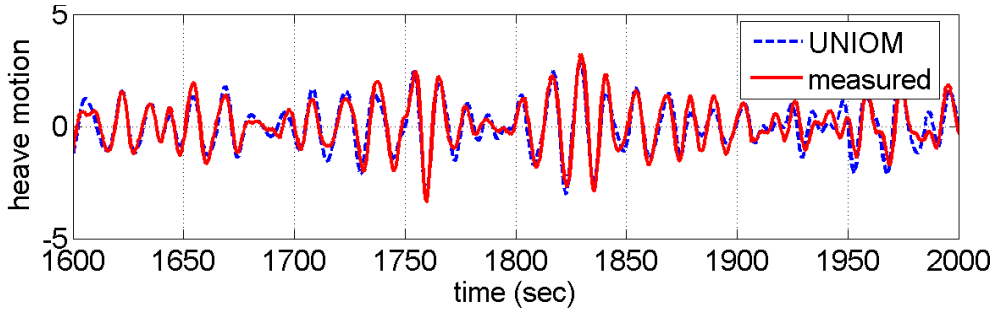


Figure 7-4 Heave response from UNIOM compared with measured response (Hs=10.0m)

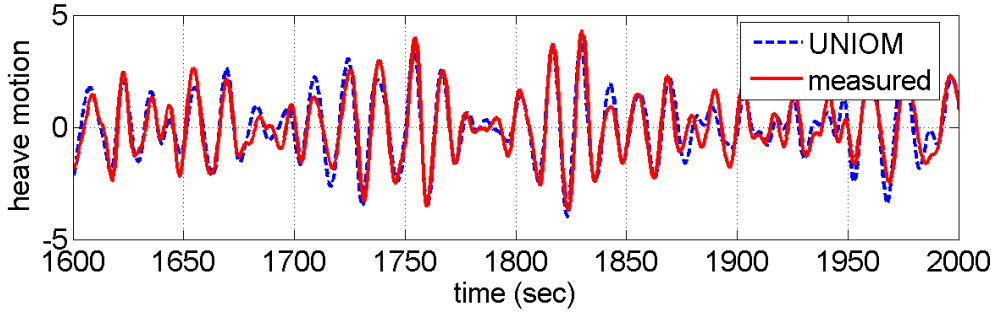


Figure 7-5 Heave response from UNIOM compared with measured response (Hs=12.2m)

Heave response were calculated using UNIOM- LTF and were plotted along with measured response as shown in

Figure 7-2 to Figure 7-5 . It was clearly visible that UNIOM response almost exactly follows the measured response. But it is necessary to have clear picture of the comparison so we compared the responses in terms of variances. The variance was calculated up to 2000 sec as shown in Table 6.1. The variances of UNIOM are higher than those of experiment above sea state Hs =10.0 m. The UNIOM seems to work for the first three sea states. Thus UNIOM-Motion-LTFs does not simulate closely beyond Hs = 10 m. It may be due to the lack of the QTF.+ CTF which beyond the scope of this study.

Table 7-1 Comparison of variance of heave from experiment and UNIOM

| Significant wave height(m) | Variance (experiment) | Variance (UNIOM) |
|---|---|---|
| 4.5 | 0.1703 | 0.1466 |
| 6.5 | 0.51 | 0.4982 |
| 10.0 | 1.5225 | 1.7039 |
| 12.2 | 2.8487 | 3.2486 |

## 7.3 Comparison of peak values of heave motion from UNIOM and measured response

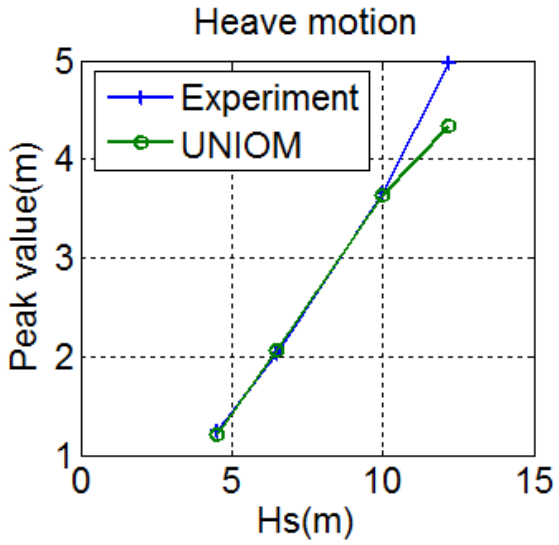


Figure 7-6 Peak values of heave motion from experiment and UNIOM

Peak values were picked from UNIOM simulated heave motion time series and experiment, compared and plotted as shown in Figure 7-6.

Table 7-2 Comparison of heave peak between UNIOM and experiment

| Significant wave height (m) | Peak value (experiment) | Peak value (UNIOM) | % error |
|---|---|---|---|
| 4.5 | 1.2457 | 1.2019 | 3.5 |
| 6.5 | 2.0298 | 2.0574 | 1.36 |
| 10.0 | 3.6519 | 3.6434 | 0.2 |
| 12.2 | 4.976 | 4.3406 | 12.7 |

The peak responses simulated are within 10% error for the first three seas. Here again we have relatively large discrepancy at the 4$^{th}$ sea, i.e., the simulated peak is found to be less than the measured. The foregoing comparisons indicate that the UNIOM-diffraction-LTFs does not simulate closely when the seas are higher than the sea of significant wave height 10.0 m. This situation indicates that the deficit might be due to the lack of higher-order frequency response function such as QTFs and CTFs.

## 7.4 Comparison of pitch response from UNIOM with measured response

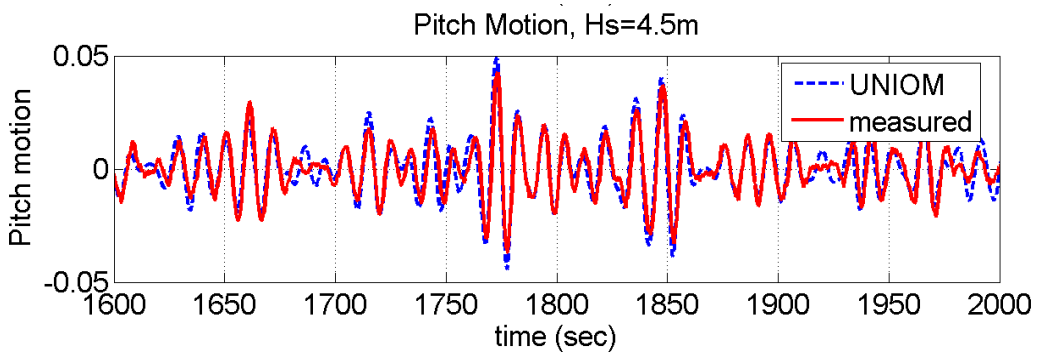


Figure 7-7 Pitch response from UNIOM compared with measured response (Hs=4.5m)

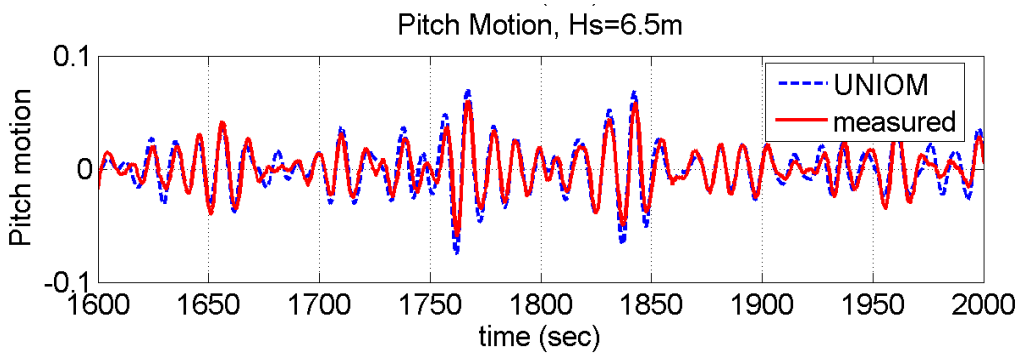


Figure 7-8 Pitch response from UNIOM compared with measured response ( Hs=6.5m)

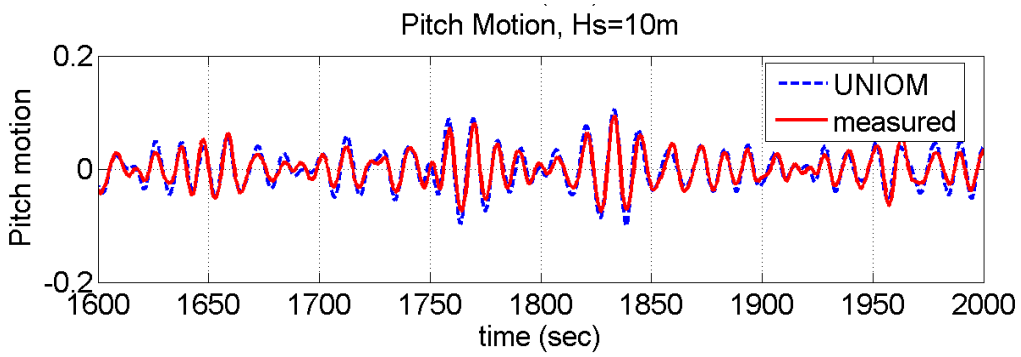


Figure 7-9 Pitch response from UNIOM compared with measured response ( Hs=10.0m)

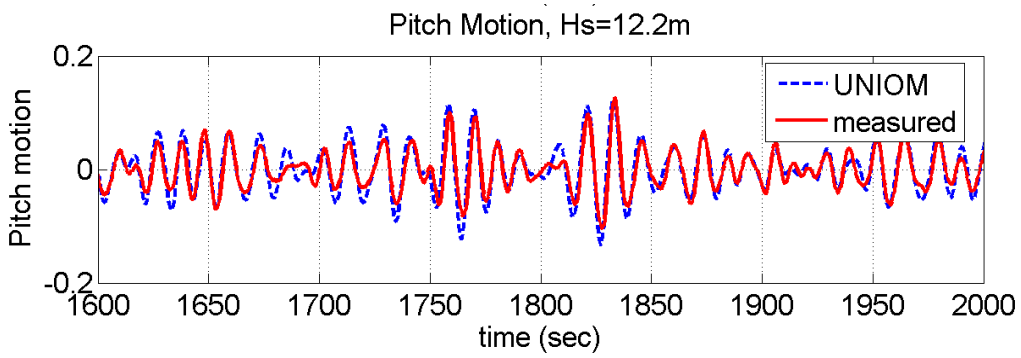


Figure 7-10 Pitch response from UNIOM compared with measured response (Hs=12.2m)

It is clearly visible from Figure 7-7 to Figure 7-10 that UNIOM-Pitch motion time series follows almost similarly to the measured response. But it is necessary to check the difference in variance of the simulation and measured responses.

Table 7-3 Pitch motion variance compared for UNIOM and experiment

| Significant wave height(m) | Variance (experiment) | Variance (UNIOM) |
|---|---|---|
| 4.5 | 0.0002 | 0.0002 |
| 6.5 | 0.0005 | 0.0006 |
| 10.0 | 0.0014 | 0.0019 |
| 12.2 | 0.0020 | 0.0030 |

The difference in variance between UNIOM and measured becomes larger as it goes to higher sea state as shown in Table 7-3.

## 7.5 Comparison of peak values of pitch motion from UNIOM and measured response

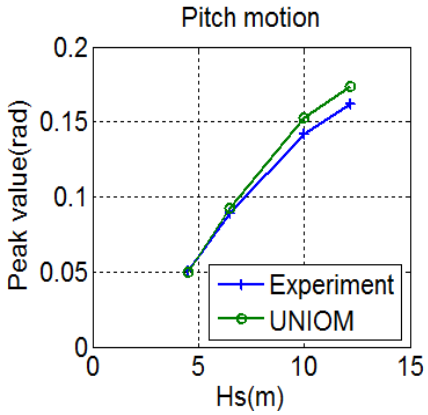


Figure 7-11 Peak values of pitch motion from experiment and UNIOM

Peak values of pitch motion were computed and plotted as shown in Figure 7-11 and difference in their values were given in the below table.

Table 7-4 Pitch peak comparison between experiment and UNIOM

| Significant wave height (m) | Pitch Peak value for 4000sec (experiment) | Pitch Peak value for 4000 sec (UNIOM) | % error |
|---|---|---|---|
| 4.5 | 0.0504 | 0.05 | 0.79 |
| 6.5 | 0.0889 | 0.0922 | 3.71 |
| 10.0 | 0.1418 | 0.1531 | 7.96 |
| 12.2 | 0.1619 | 0.1733 | 7.04 |

It can be seen that error in the peak value estimation is less than 10% which implies UNIOM-Model as a good prediction model in high seas.

# CHAPTER VIII

## SUMMARY AND CONCLUSION

Linear transfer functions are generally considered as a system characteristics and are completely independent of sea states. But this assumption was questioned by Dalzel.et.al (1962) by conducting experiment on pitch motion of destroyer. He found that in addition to system characteristics, transfer functions also depend on sea severity. This research reinvestigated and validated this result by studying the heave and pitch motion of a conventional 175 m container ship with zero speed. We found that vertical response transfer function decreases as sea severity increases and theory overestimates the peak up to 42% in the case of heave motion and 30% in the pitch motion. We again reconfirmed this difference by comparing the experimental LTF with theoretical LTF. The same study was conducted on second order responses. QTFs were extracted from the second order vertical response using Blackman-Tuky method. From this study it was found that QTF is also a function of sea severity and it decreases as sea state increases even though discrepancy was found in the case of response due to input wave of Hs=12.2m.

Volterra quadratic model was found to be a powerful tool for the estimation of QTF and extraction of second order response. In this study non Gaussian waves were used for the generation of vertical response. A complete decomposition of the measured responses into linear responses was not possible due to uncertainty regarding the involvement of higher order terms. Over estimation of second order vertical responses in the low frequency range was observed for two cases which may be due to low values of

energy spectra at the tails during the approximation of Volterra model. Still the research had given insight into overall effect of second order motion in the vertical response of a ship. The effect of sea severity on QTF was clearly observed in the behavior of responses due to input wave of Hs=4.5 and 10m. Second order response frequencies were found to be outside the heave and pitch natural frequency. Further study of variances between reconstructed second order responses and measured responses showed that second order motion have negligible effect on the vertical response (pitch and heave) of a ship (1 to 2% of measured response) . Mean components of the second order responses were noticed and slowly varying heave motion were observed for all the seas except for the lowest one (Hs=4.5m).

Reconstruction of the responses using our assumed linear frequency range alone was found to be closely following the measured responses. Addition of second order responses was having negligible effect. The effect of second order responses on the total responses were further studied in the Coherency value and found that effect of second order responses were negligible in the frequency range 0.35 to 0.9 rad/sec which was our area of interest.

In the second stage of the research a preliminary study on the UNIOM-Model was done. In this study, the UNIOM simulated vertical response and measured responses were compared. In addition, we calculated the peak values of the simulation and compared with the peak values of experiment. It was seen that UNIOM –Motion gives a good prediction of the response especially for response due to input wave of Hs=10.0m. Error in pitch motion peak value prediction was less than 10% which is a noticeable

result. Since we confined our UNIOM study to theoretical LTF it was expected that inclusion of higher order system characteristics will drastically improve the method.

# REFERENCES

Adil, A. (2004). "Simulation of ship motion and deck wetting due to steep random sea," *Master Thesis*, Texas A&M University, College Station, Texas.

Barret, N (1963). "The use of functional in the analysis of non-linear physical systems," *J. of Electronics and Control*, 15(6), pp.567-615.

Cummins, W. E. (1973). "Pathologies of the transfer functions," *The Seakeeping Symposium Commemorating the 20th Anniversary of St. Denis-Pierson Paper,* National Ship Research and Development Centre, Bethesda, Maryland.

Dalzell, J.F. (1962). "Application of cross bi spectral analysis to ship resistance in waves," *Stevens Institute of Technology*, Hoboken, New Jersey, May.

Dalzell, J.F. (1974). "Cross bi spectral analysis: Application to ship resistance in waves," *J. Ship Res*., 18(1), pp.62-72.

Dalzell, J.F. (1976). "Application of functional polynomial model to the ship added resistance problem," *11th Symposium on Naval Hydrodynamics*, London.

Dalzel, J.F and Kim, C.H. (1979). "An analysis of quadratic frequency response for added resistance," *J. Ship Res.*, 23(23), pp.198-208.

Hasselman, K (1966) . "On non-linear ship motion in irregular waves," *J. Ship Res.,* 10(1), pp.64-68

Kim, C.H. (2008). "Nonlinear waves and offshore structures," *World Scientific Publishing Co.*, Singapore, in print.

Kim, C.H. and Dalzell, J.F. (1981). "An analysis of the quadratic frequency response for lateral forces and moments," *J. Ship Res.*, 25(2), pp.117-129.

Kim, KI and Powers, EJ (1988). "A digital method of modeling quadratically nonlinear systems with a general random input," *IEEE Trans Acoustics, Speech , and Signal Processing*, 36, pp.1758-1769

Kim, N.S. and Kim, C.H. (2002). "Cross bi spectral estimation of non linear force on fixed structure in nonlinear waves," *Proc., 12th Int. Offshore and Polar Eng Conference,* Kitakyushu , Japan , l3 , pp.188-195.

Kim, N.S. and Kim, C.H. (2003). "The effect of sea severity on the cross bi spectral estimate of quadratic response function for surge exciting force," *Proc., 13th Int. Offshore and Polar Engineering Conf.*, Honolulu, Hawai, 3, pp.416-423.

Kim, N.S. (2004). "Extraction of the second order non-linear response from model test data in random seas and comparison of Gaussian and non Gaussian model," *Doctoral Thesis*, Texas A&M University, College Station, Texas.

Kim, C.H., Rajendran, S. and Kwon, S.H. (2008). "Nonlinear vertical motion affected by sea severities," *18th Int. Conf. of Offshore and Polar Engineering*, Vancouver, Canada, July 6-10.

Kumar A, Kim, C.H. and Zou, J. (2003). "Limitation of the 2nd order theories for laboratory high sea waves and forces on structures," *Int. J. of Offshore and Polar Eng.*, 12(4), pp.243-248.

Rajith Padmanabhan. (2006). "Experimental wave effects on vertical relative motion," *Master Thesis*, Texas A&M University, College station, Texas.

Richer, J. (2005). "The effects of wave groups on the nonlinear simulation of ship motion in random seas," *Master Thesis,* Texas A&M University, College station, Texas.

Tupper, E. (1996). *Introduction to naval architecture,* 3rd edition , Butterworth-Heinemann, Oxford.

Vassilopoulos, L.A. (1966). "The application of statistical theory of non-linear systems to ship motion performance in random seas," *International Shipping Progress*, 14(150), pp.54-65.

# VITA

Suresh Rajendran received his Bachelor of Technology in naval architecture and ship building from Cochin University of Science and Tecnology, Cochin, India in 2002. He entered the graduate school in ocean engineering program at Texas A&M University in January 2007 and received his M.S degree in December 2008.

His address is:

Suresh Rajendran

CE/TTI 808-F

3136 TAMU

College Station,TX 77843-3136

Email:sureshr80@gmail.com